Self-archived version:
A. Campione, L. Gurreri, M. Ciofalo, G. Micale, A. Tamburini, A. Cipollina Electrodialysis for water desalination: a critical assessment of recent developments on process fundamentals, models and applications, Desalination, 434 (2018) 121–160, https://doi.org/10.1016/j.desal.2017.12.04

Electrodialysis for water desalination: a critical assessment of recent developments on process fundamentals, models and applications

A. Campione, L. Gurreri*, M. Ciofalo, G. Micale, A. Tamburini, A. Cipollina

Dipartimento dell'Innovazione Industriale e Digitale (DIID), Università degli Studi di Palermo, viale delle Scienze Ed. 6, 90128 Palermo, Italy

****Corresponding author: luigi.gurreri@unipa.it***

Abstract

The need for unconventional sources of fresh water is pushing a fast development of desalination technologies, which proved to be able to face and solve the problem of water scarcity in many dry areas of the planet. Membrane desalination technologies are nowadays leading the market and, among these, electrodialysis (ED) plays an important role, especially for brackish water desalination, thanks to its robustness, extreme flexibility and broad range of applications. In fact, many ED-related processes have been presented, based on the use of Ion Exchange Membranes (IEMs), which are significantly boosting the development of ED-related technologies. This paper presents the fundamentals of the ED process and its main developments. An important outlook is given to operational aspects, hydrodynamics and mass transport phenomena, with an extensive review of literature studies focusing on theoretical or experimental characterisation of the complex phenomena occurring in electromembrane processes and of proposed strategies for process performance enhancement. An overview of process modelling tools is provided, pointing out capabilities and limitations of the different approaches and their possible application to optimisation analysis and perspective developments of ED technology. Finally, the most recent applications of ED-related processes are presented, highlighting limitations and potentialities in the water and energy industry.

Keywords: electrodialysis; water desalination; ion exchange membrane; concentration polarization; energy.

Contents

1. Introduction

Seawater desalination is the main non-conventional source of fresh water in many countries all around the world. In some specific areas, facing severe water scarcity conditions, it is indeed the first source of fresh water for the local population. Recent figures about desalination industry indicate a cumulative contracted capacity of desalination plants in 2016 of almost 100 Mm^3/day, with an average contracted capacity per year between 3 and 5 Mm^3/day in the last 5 years [1], and a continuous increasing trend is expected in the next decades. Interestingly, seawater desalination led the desalination market in the first decade of the third millennium, with a dramatic capacity increase for SW-desalination plants in those years. Conversely, during the second decade the desalination industry experienced a growth of the applications to the desalination of brackish water and other types of water streams (e.g. tertiary waste waters, surface saline waters, etc.), where the typical capacities are small or medium (below 50.000 m^3/day) [1].

Among several different technologies, membrane processes nowadays have the leading role. In particular, looking at the new contracted plants (2010-2016), Reverse Osmosis now holds by far the majority of the global market share, ranging from 60% to 90% depending on the geographical areas. Thermal evaporative processes (mainly Multiple Effects Distillation and Multiple Stage Flash technologies) are still keeping an important role in Gulf countries, historically characterized by the operation of huge thermal desalination plants, thanks to their robustness, small sensitivity to low quality seawater feed and salt concentration and to the large availability of low-temperature waste heat for powering the thermal evaporative plants.

Within this context, electromembrane processes, e.g. electrodialysis (ED), electrodialysis reversal (EDR) and electrodeionization (EDI), have a small, yet stable share in low-salinity desalination applications. New ED/EDR and EDI contracted plants in 2015-2016 covered between 1 and 2% of the total desalination installed capacity, with the majority of plants processing brackish water and with a size ranging between few tens of m^3/day up to a maximum of 10,000m^3/day, reached by an EDR plant installed in South Africa [1].

Such limitation in installed capacity and type of treated feed is mainly due to the relatively higher cost of ion exchange membranes (IEMs) compared to RO membranes, and to the significant reduction of membrane selectivity when seawater is used as the feed solution.

A very recent development in the field of electromembrane processes has been the launching of reverse electrodialysis (RED) for energy generation from salinity gradients. In this new application, the salinity difference between two streams (e.g. seawater and river water, or concentrated brines and

brackish water) is converted into electricity by means of a controlled mixing of the two solutions. RED significantly promoted the development of new membranes and new plant configurations suitable for operations at high salinity, with optimized process efficiencies [2–8].

Electromembrane processes are thus experiencing a very promising revival era, pushed by R&D and industrial developments carried out by research institutions and major industrial stakeholders in the US, Europe and Japan [9].

In addition to that, a number of novel applications have been proposed in other industrial sectors, where the features of ED (or EDI) are more suitable than RO. Examples of these applications are the use of ED for brine concentration in sea-salt production facilities in Japan [10, 11]; in food industry (e.g. for juice de-acidification) [12–14]; in electronics (e.g. for ultrapure water production) and wastewater treatment, especially for heavy metals removal [15–17]. Moreover, the recent trends in the field of renewable energy desalination have also highlighted the promising features of photovoltaic (PV)-ED coupling, made possible by the extreme flexibility of the ED process, which can follow the oscillating behaviour of PV power production [18]. The same features make ED extremely suitable also for coupling with other off-grid sources, such as wind energy [19].

Finally, several special applications of electromembrane processes are gaining room in the scientific-technological community, which is more and more engaged in developing new IEMs and devices, enlarging the potential for the application of this flexible and multi-faceted class of technologies. Among these, it is worth to mention the growing field of bipolar membranes for acid and alkali production and electrochemistry applications [20–26], the development of selective-electrodialysis for selective salt separation from saline streams [26–29], and the application of the electrodialysis metathesis (EDM) in Zero Liquid Discharge (ZLD) desalination [30–33].

An overview of ED technologies for water desalination and related processes is presented here, with a specific focus on the most challenging topics for the growth of the technology, such as IEM development, modelling tools for process optimization, and innovative applications.

In particular, an extensive review of literature studies on the hydrodynamics, mass transport and fundamental phenomena governing the operation of electromembrane processes is given, with the aim of providing the reader with a comprehensive collection of all the main findings published in this field so far. The most important physicochemical phenomena are critically analysed for an in-depth knowledge of what governs ED and related processes. Finally, the most significant mathematical modelling approaches to the design and simulation of electromembrane processes are presented.

2. Historical development and working principle

2.1 From early steps to commercialisation

ED was proposed for the first time in 1890 by Maigrot and Sabates [34]. They built an early concept unit to demineralize sugar syrup by using carbon as electrodes and permanganate paper as membrane. A dynamo served as current supply.

However, Maigrot and Sabates never used the term electrodialysis, which can be officially found for the first time in a patent in 1900 [35]. In this patent, Schollmeyer aimed to purify sugar syrup using the same technology as in [34], but with soluble zinc or iron anodes. Despite this, it is generally argued that ED was not actually theorised until 1911 [35–37], when Donnan presented his exclusion principle, experimentally confirmed by Teorell few years later. According to this principle, it is possible to manufacture membranes selective to cations using fixed negative charges and membranes selective to anions using fixed positive charges.

The theorisation of electrochemical principles governing the behaviour of IEMs opened the way to the development of new membranes and to the conceptualisation of an electrodialyzer with multiple compartments [34]. However, the actual concept of multi-compartment ED where anion and cation exchange membranes are alternated could be only realised in 1950, when W. Juda and W. A. McRay manufactured the first synthetic ion-exchange membranes from ion exchange resins [35]. These membranes were used by Ionics (US) in 1954 to build the first ED desalination plant for Aramco (Saudi Arabia) [35]. Since that year, many other ED units were built.

In 1974, ED faced the main breakthrough with the development of the electrodialysis reversal concept (EDR) [35, 38]. This new operational strategy allowed ED to work by periodically inverting the current, offering the main advantage of membrane fouling control and generating a breakthrough in the implementation of ED at the larger industrial scale.

By then, a number of "ED-derived" alternatives, applications and processes have been developed and presented in the literature, providing a further booster to the development of electromembrane technologies in general. Figure 1 represents a synthetic timeline of the most critical development steps for ED and related technologies, indicating from the first important milestones to the more recent and very differentiated applications presented so far, including the first laboratory- or pilot-scale experiences and the first commercialisation attempts of the most recent ED derived processes. A deeper insight on these special applications will be given in Section 6.

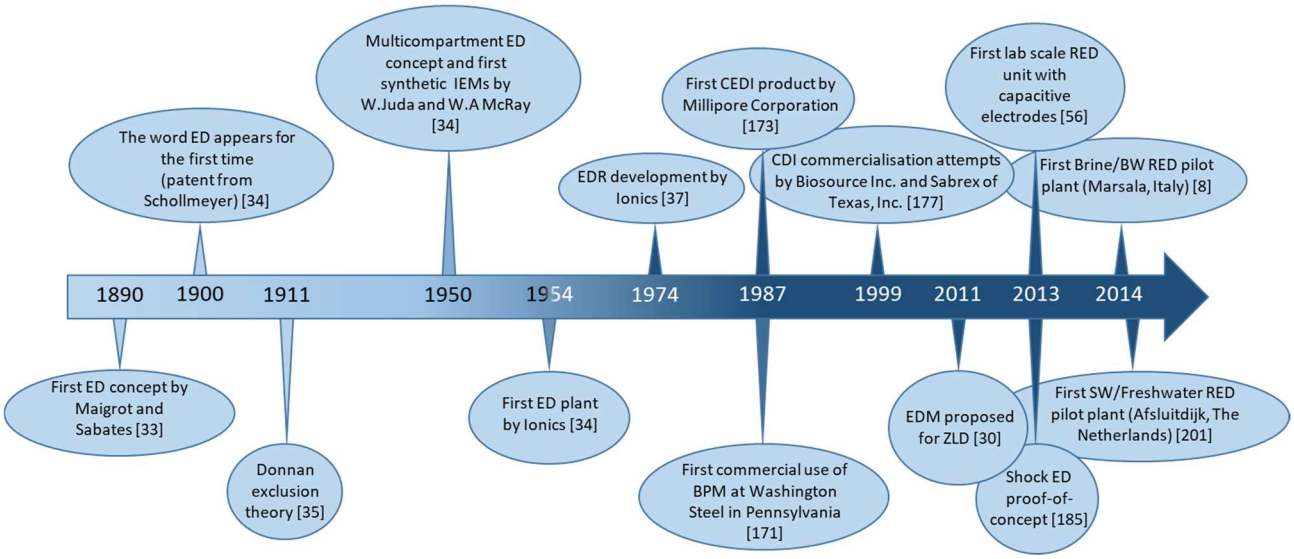

Figure 1. Timeline of the most important developments for ED and related processes.

2.2 ED devices: cell pair and stack

Electrodialysis (ED) is an electrically driven process. An ED unit is typically constituted by a train of ion-selective anion and cation exchange membranes (AEMs, CEMs), interleaved with alternating concentrate and dilute solution compartments and ending at both sides with an electrode compartment (Figure 2).

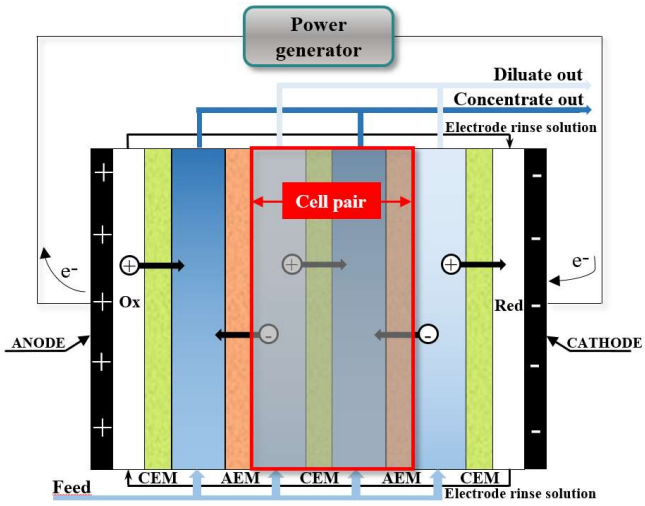

Figure 2. Schematics of an electrodialysis system, identifying the repeating unit (cell pair).

When the electrodes are electrically charged (by connecting them to a power source), an electrical current flows through the ED stack. As a consequence electrically charged solutes are forced to move according to the electric field. In particular, anions migrate towards the anode (positively charged) and cations towards the cathode (negatively charged). The presence of IEMs, as ideally selective

barriers to ions, ensures that anions move freely through the nearest AEM and are blocked by the nearest CEM. Conversely, cations move through CEMs and are blocked by AEMs, which leads to the depletion of salt content in the dilute compartments and the enrichment of the concentrate one (see Figure 2). The repeating unit of ED, namely the *cell pair*, consists of an AEM, a CEM, a dilute channel and a concentrate channel. An ED stack contains from a few cell pairs (in laboratory-scale units) up to several hundreds of cell pairs (values around 500 cell pairs or more are common in industrial units) and the two electrodic compartments, which allow the current of ions to be converted into a current of electrons flowing through the external electrical circuit. The active area of a single membrane goes from ~0.01 to ~0.06 m^2 for laboratory scale units [39–43], reaching values around 1 m^2 for large industrial scale units [44, 45].

In conventional electrodialyzers with the classical plate-and-frame equipment (see Figure 3), the feed channels are created by interposing between the membranes net spacers, maintaining a fixed inter-membrane distance and providing some mixing promotion in the channels. Spacers are provided with gaskets along the perimeter of the channels, which seal the channels and guide the solutions through them. Holes in spacers and membranes create special ducts for the two hydraulic circuits acting as manifolds for distributing/collecting the solutions to/from the channels. The ED device is closed with two end plates and compressed by bolts and nuts. ED stacks can be also built without spacers, by using profiled membranes (spacers and profiled membranes will be discussed in detail in Section 4.4). The inter-membrane distance in ED stacks typically ranges from ~0.3 to ~2 mm [10, 39, 41, 44–50].

The electrodic compartments are typically obtained from the end plates and contain the two electrodes and the electrodic solution adopted for the conversion of ionic into electric current. NaCl has been used in the past as the electrodic solution, although this causes the production of active Cl_2 [42] in the anodic compartment. For this reason, electrode rinse solutions containing SO_4^{2-} salts are now usually preferred in order to avoid damages to the anode [51].

Recently, the use of capacitive electrodes instead of conventional ones has been studied [52, 53]. These electrodes are composed by an active carbon layer and a current collector. Ions are adsorbed/desorbed in the active layer; this releases/captures free electrons, which pass through the collector thus reaching the external electrical circuit. In this way, it is possible to convert the ionic current into an electronic one without the need for a redox reaction, thus providing advantages such as the absence of unstable or toxic products (i.e. Cl_2) and the reduction of the electrodic potential drop [54]. On the other hand, capacitive electrodes suffer from saturation of the carbon layer, so that the electrical polarity needs to be periodically switched in order to operate the unit in a continuous way.

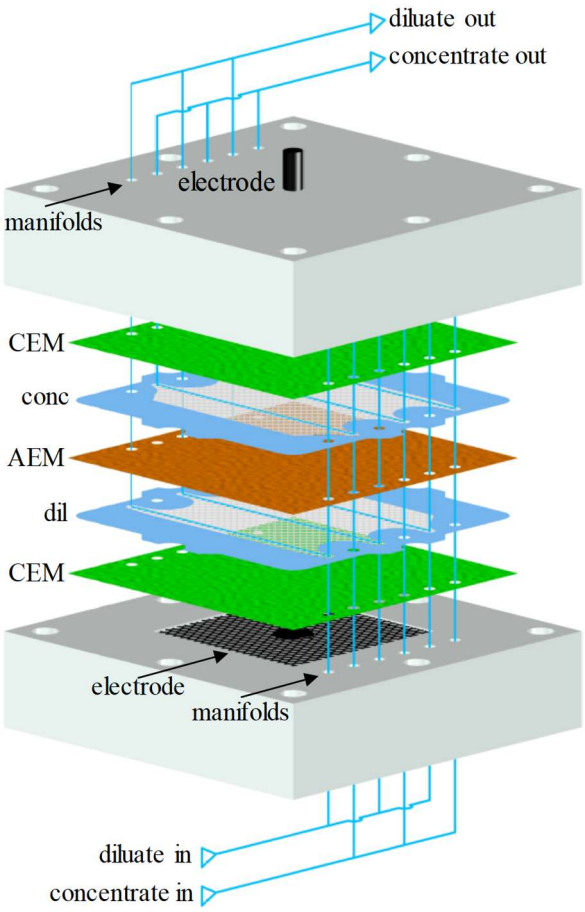

Figure 3. ED stack in the sheet flow arrangement of a laboratory scale unit with net spacers. A single cell pair and an additional CEM are represented.

The ED process can operate in batch or continuous mode. The first operating strategy is usually limited to small scale applications [42], while continuous operation is more common at industrial scale [49]. Typically, a single stack is not sufficient to reach the desired product specifications, and a multistage configuration is adopted. This configuration has also the potential to reduce the energy consumption and is particularly interesting for seawater desalination [49]. Alternatively, when a recovery higher than 50% is required, a feed and bleed operation mode can be adopted. In this case part of the concentrate, of the diluate or of both streams is recirculated back to the stack inlet, in order to independently control outlet brine and diluate concentrations [49]. Finally, an alternative, though not common, configuration includes the presence of a circulation flow on the diluate side (as it happens in a batch process) and of segregated concentrate compartments, filled with non-circulating solution. This particular arrangement has been used at laboratory scale to obtain extremely concentrated solutions [55, 56].

3. Overview of Ion Exchange Membranes

Ion exchange membranes (IEMs) represent the key components of all electromembrane processes. IEMs are typically thin polymeric films containing fixed charged groups which are ionisable in water [10, 57]. On the basis of the presence of positive or negative charged groups, these membranes can be firstly classified into anion and cation exchange membranes, respectively.

A cation exchange membrane (CEM) is characterized by the presence of fixed negative charges. Thus it is able to let positive ions (counter-ions) move across it and to block anions (co-ions). Conversely, the anion exchange membrane (AEM) blocks cations allowing the transport of anions. This exclusion principle, firstly theorized by Donnan [58], represents the fundamental IEM feature that makes the operation of all electromembrane processes possible.

The following sections are intended to give a general overview of IEMs fundamental theory, manufacturing and characterisation. For a more detailed insight on these topics, readers can refer to some more specifically focused reviews [59–61].

3.1 Donnan equilibrium and membrane potential

When an IEM is in contact with an electrolyte solution, the fixed charges on the surface of the IEM attract counter-ions by Coulomb forces and generate an electrical field. The Donnan exclusion [49, 62] causes a sharp change of concentration at the IEM-solution interface, thus generating a very thin charged region called electrical double layer (nanoscale, Debye length), where the counter-ions neutralize the fixed charges, and their concentration is much higher than the co-ions concentration (Figure 4). Therefore, counter-ions tend to diffuse from the IEM to the electrolyte solution while co-ions diffuse in the opposite direction. However, the large gradients of chemical potential are counter-balanced by a large gradient of electrical potential, the so-called Donnan potential, so that the electrochemical potential is conserved (Donnan equilibrium) and the net flux of ions is null.

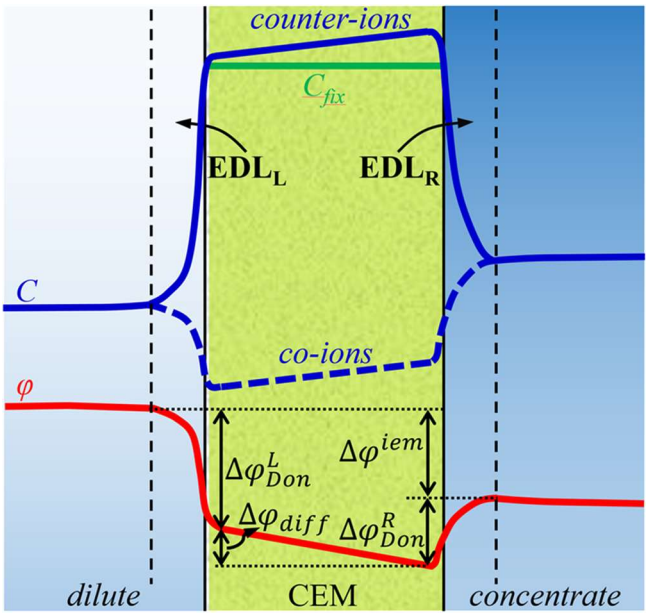

Figure 4. Schematic representation of ions concentration and electrical potential for a binary monovalent electrolyte solution in a cation exchange membrane immersed between a dilute and a concentrate solution.

By imposing the equivalence between the electrochemical potentials of ions in the electrolyte solution and in the IEM in equilibrium with it, the Donnan potential (φ_{Don}) can be expressed [49, 57] as

$$\Delta\varphi_{Don} = \varphi^{iem} - \varphi^{SOL} = \frac{1}{z_i F}\left[RT\ \ln\left(\frac{a_i^{SOL}}{a_i^{iem}}\right) + \bar{V}_i\Delta\pi\right] \tag{1}$$

where φ^{iem} is the electrical potential on the IEM side, φ^{SOL} is the electrical potential on the solution side, F is the Faraday constant, z is the valence, R is the universal gas constant, T is the absolute temperature, a is the activity of the ion, $\bar{V}$ is the partial molar volume, $\Delta\pi$ is the osmotic pressure difference between the two phases, the subscript i refers to the salt ion i and the superscripts iem and SOL indicate the membrane and the solution, respectively. By equating the Donnan potentials for cation and anion, being the osmotic pressure term $\bar{V}_i\Delta\pi$ negligible with respect to the RT-logarithmic one [49], and by assuming that the activity coefficients are equal in both phases [62], the Donnan equilibrium for the concentration can be obtained as [58, 62]

$$C_{co}^{iem} = \sqrt{\left(\frac{C_{fix}}{2}\right)^2 + C^{SOL\,2}} - \frac{C_{fix}}{2} \tag{2}$$

where C_{co}^{iem} is the co-ion concentration in the membrane, C_{fix} is the fixed charge concentration and C^{SOL} is the salt concentration in the solution.

An IEM immersed between two solutions at different concentrations is subject to a voltage difference over the two sides, referred to as "membrane potential". According to the well-known theory by Teorell-Meyer-Sievers (TMS), the membrane potential is [62–64]

$$\Delta\varphi^{iem} = \Delta\varphi^{L}_{Don} - \Delta\varphi^{R}_{Don} + \Delta\varphi_{diff} \quad (3)$$

where $\Delta\varphi^{L}_{Don}$is the Donnan potential on the left side, $\Delta\varphi^{R}_{Don}$ is the Donnan potential on the right side and $\Delta\varphi_{diff}$ is the diffusion potential arising from the concentration gradient within the membrane and from the different diffusivity of the two ions. The simplest expression of the membrane potential that can be derived from the TMS theory is [49, 62, 63]

$$\Delta\varphi^{iem} = \left(2\, t^{iem}_{counter} - 1\right)\frac{RT}{z_i F} ln \frac{a^{SOL,R}}{a^{SOL,L}} \quad (4)$$

where $t^{iem}_{counter}$ is the transport number of the counter-ion in the membrane, while $a^{SOL,R}$ and $a^{SOL,L}$ are the activities in the right and left solution, respectively.

The one-dimensional TMS model is based on several simplifying assumptions [63, 64] and predicts the membrane potential well within a certain range of solutions concentration, while deviating from experimental data in other conditions, e.g. with large concentration ratios [64, 65]. Models accounting for the effect of the membrane nano-pore radius have been developed, such as the "uniform potential" model and the "space charge" model [64, 65]. The discussion of these models goes beyond the scope of this work; however, the simple mathematical formulation of the TMS theory makes it the most commonly adopted for practical uses. Therefore, in the following the membrane potential will be intended as derived from the TMS theory.

3.2 IEMs preparation and classification

Based on their morphology, IEMs can be classified into two main categories: homogenous and heterogeneous [57, 66]. A more detailed classification based on the degree of homogeneity of the structure can be made [66, 67], which is particularly useful for IEMs characterized by micro-inhomogeneities.

Homogeneous membranes are the most commonly used in ED and other electro-driven processes [66, 68–72]. Such membranes appear homogeneous at the microscopic scale, but at the nanoscopic scale they can be observed as multiphase (i.e. microheterogeneous) systems composed by at least two phases: the polymer matrix with the fixed charges and the interstitial (electroneutral) salt solution. A more rigorous description, as given by Zabolotsky *et al*. [73], recalls the presence of a gel phase, generated by a thin layer of solution, and of fixed charges located at the internal walls of interstitial vescicles (Figure 5). This phase is also related to the formation of an electrical double layer (EDL), where electroneutrality is not maintained due to the split of anions and cations concentration profiles, which actually generates the Donnan potential at the interface [60, 66, 74, 75]. The

microheterogeneous model in [73] is particularly useful for the estimation of structural parameters as well as for the description of the peculiar behaviour (i.e. dependence on electrolyte concentration) of fundamental properties such as permselectivity and electrical conductivity.

Nevertheless, Kamcev *et al.* [76] recently discarded the actual existence of such a microheterogeneous structure discussing data of membrane resistance measurements. Therefore, this is still an open issue which will require further research activities.

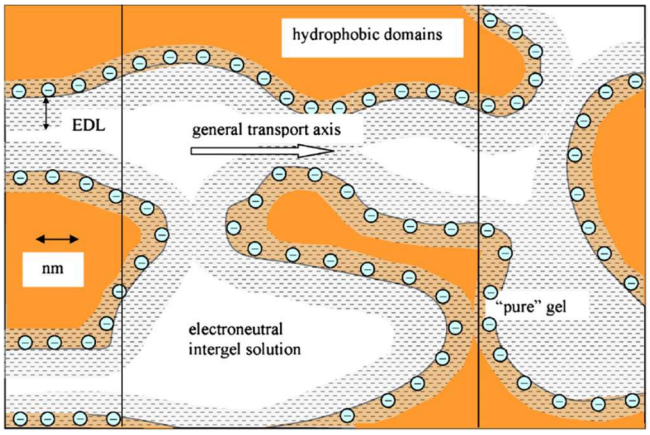

Figure 5. Representation of the structure of a homogeneous CEM, with the three different phases: polymeric hydrophobic, electroneutral solution and gel phase [74].

For homogeneous membranes, three main manufacturing methods can be identified [57, 66, 77]:

1. Polymerisation of monomers: at least one of these monomers must contain ionisable groups;
2. Introduction of charged moieties into a polymeric film: this can be done by adding either a charged monomer or a non-functional monomer to be functionalized afterwards;
3. Introduction of charged moieties into a polymer, followed by polymer melting (or solvation in a solvent) and casting into a film.

Styrene-divinylbenzene-based membranes represent one of the most remarkable examples of homogeneous structures produced starting from monomers. These membranes have been widely used in ED and are obtained from sulfonated or aminated styrene-divinylbenzene copolymers [70, 71]. These IEMs have been also used in ED plants concentrating seawater in order to produce table salt, where it is essential to increase the monovalent ion selectivity [70].

Concerning the second class of manufacturing methods, polyethylene, polypropylene and fluorocarbon polymers are used for IEMs production from a preformed polymeric film [77]. In this case, films are commonly functionalized by grafting acrylic monomers to obtain weak acidic CEMs [78–82]. Alternatively, vinyl monomers such as styrene are grafted to the polymer film and

subsequently sulfonated or aminated in order to produce strong acidic CEMs [83–86] or AEMs [87, 88].

The third manufacturing method is commonly adopted for soluble polymers such as polyether ketone and sulfonated polymers [77, 89]. These latter are particularly important as they represent a promising option for producing cheap membranes to be used for ED and other processes when working under severe conditions such as high temperature [66]. Production processes and properties of IEMs based on polysulfone block copolymers, polyether sulfone and polyarylene ether sulfone have been widely described in the literature [90–95].

Though still at a laboratory scale, electrospinning (coupled with hot-pressing) has recently been proposed for the production of nanoporous IEMs [59]. By this method it is possible to produce nanofibrous structures combining high porosity and large surface area with higher tensile modulus compared to the bulk material. In particular, very good performances of these new IEMs have been found for diffusion dialysis applications [59].

Heterogeneous membranes are characterized by ion-exchange particles (of macroscopic size, compared to the nano-scale of phase discontinuities of homogeneous membranes) incorporated in a continuous phase made of a binding polymer [57]. These membranes are usually thicker, with higher mechanical strength but poorer electrochemical properties. The use of cheap binding polymers allows for a significant reduction in the IEMs specific price, and the best trade-off is to be found between these aspects [66]. Heterogeneous membranes are usually manufactured by incorporating ion-exchange resins into polymer sheets (the binder polymer) with three main alternative procedures [66, 96]:

1. calendering the particles into the polymeric sheet;
2. dry moulding of the inert polymer film and the resin particles followed by milling;
3. dispersion of resin particles in a solution containing a film-forming binder followed by casting and solvent evaporation.

In addition, new preparation methods have been recently engineered with the aim of improving IEMs structure. In this context, polymer blending and pore filling methods represent recently proposed alternatives [59].

An important feature strongly affecting the mechanical behaviour of heterogeneous membranes is the particle size distribution. In particular, it was observed that the flexibility increases when decreasing the particle size, while the brittleness increases with the particle loading [97].

Special ion exchange membranes have also been developed through several research efforts focused on the optimal tuning of membrane properties. These efforts led to special membranes characterised by hybrid structures and particular manufacturing methods [66, 77]. Interpenetrating (IPN) and semi-interpenetrating (sIPN) polymer network IEMs are examples [98–103]. IPN are prepared by mixing two polymers that cross-link due to permanent entanglement, while sIPN are composed by a linear or branched polyelectrolyte immobilised in a cross-linked polymer matrix. This particular structure allows electrochemical and mechanical properties to be tailored for specific applications [98, 103]. Membranes prepared by radiation grafting represent another class of IEMs, in which this new technique allows incompatible polymers to be linked, thus combining their properties. In addition, these properties can easily be tuned by choosing the degree of grafting [66]. Several works deal with the preparation and characterisation of IEMs through the grafting method, and the possibility of using them in ED has been assessed [104–108].

The last group of special membranes is represented by the hybrid organic-inorganic IEMs. Combining the properties of polymers with those of inorganic materials, chemical, mechanical and thermal stability can be significantly enhanced [77]. For this reason, these membranes are mainly used in fuel cell applications [109–117]. Hybrid structures are usually obtained through intercalation, blending, in situ polymerization, molecular self-assembling or sol–gel process, with this latter being the most widespread method [118, 119].

A particular development has led to special membranes incorporating both positive and negative fixed charges within the same membrane [77].

Bipolar membranes (BPM) are the most remarkable example of this class. BPM are constituted of an anion exchange layer overlapped with a cation exchange layer. These membranes are mainly used in a special application of electrodialysis, where water splitting is induced to produce acid and alkaline solutions [57, 77]. Bipolar membranes can be manufactured by different methods such as casting a cation exchange polyelectrolyte solution on an anion exchange membrane (or *vice versa*) [120], adhering commercial cation and anion exchange membranes [23], or functionalizing the two sides of a standard membrane [121–124].

Two other interesting classes of membranes containing both type of charges are the amphoteric and the mosaic membranes [77]. The former present randomly distributed weak acid and weak basic groups. Their main feature is that charged groups respond to pH variations, thus modifying the cationic or anionic selective character of the membrane. This makes amphoteric membranes particularly useful in special applications such as in biomedical and industrial fields [77].

Mosaic membranes are characterised by anion and cation exchange areas arranged in a parallel way within a single membrane [125]. This allows individual current circulation in each layer, leading to negative osmosis and a salt permeability higher than that of neutral species. These special properties make mosaic membranes a promising candidate for the treatment of waste streams where salt should be separated from organic compounds. However, these membranes are not yet commercially available [77].

3.3 IEMs properties and characterisation

In order to evaluate the performance of a membrane it is necessary to estimate several properties which can be grouped into three main categories: mechanical, physicochemical and electrochemical properties.

Mechanical stability is essential for a membrane to be used in industrial applications such as ED. Several mechanical tests are performed for the mechanical characterization of membranes [126]. In particular:

- Uniaxial tensile test. It is the most common test to evaluate Young's modulus, yield strength, elongation at break, strain-softening and strain-hardening.
- Creep and relaxation tests[127].
- Dynamical mechanical analysis. It is widely adopted to investigate the viscoelastic properties and the glass transition temperature.
- Bursting test. During the test, a membrane is exposed to an increasing pressure (simulating the presence of a differential pressure between the two channels of a cell pair) until failure occurs.

The mechanical behaviour of IEMs is affected by several features of the membrane material, e.g. cross linking degree, water uptake, aging, and by operating conditions, e.g. temperature [68]. In particular, Young's modulus decreases as the temperature increases [128] and membranes become stiffer as the cross-linking degree increases On the contrary, membranes plasticize at high level of water uptake [129].

Physico-chemical properties to be characterised in IEMs are swelling, ion-exchange capacity (IEC), chemical stability and permeability to ions (conductivity and diffusive permeability) and neutral species (diffusive permeability).

The swelling degree can have a direct influence on the dimensional stability, permselectivity and specific electrical conductivity. The swelling degree can be evaluated by measuring the weight difference between dry and swollen membrane [130, 131]. In order to calculate the volumetric swelling, the membrane material density is needed [66].

The IEC indicates the amount of fixed charges in the IEM. It is commonly expressed as milli-equivalent (meq) of functional groups per gram or cm^3 of dry membrane (though in some cases they can be expressed per gram or cm^3 of swollen membrane) and it is useful to estimate the fixed charges concentration. The main technique for the measurement of IEC is titration with NaOH for negative groups and with HCl for positive groups [89, 130, 131].

In ED and related processes, very large concentration differences can be achieved in the two compartments. For this reason, salt and water diffusion through IEMs can represent an important factor for determining process performance.

Salt diffusion can easily be measured using the time-lag method or a more advanced method adopting radioactive tracers [49].

Water moves across membranes by two main mechanisms: osmosis (water passage driven by an osmotic pressure difference) and electroosmosis (passage of water molecules entrained in the solvation shell of ions, thus proportional to the ions flux). In order to determine the water osmotic permeability it is possible to measure the water flux in an ED batch process by simply measuring the weight change in the reservoirs, periodically switching off the stack current to exclude the electroosmotic effect [42].

Electrochemical properties have the most important influence on the performance of IEMs. In particular, the two main electrochemical properties to be measured are permselectivity and electrical resistance.

Permselectivity indicates how selective the membrane is to the passage of counter-ions. A low perm-selective membrane will allow the passage of co-ions between compartments, thus negatively affecting the separation efficiency. The fastest method to estimate membrane permselectivity is by measurement of non-Ohmic membrane potential [66, 132]. The real (measured) membrane potential in the case of a single electrolyte in solution can be written as [32]:

$$\Delta\varphi_{measured}^{iem} = \alpha_{iem}\frac{RT}{z_i F}\, ln\frac{a^{SOL,R}}{a^{SOL,L}} \tag{5}$$

where $a^{SOL,R}$ and $a^{SOL,L}$ are the salt activities in the solutions at the two sides (right and left) of the membrane and α_{iem} is the membrane permselectivity, which can be seen as the ratio between the

actual membrane potential and the theoretical one given by the Nernst equation (5) for α_{iem} = 1, i.e. $\alpha_{iem} = 2\, t^{iem}_{counter} - 1$ (see eq. (4)).

It should be noted that the transport number (and thus the permselectivity) evaluated with this simple method is generally underestimated. In fact, this measurement leads to an apparent transport number that should be corrected by the water transport number. A more detailed discussion of this issue can be found in [61].

By a more rigorous definition, the permselectivity can be expressed as [49, 66]:

$$\alpha_{iem} = \frac{t^{iem}_{counter} - t_{counter}}{1 - t_{counter}} \tag{6}$$

where $t^{iem}_{counter}$ and $t_{counter}$ are the counter-ion transport numbers in the membrane and in the solution, respectively. In particular, it is possible to experimentally estimate transport numbers using Hittorf's method [61, 66, 134, 135] or by chronopotentiometric measurements [136–140]. One of the most critical aspects is that the concentration of electrolytes in solution affects permselectivity [5, 141]. For this reason, multiple measurements at different concentrations are necessary in order to get the different permselectivity values in the whole operational range.

The membrane electrical resistance (ER), inversely related to the electrical conductivity, generates Ohmic potential drops when an electrical current passes through the membrane pile, thus dramatically affecting the process energy consumption. As in the case of permselectivity, electrical resistance is influenced by solutions concentration [60, 75, 142]. This dependence can be explained with the typical multiphase structure of IEMs, widely reported in the literature [60, 73, 143]. In order to characterise membranes ER, direct current (DC) or alternating current (AC) measurements can be carried out.

The simplest method consists of estimating ER from the slope of an *I-V* (current-potential) curve in DC mode, limited to the region where a linear relationship between voltage and current is maintained. This curve can be obtained using a test-cell with two chambers separated by one membrane [144] or by chronopotentiometry in a six-cell compartment device [75, 140]. Another option involves the use of a *clip cell*, composed by two black graphite electrodes fixed on Plexiglas plates and used to "clip" a conditioned wet membrane [145, 146]. ER can thus be measured by the previously mentioned DC method but also by means of AC methods (as described in the following lines).

It should be noted that *I-V* curves (and, more generally, the use of DC methods) give reliable results only when IEMs are placed in contact with a sufficiently concentrated solution. The reason is that this method is not suitable for low concentrations as it cannot separate the effects of electric double

layer formation and concentration polarisation. In addition, the presence of DC leads to concentration polarisation in the internal pores even when the external diffusion layers are not present [147]. Finally the blank resistance to be subtracted in order to separate the resistance of the membrane from that of the solution can be relatively very high for low concentration, thus affecting the accuracy of the method.

As an alternative to DC-based methods, AC-based measurements can be performed adopting the Electrical Impedance Spectroscopy (EIS) method, able to distinguish among the contributions due to Ohmic effects, electric double layer and diffusion boundary layer and, thus, to estimate the pure membrane resistance [75, 142, 148, 149]. On the other hand, EIS is the most complex methodology, as it requires the identification and implementation of an "electrical model" fully describing all phenomena involved, in order to properly interpret the experimental data and convert them into the desired information.

3.4 Fouling and electrodialysis with polarity reversal (EDR)

Although ED is not generally affected by fouling and scaling phenomena as much as other desalination processes such as RO [150], IEMs fouling can still be a limiting factor for maintaining good process performances. In particular, this phenomenon can significantly enhance membrane resistance and pressure drops along the channel and, in some cases, even reduce membrane permselectivity [151]. *I-V* curves are often used to characterise membrane fouling, though this method does not provide information on the properties of fouling layers. EIS has been proposed as a supplementary investigation method in order to capture more details on interfacial layers [152].

Three main classes of fouling compounds can be identified: scalants, colloidal particles and organic materials [153].

Scaling is one of the most important problems in desalination, especially when the feed water is rich in low-solubility salts such as $CaCO_3$ and $CaSO_4$. The most common methods for reducing it include the use of lower recovery rate, the adjustment of pH and cleaning procedures with citric acid or EDTA [153]. In addition, the possibility of treating the concentrate stream (i.e. the one with highest scaling potential) of a batch ED unit by magnetic or ultrasonic field has been reported [154]. In particular, the magnetic field was applied to a part of the feeding line, while an ultrasonic bath was used as the concentrate tank. Interestingly, the last method not only results in a scaling reduction but also in an improvement of ions transport.

Colloidal particles can be abundant in sea or brackish waters and they are often negatively charged. Their deposition on the membrane surface is driven by the electric field pushing the colloidal particles towards the positive electrode. Such migration is stopped by the presence of the membranes, acting as a mechanical barrier and being covered by a growing deposited layer of colloids on their surface. Similarly to scaling, colloidal-fouling prevention strategies include the reduction of recovery and pH adjustment. Besides, micro and ultrafiltration can be used as pre-treatments, while a higher fluid velocity inside the stack can help particles displacement from the membrane surface [153]. The most effective action for colloidal and organic foulants, however, is the use of a polarity reversal strategy, which will be presented in the following lines.

Fouling due to organic matter can be very severe when ED treats food industry streams [155, 156] and in water reuse applications [151, 157]. In these cases, the presence of organic compounds can dramatically affect fouling phenomena leading to a huge decline in process performances. For this reason, several research works have adopted model foulants such as bovine serum albumin, humate and sodium dodecylbenzene-sulfonate in order to investigate the phenomenon in depth [152, 158].

The molecular size of organic particles can significantly affect their fouling behaviour. In fact, particles with a molecular weight of 200 - 700 Da can cause internal membrane fouling, being able to penetrate membrane pores. On the other side, larger molecules cannot enter inside pores, thus being blocked on the external surface, while, conversely, much smaller molecules pass freely through membrane pores, thus not generating any internal blocking and fouling in the IEM [157]. In order to reduce organic fouling pre-treatments such as microfiltration, ultrafiltration or activated carbon have been proposed and cleaning actions with NaOH solutions are also possible [153].

Regardless of the different classes of materials, most foulants present in feed waters exhibit electrostatic features which enhance the fouling risk for AEMs [151, 159]. In this respect, many efforts have been made through years in order to increase AEMs antifouling properties by surface modification processes [160–162]. Grebenyuk. *et al*. [160] modified AEMs by adding high molecular mass surfactants obtaining an increased resistance against organic deposition. Alternatively, modification with poly(sodium 4-styrene sulfonate) [161] or polydopamine [162] can also reduce fouling, while negligibly affecting other IEMs properties.

Despite the different strategies proposed for reducing fouling in IEMs, standard ED operation always require in-place-cleaning procedures, resulting in a cost increase for the process [153]. For this reason, the development of the electrodialysis reversal (EDR) concept represented one of the main breakthroughs for the ED technology, succeeding in dramatically reducing the fouling tendency of IEMs in ED stacks for very long lifetimes. The EDR concept is based on the idea of reversing the

polarity of the electrodes at regular time intervals [163]. Consequently, diluate and concentrate channels are inverted and the reverse electric field promotes the periodic removal of electrically-charged foulants (e.g. colloids or organic matter) deposited on membranes surface. In this way, detached particles are entrained by the flowing solutions and discharged with the exiting streams ("off-specification" outlet), which are therefore disposed back to the sea (or to another receiving body) for a time interval allowing the complete cleaning of the feed compartments, typically ranging from a few seconds up to 1-2 minutes [163]. EDR adds complexity to the process as it requires a triggering control unit, electric control systems to change polarity and automatic valves for compartments switching . In addition, some of the feed is wasted during the "off-spec transition", which leads to a reduction in the conversion rate of the process.

Nevertheless, EDR offers significant advantages in terms of minimisation of cleaning procedures and pre-treatments and avoids the presence of acids tanks, complexing agents tanks, dosing pumps and pH controllers inside the desalination plant [163]. Moreover, the polarity reversal technology is able to operate under extreme conditions, such as salt supersaturation, with examples of plants operating under a super-saturation level of $CaSO_4$ higher than 175% [164]. More importantly, EDR has allowed the operation of brackish water ED industrial plants for more than 30 years, with IEMs lifetime reaching up to 10-15 years.

More recently, a concept similar to polarity reversal has been investigated, namely the pulsed electrical field (PEF) [153, 165, 166]. The PEF operating mode consists of discontinuously applying the electric field and generating a constant current, leaving some time intervals without any electric field applied. This method is claimed to reduce membrane fouling, thus increasing process performances, by disturbing the deposition of charged species. In addition, a reduction of the polarisation layer has also been experienced [165, 166]. PEF has been recently compared with EDR, showing similar performances or even lower energy consumption under certain conditions [167].

4. Hydrodynamics and mass transport in electrodialysis: from fundamentals to recent developments

The role of hydrodynamics and associated phenomena of mass transport is crucial in determining the performance of ED stacks and the capital and operating costs of the process. It is well known that mass transfer limitations and non-Ohmic voltage drops arise because of the so called "*concentration polarization phenomena*" and can be mitigated by convective motions enhancing mixing. The energetic cost of the process may also be affected by the power consumption for pumping the solutions through the channels. Moreover, the channel features, which are essential for

hydrodynamics and mass transport, also affect other aspects that may be critical, such as the Ohmic voltage drop. Finally, pressure drop in the manifolds, voltage losses caused by a non-uniform flow distribution among and in the channels, internal leakages due to pressure gradients across the membrane are additional phenomena depending on the stack hydrodynamics.

Clearly, the optimization of ED (or EDR, or other electromembrane processes) units is based on a very delicate equilibrium among the stack features (including the membranes properties) and the operating conditions. The following sections will examine in detail the fundamentals of hydrodynamics and mass transport in ED and the way these affect the operation of ED and related processes, together with more recent strategies for the improvement of hydrodynamics performances and novel experimental techniques for their characterisation.

4.1 Concentration polarization phenomena

In membrane separation processes, concentration polarization is a well-known phenomenon which manifests itself as a concentration gradient within the solution and perpendicular to the membrane surface. In the case of IEMs-based processes, the electrical current is carried roughly in the same amount by cations and anions migrating through the solution in opposite directions. On the contrary, inside the membrane current is carried mainly by counter-ions, while co-ions are (ideally) excluded. As a consequence, at the solution-membrane interface the migrative flux of co-ions (typically directed from the interface to the bulk of the solution) has to be counterbalanced by a diffusive flux in the opposite direction, intrinsically accompanied by a concentration gradient able to generate such diffusive flux according to Fick's law [10, 168–170].

Concentration polarization and transport phenomena near interfaces have commonly been analysed by the Nernst film model [171, 172]. The basic assumption of this theory is the existence of a "Nernst diffusion layer" between the membrane-solution interface and the fluid bulk with uniform composition. This is also known as "diffusion boundary layer" (DBL) and can be considered as a thin stagnant layer where no convection occurs and mass transfer is controlled by diffusion-migration, resulting in a linear concentration profile (Figure 6 (a)). The Nernstian idealization was improved by Levich [172], showing that the presence of convective transport within the DBL results in a smooth monotone concentration profile asymptotically approaching the bulk concentration.

Mass transport in IEMs and electrolyte solutions has been widely studied by the theoretical description given by the Nernst–Planck formalism [62, 171], which can also lead to a more rigorous

definition of the concentration polarisation gradient. In fact, under certain hypotheses (for more details see Section 5.1.1), the flux $\vec{J}_i$ of type-i ions can be expressed as

$$\vec{J}_i = -D_i\vec{\nabla}C_i - z_iFD_iC_i\vec{\nabla}\varphi + C_i\vec{u} \tag{7}$$

where D_i is the ionic diffusion coefficient, C_i is the concentration, z_i is the valence, F is Faraday's constant, φ is the electric potential, and $\vec{u}$ is the velocity vector. Hence, the total flux is given by the sum of diffusive, migrative and convective flux. The ion diffusion-migration flux can also be expressed as a chemical diffusion-Ohmic conduction flux [62], so that, for a strong binary electrolyte, it can be written as:

$$\vec{J}_i = -D\vec{\nabla}C_i + \frac{t_i\vec{\imath}}{z_iF} \tag{8}$$

where D is the electrolyte diffusion coefficient, t_i is the migration transport number and $\vec{\imath}$ is the current density. At the membrane-solution interface, the mass balance under steady state conditions is obtained by equating the flux on the solution side (eq. (8)) with that on the membrane side. Considering only the component normal to the membrane surface (y coordinate) one has:

$$-D\frac{\partial C_i}{\partial y} + \frac{t_i i}{z_iF} = \frac{T_i^{iem} i}{z_iF} \tag{9}$$

where T_i^{iem} is the integral transport number within the membrane [62, 173, 174] accounting for both ionic diffusion and migration (i is positive if directed towards the positive y axis). Therefore, the following boundary condition can be written:

$$\frac{\partial C_i}{\partial y} = -\frac{i}{z_iFD}\left(T_i^{iem} - t_i\right) \tag{10}$$

In the literature, this boundary condition is often given by a less rigorous expression where T_i^{iem} is replaced by the migration transport number within the membrane t_i^{iem} [168–170, 175–178], but the approximation is legitimated by the fact that diffusion inside the IEM is often negligible.

Moreover, commercial membranes normally have high permselectivity, i.e. the counter-ion transport number is close to 1 in the membrane, while being close to 0.5 in solution (NaCl). As a result, a diffusive flux roughly equal to 50% of the current density (i) divided by z_iF, i.e. equal to the conductive transport for each ion, is established at the IEM-solution interface. Thus, salt diffusion (of both co- and counter-ions due to electroneutrality) between the solution bulk and the interface takes place, in the same direction of migration for counter-ions and in the opposite direction for co-ions. Salt depletion occurs at the IEM-diluate channel interface, while salt enrichment occurs at the IEM-concentrate channel interface, affecting the electric potential profile as shown in Figure 6 (b).

Typically, the electrolyte concentration profile in solution is slightly asymmetric, due to the difference in the transport number of cation and anion (e.g. $t_{Na+} \approx 0.4$ and $t_{Cl-} \approx 0.6$).

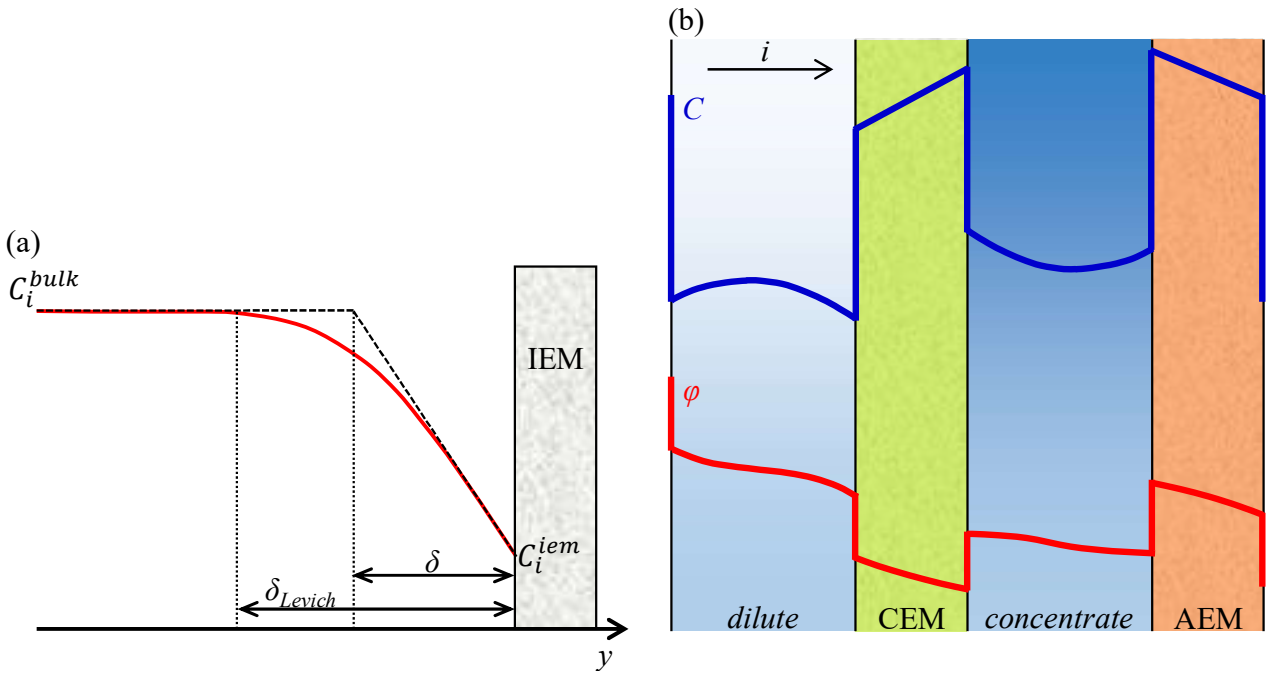

Figure 6. (a) Concentration profile within current-induced diffusion layer in steady-state conditions: Nernst's linear concentration profile (dashed line); Levich's profile taking into account convection contribution (solid line), where the concentration differs from the bulk concentration only by 1% at the distance δ_{Levich} from the IEM [74]. (b) Qualitative profiles of electrolyte concentration and electrical potential within an ED cell pair. Inside the IEMs the concentration of counter-ions is depicted. Electrical double layer phenomena are represented as sudden jumps at each IEM-solution interface.

Experimental observations of concentration polarization gradients have been carried out by several techniques. Choi *et al.* [179] measured the potential drop by a mobile micro-electrode at various distances from a CEM (two-compartment cell), obtaining the concentration profiles in the depleted side by letting the current vary. Tanaka [180, 181] reported data on the electrolyte concentration profile obtained by the so-called Schlieren-diagonal method, based on the measurement of the refractive index in a three-compartment optical glass cell. Another method of visualization of the concentration profile is laser interferometry, firstly introduced by Forgacs *et al.* [182] and then applied in several works [183–187], some of which were used to validate models simulating ED stacks equipped with ion conducting spacers or profiled membranes [185, 187], or analysing intensive current regimes ("overlimiting" region) [186]. Kwak *et al.* [188] fabricated a microfluidic ED device and applied a technique for the direct visualization of fluid flows and salt concentration profiles using charged fluorescent dyes over a wide range of voltage (0-100 V). Recently, the same research group [189] used the microscale ED system for studying the effects of floating spacers and validate their model for fluid dynamics and mass transport phenomena.

4.2 Mass transport equations and limiting/overlimiting current conditions

4.2.1 Formulation of mass transport equations in ED and related processes

Regardless of the true concentration profile, the interfacial condition expressed in eq. (10) can also be written in Nernstian form, taking into account the DBL thickness (δ) [169, 170, 173, 178, 190, 191] or the Sherwood number (*Sh*) [50, 174, 178, 192]:

$$\frac{\partial C_i}{\partial y} = \pm \frac{C_i^{iem} - C_i^{bulk}}{\delta} = \pm \frac{Sh\left(C_i^{iem} - C_i^{bulk}\right)}{d_{eq}} = -\frac{i}{z_i F D}\left(T_i^{iem} - t_i\right) \tag{11}$$

where C_i^{iem} is the concentration at the IEM-solution interface (solution side), C_i^{bulk} is the bulk concentration, d_{eq} is the equivalent diameter. In eq. (11) the sign + has to be considered when moving from bulk to interface, while the sign – in the opposite case. For simplicity, the difference of the transport numbers is often assumed equal to 0.5 [6, 192, 193]. Eq. (11) identifies the most common expressions of mass transfer rate in these systems, also allowing an in depth comprehension of mass transport phenomena at the boundaries. In fact, under steady state conditions, both diffusion and convection in solution from bulk to interface or *vice versa* compensate for the difference between the migrative fluxes across solution and membrane.

The Sherwood number is defined as

$$Sh = \frac{k\, d_{eq}}{D} \tag{12}$$

where *k* is the mass transfer coefficient. From dimensional analysis, it can be found that the Sherwood number depends on the channel configuration (geometry of spacer or membrane profiles, but also active walls surface, depending on the presence of conductive spacers or profiles), the Reynolds number (*Re*) and the Schmidt number (*Sc*) [194–201]. For more details, see the mass transfer correlations discussed in Section 4.4.4.

Besides concentration polarization visualization techniques, some experimental methods for the measurement/estimation of δ (and thus *Sh*) have been developed and tuned up, e.g. based on chronopotentiometry [74, 139, 202, 203] and EIS [204]. However, mass transfer characteristics are often evaluated by measurements of limiting current density, an important parameter controlling the operation of ED units.

4.2.2 Limiting current density in ED units

The increase of current density in a stack, always accompanied by an increase in diffusive transport of ions in solution, leads to a depletion of salt in the solution at the IEMs interface of the diluate

channel. Such phenomenon is allowed only until the concentration at the wall in the depleted layer becomes zero. In this condition, the so-called "*limiting current density*" is achieved, which, from eq. (11), can be expressed as:

$$i_{lim} = \pm \frac{C_i^{bulk} z_i F D}{\delta \left(T_i^{iem} - t_i\right)} = \pm \frac{Sh\, C_i^{bulk} z_i F D}{D_{eq} \left(T_i^{iem} - t_i\right)} \tag{13}$$

According to the sign conventions cited above, i_{lim} will be positive if directed towards the positive y axis. Thus the limiting current density depends on hydrodynamic conditions, channel thickness and salt transport numbers. Interestingly, once the values of i_{lim} and T_i^{iem} are known, the DBL thickness and Sh could be easily calculated from eq. (13), but it should be noted that phenomena occurring in limiting current conditions, such as electroconvection, may significantly affect the value of Sh determined with this equation [139]. Therefore, if the hydrodynamics features and mass transport coefficients have to be determined in the underlimiting range, where the above mentioned phenomena do not play a role, chronopotentiometric and EIS-based methods are more suitable.

From eqs. (11) and (13), it follows that, for a current density $i < i_{lim}$, the concentrations at the IEM-solution interface can be expressed as [169, 177, 179, 190, 205]

$$C_i^{iem} = C_i^{bulk} \left(1 \mp \frac{i}{i_{lim}}\right) \tag{14}$$

Values of limiting current density can be obtained experimentally by current-voltage curves. As the voltage increases, the current increases more and more slowly due to the higher boundary layer effects that increase the resistance (see Section 4.3), until current increases only slightly with large voltage increments, indicating the achievement of limiting current condition. However, when the limiting current is approached, experimental observations deny the presence of the plateau theoretically postulated as a curve saturation (see Figure 7), so that the classical theory of concentration polarization is not anymore considered valid since the early 1970s [40, 169, 170]. Instead, only a narrow flat region or even an inflection point are found, along with a further increase of current (*overlimiting* current), due to the onset of further phenomena that were not observed at electrode-solution interfaces. Water splitting was considered responsible of the further charge transport, thus causing such deviation. However, many other mechanisms have been more recently theorized, discussed and experimentally proven (see Section 4.3).

Figure 7 shows a typical *S*-shaped current-voltage curve, exhibiting three regions [175, 188, 190, 191, 206–210]. Region I has been often defined as Ohmic, though this may be misleading due to the coexistence of both Ohmic and non-Ohmic phenomena. In the first small tract, the curve can be well approximated by a straight line; however, as the current increases, polarization (non-Ohmic) effects

become more pronounced and cause a deviation from the linear trend. A much lower slope characterises region II, which can be regarded as a transition step following the achievement of the limiting current, conventionally identified by the intersection between the line tangent at the first tract of the current-voltage curve and the tangent of the plateau (or at the inflection point) in region II. Then, the slope increases again towards region III until reaching an asymptotic value leading to a stable linear increase of current *vs* voltage.

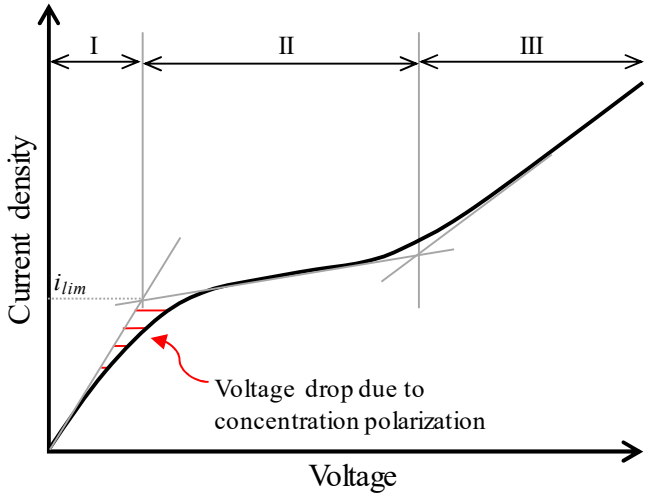

Figure 7. Sketch of a typical current-voltage curve for an IEM immersed in an electrolyte solution, showing a limiting current density and the presence of three distinct regions.

The behaviour of IEMs in current-voltage tests has been explained by the effects of the conductive heterogeneity of the membrane surface [138, 207, 208, 211–216], which can be viewed as a mosaic of alternating conductive and insulating regions of size ranging from micrometers to tens of micrometers. Therefore, for any given average current density, the local current density on the conductive areas is larger. This results in a decrease in the average value of i_{lim} compared to a membrane having an electrically homogeneous surface, or to a metal plate electrode. Hence, region II of the current-voltage chart is due to a gradual achievement of the local i_{lim} in the non-conductive regions, at the cost of a much larger voltage drop. Another effect of the conductive heterogeneity is the alteration (elongation or shortening, depending on the distance between the surface heterogeneities) of the plateau length, i.e. of the onset of the overlimiting transport phenomena, namely electroconvection, associated to the generation of a non-uniform electric field with tangential components. Also geometrical heterogeneities of the membrane surface affect current-voltage curve features such as the i_{lim} value, the plateau length and the amount of overlimiting transport through electroconvection. Profiled membranes may enhance the mass transfer rate by the increase in the membrane active area, the promotion of fluid mixing and the increase of electroconvective mixing due to larger tangential components of driving force [217]. More recent studies [173, 217–219] have

proven that also other membrane properties, such as roughness, degree of hydrophobicity and surface charge density, affect the current-voltage curve characteristics.

Figure 8 (a) shows experimental current-voltage curves of a six-compartment stack with and without the central membrane. By subtracting these results, the current-voltage curve of the central membrane can be obtained [178]. The limiting current density is often identified as the point where the slope change occurs in the corresponding *Cowan plot* [169, 178, 191, 209, 220–226] reporting the apparent resistance as a function of the reciprocal of current density (or, simply, of electrical current) as shown in

Figure 8 (b). Measurements of i_{lim} have been carried out in several works in order to assess the effect of spacers or profiled membranes on mass transfer. Values of i_{lim} are reported as functions of the fluid velocity [39, 177, 209, 221, 222, 226, 227] and fitted by power laws. Other works report *Sh* values determined from i_{lim} measurements according to eq. (13) [50, 178, 195, 200, 224, 228–232] and correlations as power laws (see Section 4.4.4).

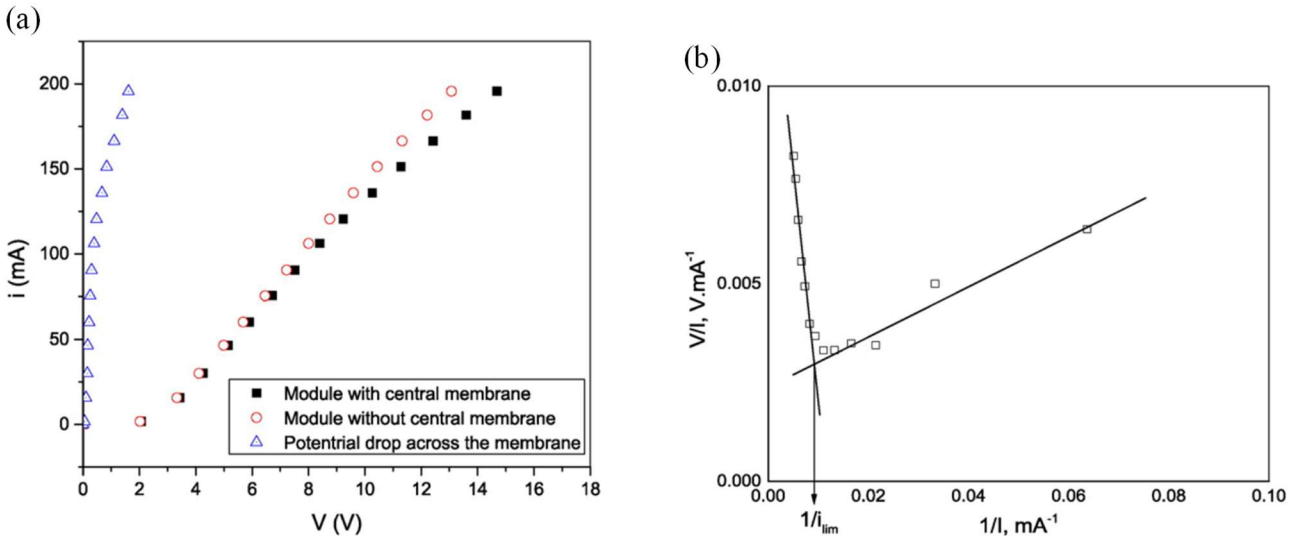

Figure 8. (a) Experimental current-voltage curve and (b) apparent resistance over the membrane as a function of the reciprocal of electrical current (*Cowan plot*) for the estimation of i_{lim} [178].

Sh values have also been obtained by measurements of i_{lim} on electrodes of simple electrochemical cells without membranes [200, 229–232]. However, these devices simulate only an ideal mass transfer of an IEM-based system, as membrane properties govern the mass transfer mechanisms. In fact, as claimed by Rubinstein and Maletzki [207], membranes with the same permselectivity may exhibit a markedly different behaviour even in the underlimiting region, significantly affecting polarisation phenomena.

Finally, when overlimiting conditions occur, mass transfer characteristics can be assessed by the approach proposed by Nikonenko *et al.* [192] and Larchet *et al*. [50] based on the experimental procedure described in [233].

4.2.3 A critical outlook of ED operations under limiting and overlimiting current conditions

In common ED operations, i_{lim} has been assumed as a practical upper threshold for optimal operation [49, 195, 217, 234, 235]. In fact, despite the advantages of enhancing the current thus reducing membrane area requirements, a number of detrimental effects may be encountered in limiting current conditions, such as fouling, scaling and membrane deterioration due to extreme pH values [169, 170, 191, 235, 236].

On the other hand, all complex phenomena occurring in the limiting and overlimiting regions have been misunderstood for long periods in the past and a debate has been on-going in the last 10-20 years on how these can actually affect the operation of an ED stack.

Recent publications outline a clear and complete picture of the multifaceted nature and of the complexity characterizing such phenomena [138, 173, 210, 217]. The existence of the overlimiting region was originally attributed to water splitting, i.e. the generation of H^+ and OH^- ions that contribute as charge carriers [169, 170]. Water splitting has also a secondary effect consisting in the disturbance of the electric field that exalt the transport of salt ions (Kharkats effect of current exaltation [237]). Later, water splitting was found to be promoted by the catalytic activity of some functional groups on the membrane surface in contact with the solution, giving rise to reversible protonation and deprotonation reactions. For example, the splitting reaction occurs intensely in the case of AEMs containing secondary and tertiary amino groups on the surface [238, 239] or CEMs with surface phosphoric acid groups, while it is significantly suppressed in AEMs modified by surface treatment with a strong electrolyte that converts the tertiary and secondary amino groups into quaternary ones [173]. A strong reduction of water splitting was also obtained by AEMs containing crown ethers [240], thus suggesting the possibility to achieve significant effects in fouling prevention.

Interestingly, the transport mechanism of charges (i.e., the electrical current) in overlimiting conditions was recently proven to be actually related to the transfer of salt counter-ions by coupled current-induced convection, with water splitting having only a minor effect in generating current. Two types of coupled convection were identified: gravitational convection and electroconvection. Gravitational convection [207, 215, 237, 241, 242] arises from a non-uniform distribution of solution density due to concentration or temperature gradients. Electroconvection [175, 176, 188, 206, 207,

211, 212, 241–246] is related to the formation of an extended region (much thicker than typical EDLs) adjacent to the membrane surface, where electroneutrality is no more maintained, and to an inhomogeneous electric field affected by membrane features (geometrical and conductive heterogeneities, roughness, hydrophobicity, surface charge [173, 217–219]). The interactions generated within this charged region lead to volume forces triggering convective motions in the form of dynamic vortices in the near-wall layer, thus allowing overlimiting currents.

Therefore, when the risk of scaling is low due to the lack of poorly soluble salts, operating at high current densities, close to the limiting one, may be an option in order to improve the process efficiency [235]. Furthermore, overlimiting regimes have been tested at laboratory scale, showing enhanced mass transfer [50], thus paving the way to alternative operational regime possibilities for efficient ED systems. This is favoured by the possibility of improving the performance of IEMs simply by surface modifications [173], in order to reduce water splitting and promote mass transfer, which has attracted an increasing interest to the application of overlimiting regimes in recent years.

4.3 Influence of polarization phenomena on the voltage drop

The limiting current density is only one of the aspects related to concentration polarization phenomena. However, several other effects caused by concentration polarisation have to be characterised, as they can significantly affect the total stack voltage drop. The total potential drop between two bathing solutions (left, *L*, and right, *R*) facing an interposed IEM can be analysed following the *segmentation modelling* approach by TMS (see Section 3.1) [64, 202, 247] in a multi-layer system taking into account the presence of the DBLs, as in Figure 9.

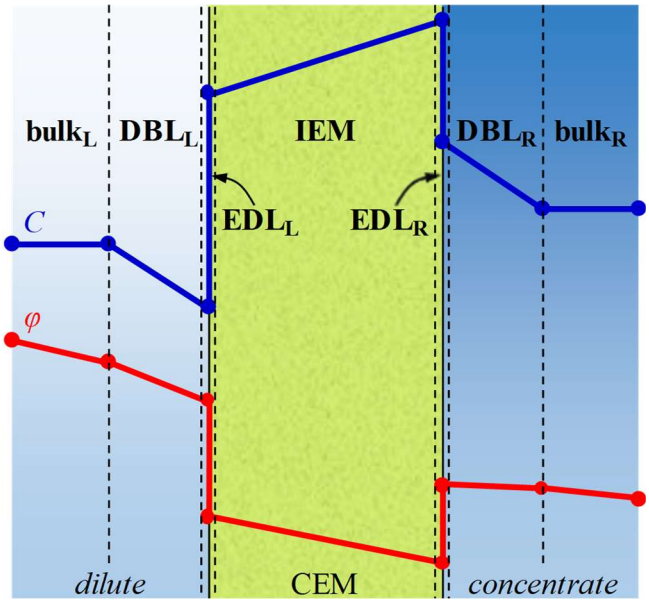

Figure 9. Segmentation of the system composed by a membrane and two bathing solutions, according to the TMS theory, showing concentration of counter-ions and electric potential changes in each layer. The example in the picture shows a CEM immersed between a dilute solution and a concentrate solution.

Some aspects related to the total voltage drop were treated in the first experimental and theoretical studies by Cooke [168] and Sonin and Probstein [236]. The topic was then treated more extensively by some authors in the early 1970s [169, 170] and many further studies have since been performed [174, 199, 202, 205, 247–254]. However, by pursuing the aim of a general discussion based on these works, the total voltage drop including all the possible contributions can be expressed as

$$\Delta V = \eta_{Ohm}^{bulk_L} + \eta_{Ohm}^{DBL_L} + \eta_{diff}^{DBL_L} + \Delta\varphi^{iem} + \eta_{Ohm}^{iem} + \eta_{diff}^{DBL_R} + \eta_{Ohm}^{DBL_R} + \eta_{Ohm}^{bulk_R} \quad (15)$$

where the different terms represent: Ohmic voltage drop within the left solution bulk, Ohmic voltage drop within the left DBL, (non-Ohmic) diffusion potential within the left DBL, (non-Ohmic) membrane potential, Ohmic voltage drop within the membrane, (non-Ohmic) diffusion potential within the right DBL, Ohmic voltage drop within the right DBL, Ohmic voltage drop within the right solution bulk.

In the case of a binary monovalent electrolyte, the membrane potential (eqs. (3)-(5)) acting as a back electromotive force [199, 255–258] can be expressed as:

$$\Delta\varphi^{iem} = \alpha_{iem}\frac{RT}{F} ln\left(\frac{C_C^{iem}\gamma_C^{iem}}{C_D^{iem}\gamma_D^{iem}}\right) \quad (16)$$

where C_{SOL}^{iem} and γ_{SOL}^{iem} represent the electrolyte concentration and the electrolyte activity coefficient at the IEM-solution interface (solution side) and the subscripts *C* and *D* refer to the concentrate and the dilute channel, respectively. It is useful to resort to polarization coefficients [6, 193], whose values range from 0 (maximum polarization) to 1 (no polarization), defined as:

$$\theta_D^{iem} = C_D^{iem}/C_D^{bulk} \tag{17}$$

$$\theta_C^{iem} = C_C^{bulk}/C_C^{iem} \tag{18}$$

where C_{SOL}^{bulk} is the electrolyte concentration at the solution (dilute or concentrate) bulk. In a cell pair, there are four polarization coefficients, one for each IEM-solution interface. Values of θ_{SOL}^{iem} can be derived from eq. (14), though a more rigorous approach relates them to eq. (11). The membrane potential can then be split into two terms, one accounting for the potential of a membrane ideally in contact with the bulk solutions ($\Delta\tilde{\varphi}^{iem}$), and the other accounting for the concentration overpotential due to polarization in the DBLs (η_{COP}^{iem}) [168, 179, 190, 202]:

$$\Delta\varphi^{iem} = \Delta\tilde{\varphi}^{iem} + \eta_{COP}^{iem} = \alpha_{iem}\frac{RT}{F}\left[ln\left(\frac{C_C^{bulk}\gamma_C^{bulk}}{C_D^{bulk}\gamma_D^{bulk}}\right) - ln\left(\theta_C^{iem}\theta_D^{iem}\xi_C^{iem}\xi_D^{iem}\right)\right] \tag{19}$$

where $\xi_D^{iem} = \gamma_D^{iem}/\gamma_D^{bulk}$ and $\xi_D^{iem} = \gamma_C^{bulk}/\gamma_C^{iem}$ (often assumed equal to 1).

Interestingly, focusing on hydrodynamics-related features, the DBLs contribute to the total potential drop by means of both Ohmic and non-Ohmic phenomena, which can easily be calculated assuming a linear concentration profile. η_{Ohm}^{DBL} can be computed by Ohm's law integrating the resistivity over δ and multiplying by the current density (1-dimensional approach, where i = cost). η_{diff}^{DBL}, also called concentration potential or junction potential, is strictly non-Ohmic and originates from the difference in the ionic diffusion coefficients and the need to maintain the local electroneutrality [62]. Note that η_{Ohm}^{DBL} has a dissipative nature, i.e. it is caused by the irreversible process involving Joule's effect [62]; conversely, non-Ohmic phenomena are (at least ideally) reversible and, ultimately, convert the electrical energy into the chemical energy of a salinity gradient. However, under the hypothesis of a linear variation of concentration within the DBL and of an equivalent conductivity (λ) independent of concentration, η_{diff}^{DBL} and η_{Ohm}^{DBL} can be expressed as [169, 170, 199]:

$$\eta_{diff}^{DBL} = \mp(t_- - t_+)\frac{RT}{F}ln\left(\theta_{SOL}^{iem}\right) \tag{20}$$

$$\eta_{Ohm}^{DBL} = -\frac{FD}{\left(t_i^{iem} - t_i\right)\lambda}ln\left(\theta_{SOL}^{iem}\right) \tag{21}$$

where t_- and t_+ are the transport numbers of anions and cations, respectively. In eq. (20) the sign – is valid when the concentration gradient is negative, as in Figure 9 (thus η_{diff}^{DBL} is positive, i.e. there is a potential drop), while the sign + is valid when the concentration gradient is positive (thus η_{diff}^{DBL} is negative, i.e. there is a potential increase).

In very recent years, researchers have shown a wide interest on transport phenomena and DBL effects in IEMs-based systems. The resistance associated with the boundary layer has been measured by

chronopotentiometry [3, 4, 139, 203, 259, 260] and EIS [140, 204, 205, 261–263]. Finally, Abu-Rjal *et al*. [264] have investigated the influence of the DBL on the membrane permselectivity, finding that concentration polarization may significantly affect counter-ions transport through the membrane, due to variation of the interface concentration and concentration profile across the membrane as the electric current changes.

4.4 Channels, mixing promotion and pressure drop

Most electromembrane processes are based on the use of plate-and-frame geometries, in which channels are constituted by two membranes (being the channel walls) and an internal spacer keeping the interspace between them and also acting as a mixing promoter. The selection of proper spacer geometry and material can thus play a fundamental role in process design and optimisation. For this reason, hydrodynamics and mass transport phenomena in channels of membrane modules have been extensively characterized, both by experiments and by simulations [196, 198, 229, 230, 265–267]. Much research effort has been addressed to these phenomena also in the very recent years [6, 268–276], thus demonstrating how this is still an open field leaving room for new developments. In the specific case of ED, several works are available in the literature which will be critically reviewed in the following sections, highlighting how researchers have approached the problem with particular focus on recent developments. Also findings on spacer-filled channels related to other membrane processes (e.g. reverse osmosis, membrane distillation, reverse electrodialysis [Section 6.6]) can provide useful information for ED applications.

Two main geometric patterns have been devised for ED channels [10]: the sheet flow and the tortuous path. In the former configuration (Figure 3), the feed channels have a rectangular (or similar) shape and the solution flows roughly straight [10, 39–41]. In the latter configuration (Figure 10), the feed channels have a narrow serpentine shape with several baffles and 180° bends [10, 45]. ED stacks in the sheet flow arrangement make use of net spacers (Figure 11), while the most commercialised tortuous flow path spacers are manufactured by gluing two sheets of polyethylene provided with straps forming an under/over flow path [45, 170] (Figure 10 (a) and (b)), but in principle they can be manufactured also with conventional net spacers or profiled membranes. Finally, flow paths with intermediate features between the sheet flow and the tortuous path have been developed, e.g. the U-shaped channels [45] (Figure 10 (c)).

Parallel-, counter-, and cross-flow arrangements are possible in ED stacks. In principle, counter-flow is preferable since it does not suffer from the strong axial increase of concentration difference typical

of parallel flow, but it causes larger pressure differences between the concentrate and dilute compartments, which may result in internal leakages and excessive membrane deformation. The cross-flow arrangement has been recently proposed, performing similarly to counter-flow [277] and allowing more efficient flow distribution strategies, which can reduce pressure losses. The parallel-flow configuration, however, remains the most common in all industrial ED applications [10].

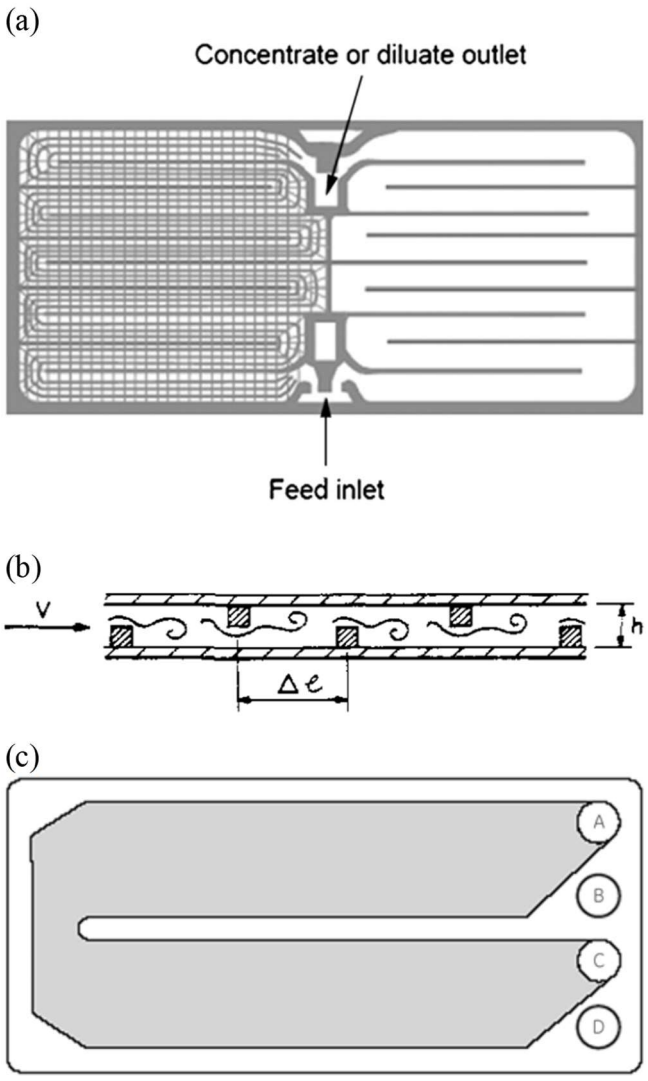

Figure 10. (a) Tortuous path spacer [10], (b) longitudinal section of a tract of tortuous path channel (longitudinal straps are not represented) [234], (c) U-shaped path [45].

4.4.1 Channels filled with non-conductive spacers

From early studies on ED applications, it is well known that different spacers exhibit different performance in mass transfer and pressure drop, thus exerting a large influence on the process efficiency and raising the issue of channel optimization [39, 44, 48, 195, 221, 228, 278, 279].

Common spacers are made by two arrays of polymeric wires either extruded (overlapped) or woven, with circular cross section, though other geometries have also been devised [39, 41, 48, 222]. Spacers are typically fabricated by non-conductive polymeric materials and can have a variety of geometries according to the filament shape/arrangement, the angle between crossing filaments, the number of layers, the filament spacing and the filament size (Figure 11).

Net spacers used in sheet flow electrodialyzers can be classified into four main categories: overlapped, woven, twisted and multi-layer. The first two types are the most common [49]. In particular, woven nets have been used in sheet flow configurations since early studies on ED systems [39, 280] and have even been recently investigated by Kim *et al*. [252, 253] through laboratory-scale ED experiments. Some interesting results comparing the performance of electrodialyzers equipped with different woven meshes (90° angled filaments) are reported in [41]. Mass transfer was enhanced by a lower distance between filaments and with a flow attack angle of 45°; this features are then reflected on the cell pair resistance. Pressure drops were higher when the distance between filaments was lower and the flow was aligned to a filament. These findings are in good agreement with results of simulations performed in several other works [6, 193, 281].

Twisted and multi-layer spacers were tested by Balster *et al*. [222] (see e.g. Figure 11 (g) and (h)), showing the possibility to improve mass transfer by swirling motions, both at any given *Re* and at any given *Pn* (power number, a dimensionless number accounting for the pumping power), with respect to a non-woven spacer. The same research group investigated also the use of air sparging [223], finding that a mass transfer enhancement may be obtained with some spacer configurations, but at the cost of increasing the resistance. Tadimeti and Chattopadhyay [178] tested a larger variety of twisted tape spacers, showing the significant effect of some geometrical features on mass transfer and pressure drop. Better performance than in an empty (spacerless) channel were obtained in some of the tested configurations, thanks to the development of longitudinal and transverse vortices. Nevertheless, some other configurations led to worse performance than in an empty channel, in which mass transfer coefficients increased as the Reynolds number increased, probably due to the small channel length (8 cm) characterized by large entrance effects (see Section 4.4.4). Moreover, several non-conventional (commercial and non-commercial) spacer geometries for applications in various membrane processes have been investigated both by experiments and simulations [230, 269–272, 274, 282, 283] (Figure 11 (i)-(n)).

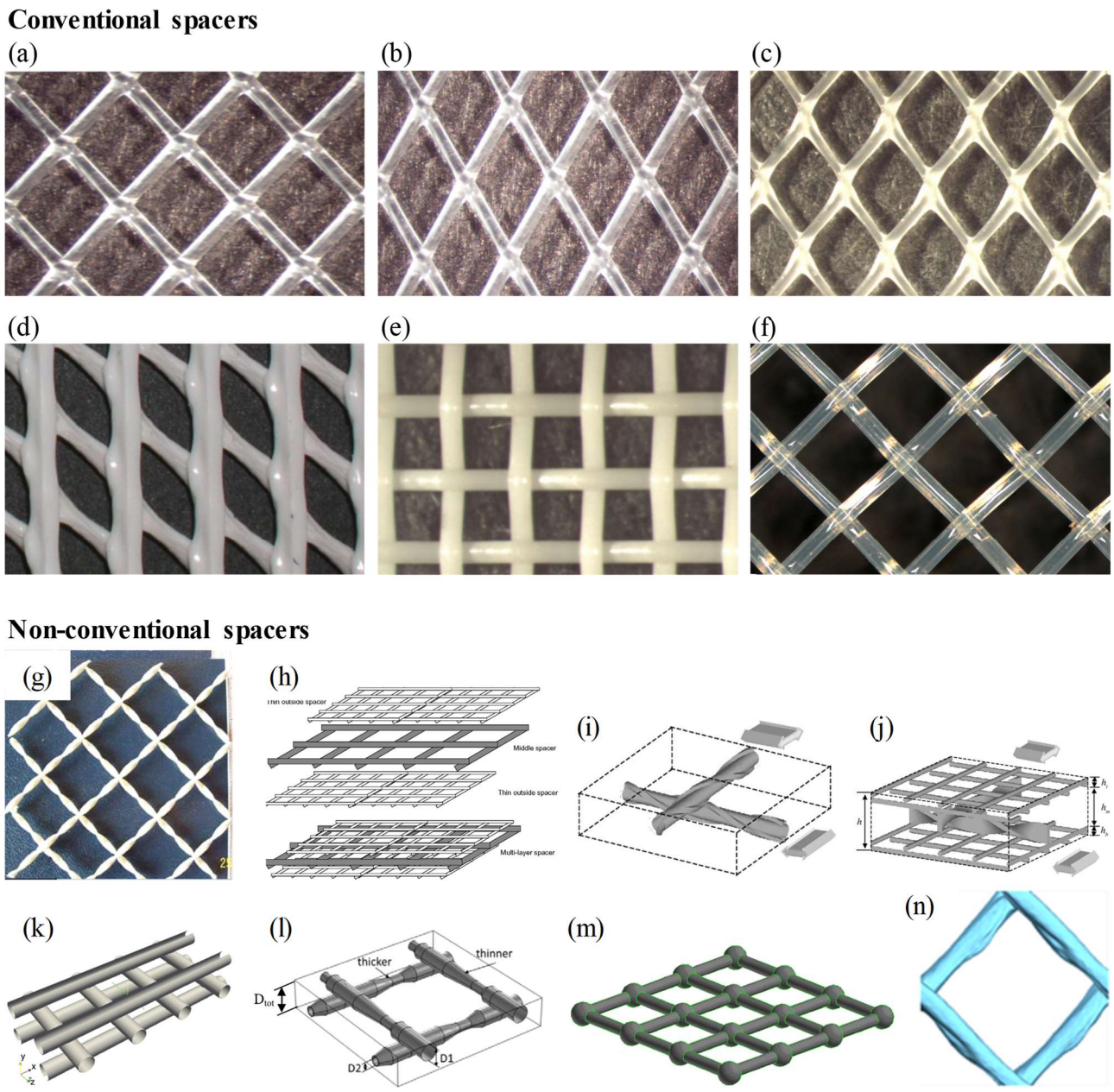

Figure 11. Different kinds of conventional [284] and non-conventional net spacer: (a) extruded with overlapped crossing filaments at 90°, (b) extruded with overlapped crossing filaments at 60/120°, (c) extruded with crossing filaments at 60/120° with irregular shape, (d) extruded with crossing filaments at 60/120°with very irregular shape, (e) with woven crossing filaments at 90°, (f) with woven crossing filaments at 90°, but coarser than (e), (g) twisted spacer [222], (h) multi-layer spacer [222], (i) spacer with modified filaments [230], (j) multi-layer spacer with twisted tapes [230], (k) triple-layer overlapped spacer [269], (l) overlapped spacer with filaments characterized by different regions [270], (m) floating one-layer net with spherical nodes spacers [271], (n) irregular overlapped spacer obtained by X-ray computed tomography of a commercial spacer [274].

Floating spacers [195] have been also devised. The main feature of the floating spacers is the ability to avoid contact areas between spacer and membrane surface, thus minimizing regions of stagnant flow. Floating spacers can be used in asymmetric stacks with different channel thickness of the diluate and of the concentrate channel caused by a stationary differential pressure over the membrane. Conversely, if dimensional stability is required, a suitable control of the pressure gradient along the

channels avoiding differential pressures is needed (this is more important in large stacks). Submerged cylinders perpendicular to the flow have been tested at lab scale and simulated in two dimensions [189, 195, 234]. Interestingly, if cations and anions have different diffusivities in solution, as in the case of NaCl ($D_{Cl^-} > D_{Na^+}$), floating promoters of mixing optimize mass transfer when placed slightly closer to the AEM than to the CEM, due to the obtained asymmetric distribution of fluid velocity inside the channel [189]. Dimensional stability can be maintained also by the novel design proposed by Koutsou *et al*. [271] (Figure 11 (m)), where the partially floating spacer comprises spherical nodes in contact with the membranes and symmetrically connected with a mesh of smaller cylindrical filaments.

4.4.2 Conductive spacers and profiled membranes

The most significant disadvantage of net polymeric spacers is that they are commonly made by non-conductive materials, thus increasing the compartment's electrical resistance; instead, the use of conductive materials spacers may be a good option for lowering the energy consumption, thus improving the efficiency of ED units. In the mid-1970s, Kedem [46, 47] prepared spacers made by ion exchange material. The multiple benefits deriving from the use of conductive spacers were evident: mass transfer enhancement (reduction of polarization and increase of i_{lim}) due to the increase of the active area, reduction of Ohmic (shadow effect) and non-Ohmic resistances, high current efficiency at high current density, stable pH (reduction of water splitting), higher effectiveness at low concentrations of diluate and achievement of very low concentrations. After more than 20 years, commercial spacers were modified into conductive spacers by chemical reaction [285] or coating [286], confirming the previous results. In addition, it was pointed out that (i) the consequences (water splitting, scaling and fouling) of uneven distributions of feed solutions among and within the channels were significantly mitigated by the lower resistance provided by conducting spacers [285]; (ii) a larger effectiveness was achieved in electrodialyzers provided with heterogeneous IEMs which are, by their nature, more polarizing, and with conductive spacers with higher ion exchange capacity [286]. The effectiveness of chemically modified spacers was also proven by a subsequent work [144]. Conductive spacers can be useful also for special applications, e.g. for the selective separation of nitrates from drinking water [287] by using a cation conductive woven spacer with granules of nitrate-selective anion exchange resin and a modified AEM. Local effects of a conducting spacer were analysed by Shaposhnik *et al*. [185] by experiments (laser interferometry) and simulations. Fragments of ion exchange material were cut and pasted on the membranes (with glue only on the non-working surface of membrane). The membrane/channel configuration obtained in this way is very similar to what can be obtained by profiling the membranes.

Notwithstanding the advantages pointed out, conductive spacers have never been implemented in real industrial ED units, likely because of higher production costs, lower robustness and larger complexity.

More recently, profiled membranes (Figure 12) have been proposed as a cheaper and more effective alternative to conductive spacers. In this case, the membrane surface (on either one or both sides) is provided with reliefs, pillars, or ridges that play the role of "spacers" [10, 50]. The use of profiled membranes leads to a simplification in stack assembly (the use of spacers is avoided), along with some advantages typical of conductive spacers, such as the reduction of Ohmic resistance and the possibility to increase the active area. The actual mass transfer rate will then depend also on the effects on the fluid mixing due to the specific geometry, which can be quite similar to that of overlapped-filaments spacers or much simpler (as in the case of one-side ridges, waves or pillar profiles, see Figure 12 (e), (f) and (g)). Similarly, pressure drops are strongly affected by the profiles geometry. Moreover, cost savings on stack components [288] and lower fouling issues [289] may be achieved.

Strathmann [10] reported data of ED stacks built with profiled membranes with trapezoidal cross section profiles as shown in Figure 12 (b), (c) and (d). The increase of membrane surface due to the profiles was between 40 and 45%. The abatement of resistance, especially at low salt concentrations, and a significant increase of the limiting current density, led to enhanced performance in salt removal as the voltage varied, with larger improvements when the inlet concentration was lower. Balster *et al*. [290] prepared and characterized a novel membrane design, referred as "membrane with integrated spacer", where the profiles were obtained by capillary forces of a drying polymer solution in contact with a net spacer (which is then removed). This membrane showed better performance than the corresponding flat membrane and the authors suggested also the application either in spacerless systems or in multi-layer systems [222] including a middle spacer. Another particular geometry of profiled membrane was obtained by hot pressing a membrane sandwiched between two fabrics [291].

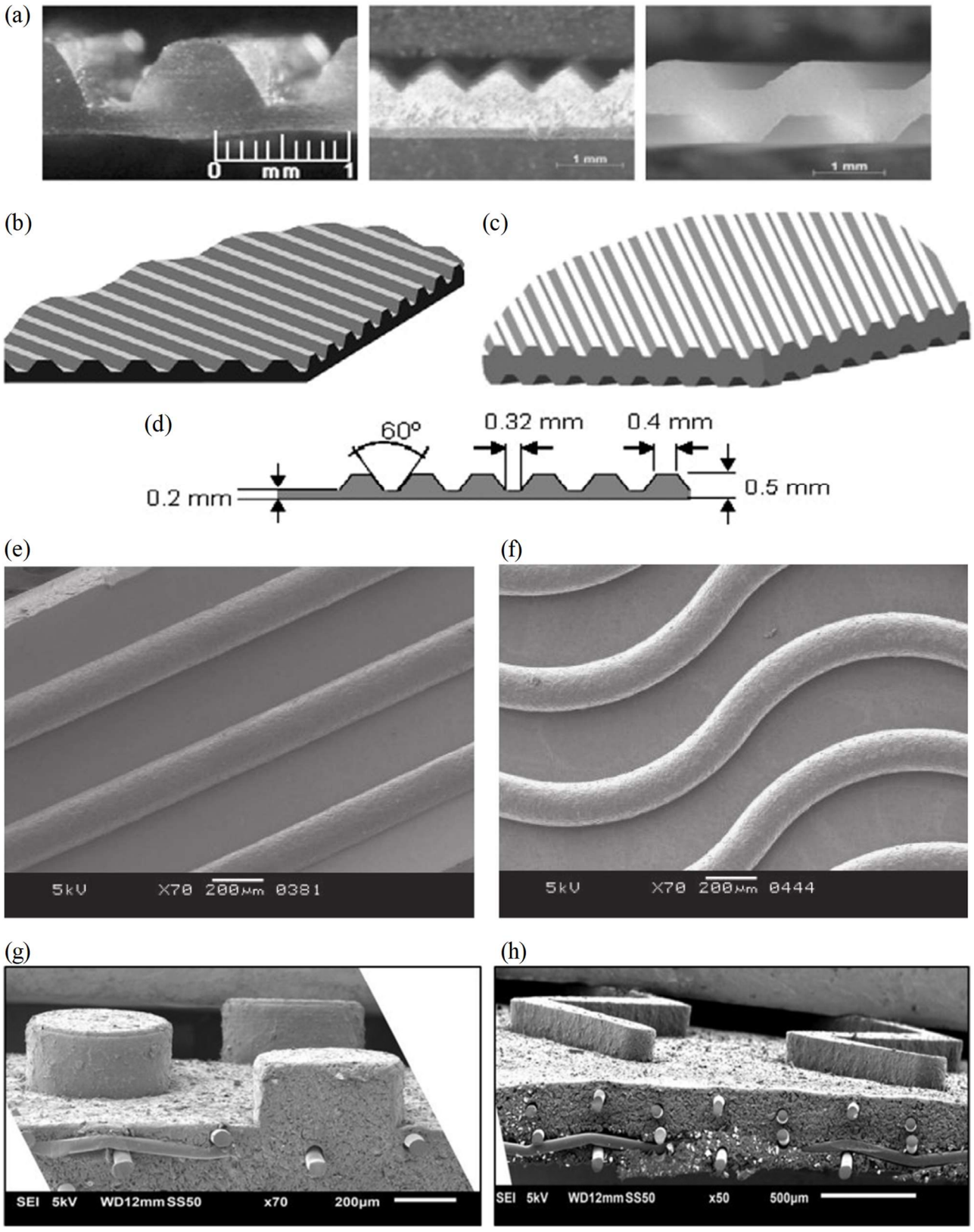

Figure 12. Profiled membranes. (a) Photos of membranes with different surface profiles on one or both sides of the membrane; (b) and (c) schematic drawings of membranes with profiles on one or both sides; (d) sketch example of a membrane profile sizes. (a)-(d) are taken from [10]. (e) Ridges and (f) waves profiled membranes by [259]. (g) Pillars and (h) chevrons profiled membranes by [292].

Other geometries can be obtained by corrugating IEMs. Mass transfer in an electrochemical cell with corrugated electrodes (mimicking membranes) was analysed by measurements of i_{lim} [293, 294], obtaining correlations for the Sherwood number. The use of actual corrugated membranes in ED was tested for the extraction of nickel and cobalt from their sulphate solutions [295], showing a significant increment of active area (60%) and a significant improvement of the current efficiency with respect to the use of flat membranes.

The possibility of improving mass transfer by profiled membranes is reported also by Nikonenko *et al*. [192], who carried out measurements in overlimiting conditions. Also Larchet *et al*. [50] tested profiled membranes in overlimiting regimes, obtaining higher Sherwood numbers with respect to flat membranes and non-conducting spacers, along with high desalination rates in a large range of concentrations.

In the last years, many research efforts have been devoted to the development and characterization of profiled membranes for reverse electrodialysis (see Section 6.6). In comparison with net spacers between flat membranes, simple profiled membranes created by either ridges or pillar profiles reduce pressure drop and Ohmic resistance, but, at least at the very low *Re* numbers typical of RED, are less effective in mass transfer [4, 259–261, 296]. Improved profile geometries, more similar to spacer filaments, lead to better trade-off between low pressure drops and good mixing, thus improving the stack performance [6, 292, 297]. Multi-physical modelling tools have been developed in order to investigate the potentials of profiled membranes by simulating simplified two-dimensional geometries for ED [187] and reverse electrodialysis [298] applications.

Nowadays, profiled membranes represent a very attracting frontier for the development of ED systems and deserve further studies especially for process optimization perspectives.

4.4.3 Flow regimes in ED channels

ED systems have been usually operated at a fluid velocity of ~2 to ~10 cm/s [10, 41, 46, 47, 49, 50], with higher values, even up to ~50 cm/s, in tortuous path configurations [10, 44, 45, 49]. Taking into account the typical channel thicknesses, the corresponding Reynolds number (calculated here by assuming as the equivalent diameter twice the channel thickness) ranges roughly from ~20 to ~400, with values up to ~2000 for tortuous paths (see also the Reynolds numbers reported in [39, 138, 185, 195, 199, 279]). In fact, tortuous path configurations are characterized by higher concentration polarization and lower pressure drop per unit length with respect to sheet flow channels with net

spacers, so that higher fluid velocities are adopted in tortuous paths in order to maintain polarization phenomena under control [10, 45, 49].

The flow regime within spacer-filled channels is steady for *Re* values roughly up to 200-300, then changes gradually (possibly through periodic flow) towards turbulent conditions, starting at $Re \approx 1000$ [39, 195, 279, 281, 299, 300]. Therefore, we can assert that the flow regime in ED units is typically steady or with incipient unsteadiness in many cases, and it reaches turbulent conditions only in some rare cases [194].

4.4.4 Correlations for mass transfer coefficients

The characterisation of mass transfer phenomena in spacer-filled channels has been often performed by means of correlations linking the *Sherwood number* to the main geometrical and operating parameters [48, 178, 195, 199, 224, 234, 278–280, 301]. The use of dimensionless numbers offers the advantages of an easy scalability of results and easy implementation/processing of results (input/output) in modelling tools [6, 174, 193]. However, also correlations for i_{lim} have been often reported [39, 177, 178, 209, 221, 226–228]. In most cases data are fitted by power laws, such as

$$Sh = aRe^{b}Sc^{c} \tag{22}$$

$$i_{lim} = dC_i^{bulk^{e}}u^{b} \tag{23}$$

Note that the exponent of *Re* in eq. (22) corresponds to the exponent of *u* in eq. (23). In some cases, *b* was found to be close to 0.5 [48, 177, 199, 209, 224, 226, 228, 234, 279], while in other cases *b* ranged from ~0.13 to ~1 [178, 195, 221, 278, 280, 301]; however, much more complex trends in a larger range of *Re* values have also been reported [39, 195], and modified correlations have been proposed [227]. It is worth highlighting that power laws and relevant coefficients' values may be suitable only in a narrow range of Reynolds numbers [6, 281], while ED stacks can operate in a relatively large *Re* range involving different flow regimes. A log-log chart of *Sh* vs. *Re* exhibits a horizontal asymptote at very low *Re* (creeping flow), where mass transfer in spacer-filled channels may be worse than in the empty channel, as shown in Figure 13 (a). Then, one or more inflections at higher *Re* follow, up to an oblique asymptote (power law) in the turbulent regime, as shown in Figure 13 (b).

The effect of the fluid properties, represented by the Schmidt number (*Sc*), was evaluated in [48, 279] and the exponent *c* in eq. (22) was found to be 1/3. This value has often been considered valid, but, in general, the effect of *Sc* can be different as *Re* and/or the spacer geometry vary [6, 197, 200, 271].

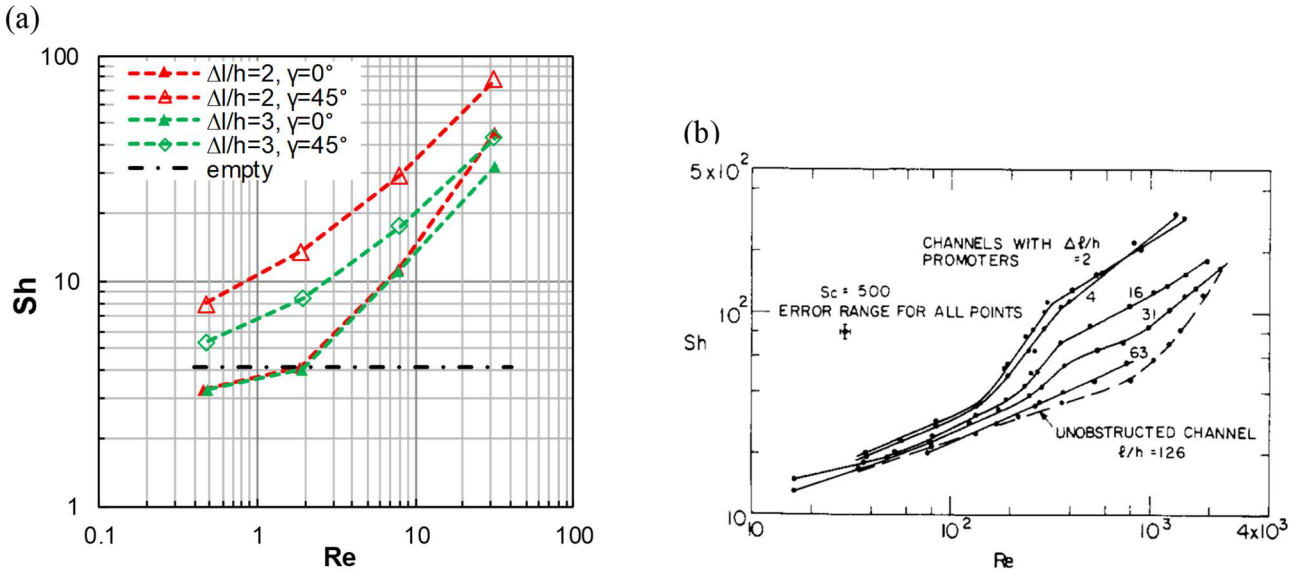

Figure 13. Sherwood number in spacer-filled channels. (a) Lower Reynolds numbers: results from CFD simulations of fully developed flow within woven spacers with different pitch-to-height ratios ($\Delta l/h$) and flow attack angles (γ) (adapted from [281]). (b) Higher Reynolds numbers: experimental data (measurements of i_{lim}) concerning floating eddy promoters with different pitch-to-height ratios ($\Delta l/h$) [195]. Note that the equivalent diameter to calculate *Re* and *Sh* is equal to the channel thickness h, according to the definitions in [195].

Note that, in the literature, plane (spacerless) channels have often been considered as an acceptable idealization/simplification of the channel geometry in models [195, 234, 236, 302–304] or as a reference case for comparison purposes both in models and in lab scale experiments [6, 50, 139, 178, 223, 281]. However, the actual use of plane channels in stacks at industrial scale is not allowed due to dimensional stability issues.

Attention should be given also to the entry effects on mass transfer phenomena. The flow field within the entire channel can be assumed fully developed, as the Reynolds number is usually sufficiently small. Nevertheless, due to the high Schmidt number (~600 for NaCl solutions at concentration below 0.5 M), the concentration field develops in a longer entrance region [184, 189, 236, 302] in which the local Sherwood number decreases towards its fully developed value. The topic of entry effects in heat and mass transfer is known as the "Graetz-Lévêque problem" [305, 306]. In the case of relatively short plane channels (length $L < 0.02uh^2/D$, being h the channel thickness), the correlation of the average Sherwood number in laminar conditions, as reported by several authors [139, 203, 216, 229, 231], is

$$Sh = 1.47\left(Re\,Sc\,\frac{h}{L}\right)^{\frac{1}{3}} \tag{24}$$

Further theoretical predictions along with experimental data have been also reported [48, 195, 307, 308]. Experimental data concerning spacer-filled channels show some entrance effects at very low

Re [231], but, contrary to what happens within plane channels, smaller entrance effects at higher *Re* [189, 229, 231, 309]. This behaviour can be explained by the convective motions perpendicular to the active walls (membranes) induced by the obstacles, which, in flow conditions intermediate between full turbulence and creeping, accelerate the development of the concentration field.

4.4.5 Correlations for pressure drop and influence of pumping power on energy consumptions

Data on pressure drops in ED systems can be found in several references [39, 177, 178, 195, 221, 228, 234, 279]. The energy consumption for feed solutions pumping is strongly dependent on pressure drops, which can be simply characterized by the correlation between the friction factor (*f*) and the Reynolds number, often reported in the literature as a power law:

$$f=ARe^{-B} \tag{25}$$

Actually, the exponent *B* tends to 1 at very low *Re* (Figure 14 (a)), but decreases as *Re* increases (Figure 14 (b)) due to higher inertial effects [281]. Therefore, we stress that correlations as those in eq. (25) are more suitable for fitting narrow *Re* ranges, similarly to the case of *Sh*. For larger ranges or ranges starting from low *Re* values, the trend of the friction coefficient normalized by that of the spacerless plane channel as a function of *Re* may be fitted by polynomial laws [6].

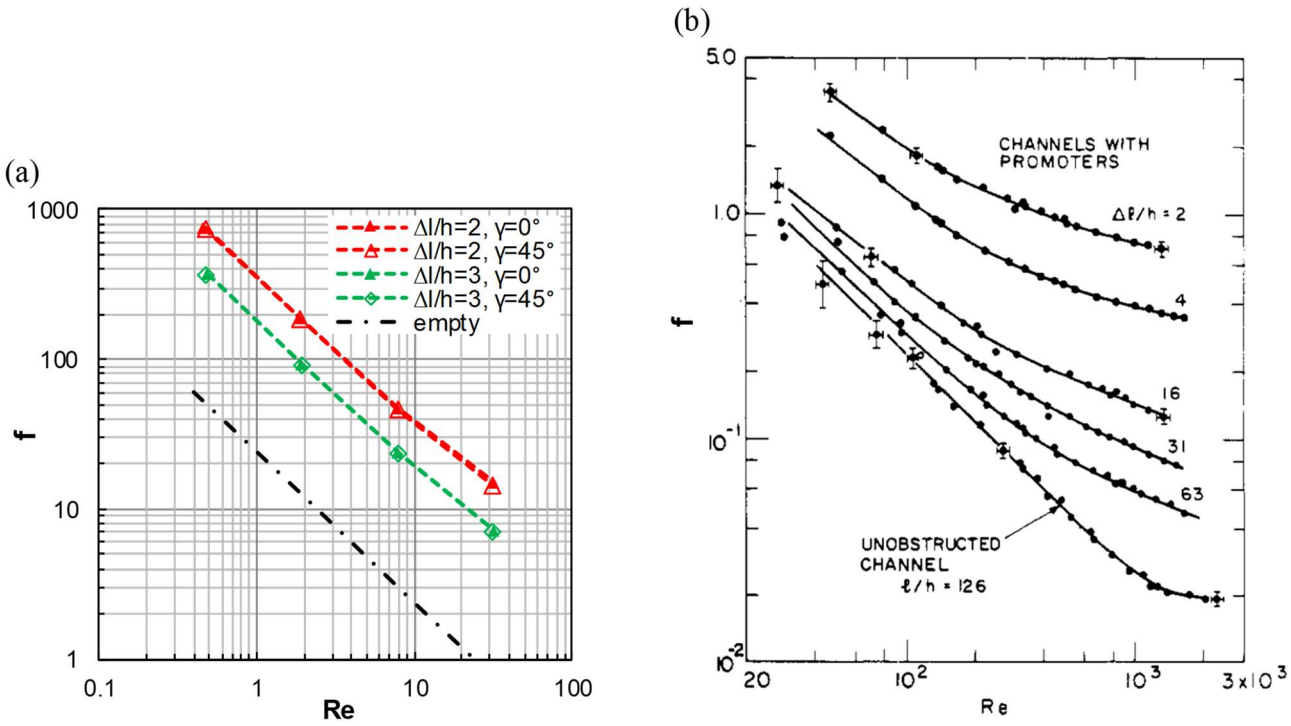

Figure 14. Darcy friction factor in spacer-filled channels. (a) Lower Reynolds numbers: results from CFD simulations of fully developed flow within woven spacers with different pitch-to-height ratios ($\Delta l/h$) and flow attack angles (γ) (adapted from [281]). Higher Reynolds numbers: experimental data concerning floating eddy promoters with different pitch-to-height ratios ($\Delta l/h$) [195]. Note that the equivalent diameter to calculate *Re* and *f* is equal to the channel thickness *h*, according to the definitions in [195].

In order to give an idea of the role played by pressure drop in determining the energetic consumption of ED systems, we report some data in the following. The influence of pumping power varies widely on the basis of the stack design and of the operating conditions [39, 226, 288, 310]. It may be relatively low in ED devices with short path lengths [226] (and even negligible in microfluidic devices for lab tests [189]), so that it has even been neglected in some cost effectiveness assessments [174]; however, it may be significant or even dominant in longer modules. Chiapello and Bernard [41] recorded pumping energy consumptions of ~23% and ~16% of the total energy in two sheet flow modules 46 cm long, while von Gottberg [45] reported values of ~24% and ~39% for a stack with U-shaped channels (with net spacers) and for a tortuous flow path stack, respectively, both at industrial scale.

4.4.6 ED stacks operated under oscillating conditions

A number of recent papers have highlighted how transport phenomena and, more in general, process efficiency can be enhanced by operating ED units in non-stationary conditions. Oscillations applied by dynamically changing either the flow rate [225, 232, 262, 311] or the electrical field [153, 154, 165–167, 173, 191, 312, 313] can achieve an intensification of ED systems performance. Pulsed flows or pulsed electric fields at relatively high frequencies (thus, with a time constant much smaller than the large characteristic time scales for diffusion typical of high Schmidt numbers systems) caused the DBL to be disrupted and the concentration profile to flatten, with transient concentration fields different from a sequence of steady states. Consequently, concentration polarization and its effects can be significantly reduced (i.e. higher limiting currents and lower resistances are achieved). Benefits coming from oscillations depend on frequency, amplitude and shape of oscillation. The correlations for the time-averaged Sherwood number will include also the Strouhal number, a dimensionless number taking into account the oscillating features of the system [225].

In a recent paper, Rodrigues *et al*. [232] measured limiting current densities with a 8-electrode cell fed by a pulsatile flow generated with solenoid valves with frequencies between 1 and 50 Hz. In the case of an empty (spacerless) channel, the pulsatile flow enhanced mass transfer at frequencies of 50 Hz, with effects that increased towards the channel outlet. When a spacer was inserted within the cell, mass transfer exhibited an increase up to 50% with respect to the stationary case, with larger effects at higher frequencies and higher *Re* values. Again, the effect was particularly intense near the channel outlet, close to the source of oscillation.

A novel concept, named “breathing cell” and based on the application of oscillating conditions, was proposed and tested for reverse electrodialysis systems (see Section 6.6) by Moreno *et al*. [262]. In

the breathing cell, the channels thickness changes dynamically over time in a two-stage cycle by closure of the outlet hydraulic circuit of the concentrated stream, operated by an electronic valve, while maintaining the pump switched on. By cutting the central part of the original spacer and replacing it with a thinner one in the diluate channel, spacers are floating periodically in dilute and concentrate channels. When the valve is closed, the pressure inside the concentrate compartments increases, thus causing the concentrate compartment thickness to increase, while the dilute channel thickness decreases. As a result, the Ohmic resistance of the dilute compartment (which is predominant with respect to the resistance of the concentrate channel) is reduced. Then the valve is opened and the initial conditions are restored. This is repeated in cycles at low frequencies (5 and 15 cycles per minute), such as to allow the complete deformation of membranes. Moreover, some effects on the concentration polarization are expected. The cyclic operation of the stack leads to higher net power densities in a wider range of flow rates with respect to the case of conventional stack with intermembrane distance in the dilute channel equal to the inner spacer thickness, although the maximum net power density was slightly lower. This resulted from a better compromise in a wider range of flow rates between the stack resistance (higher in the breathing cell) and the pressure drop (lower in the breathing cell). The breathing cell could thus be an interesting concept and, in principle, could be applied to ED units. Nevertheless, the long-term operation of the breathing system still has to be carefully analysed, in order to assess the long-time response of IEMs, which can exhibit viscoelastic behaviour. Moreover, the applicability in industrial size stacks may require some adaptations / special measures to guarantee the mechanical robustness of the overall system.

Several experimental tests with pulsed electric fields showed various benefits [153, 154, 165–167, 173, 191, 312, 313]. Besides the positive consequences resulting from a mass transfer enhancement, electrodialyzers operating with oscillating currents are less subject to fouling, scaling and water dissociation. Moreover, they allow higher current efficiencies and operation in overlimiting conditions. Finally, the simple equipment and the inexpensive technology do not pose issues in the scalability for applications also in industrial plants.

4.5 Manifolds and flow distribution

4.5.1 Inlet-outlet manifolds in plate and frame units

Although channel features likely play the main role in controlling electromembrane processes performance, attention should be addressed also to the hydrodynamics-related aspects concerning the inlet-outlet distribution systems, commonly indicated as inlet/outlet manifolds (see Figure 3).

Experimental data and simulations of sheet flow (R)ED stacks revealed that the friction losses per unit length along the channels may be much larger (by one or two orders of magnitude) than in the case of the empty channel of large streamwise and spanwise extent; however, a significant (or even dominant) contribution to the overall pressure drop can be due to the manifolds [2–4, 284, 314–319]. For example, Veerman *et al.* [316] fed a 25×75 cm^2 stack from either the long side or the short side, finding that overall pressure drops were not proportional to the path length. This indicates that pressure drops were largely due to friction losses concentrated at the inlet-outlet regions.

Moreover, Vermaas *et al.* [4] tested a stack with a very simple channel geometry (using profiled membranes), estimating that the measured pressure drops were ~13 folds higher than pressure drops theoretically predicted within the channels. These findings indicate that a large portion of the total pressure drop occurs within the manifolds. In fact, the manifolds are created by virtual cylindrical ducts in spacers, gaskets and membranes with large variations of cross-section, and thus of fluid velocity, at the inlet/outlet zones of the channel (Figure 3, Figure 15 (a)). Nevertheless, an improved geometry of the distribution system can dramatically reduce this localized loss, as it happens in stacks with wide and sufficiently thick manifolds [260, 320] (Figure 15 (b)). This kind of design is specifically suitable for cross-flow stacks, with manifolds as wide as the compartments.

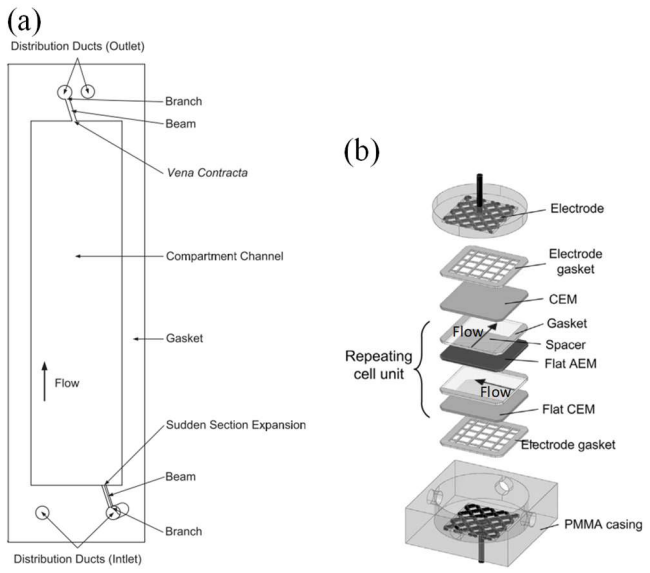

Figure 15. (a) Compartment geometry with large cross-section variations at the entrance/exit regions (adapted from [313]). (b) Stack with manifolds as wide as the channels for cross-flow configuration (adapted from [260]).

The manifolds geometry, along with the channel features and the operating conditions (flow rate and relative direction of the concentrate and diluate streams), also affect the distribution of flow rates (and thus of pressure) among the compartments and in each compartment, with consequences on non-Ohmic resistances, solution leakages from the concentrate channel towards the dilute one and *vice*

versa, and fouling [260, 318, 320–323]. The increase of non-Ohmic resistance arising from a non-uniform distribution of the flow rate can be explained by the exponential reduction of the non-Ohmic resistance with the flow rate. In fact, the increase of non-Ohmic resistance in the areas with a flow rate lower than the average is larger than the decrease generated in the other areas, thus leading to an overall increase in the total non-Ohmic losses. In this respect, wider manifolds lead to a more uniform delivery of feed solutions flow rate, with beneficial effects in terms of non-Ohmic resistances reduction [260]. Finally, large differential pressures between adjacent compartments cause solution leakages through the membrane [322], occurring especially in counter-current and cross-flow configurations [321].

4.5.2 Flow distribution within the channels

Some recent works have dealt with the flow distribution throughout a channel [259, 319, 321, 323–327]. Kostoglou and Karabelas [324] simulated the flow distribution by modelling the spacer as a continuous porous medium filling the channel, in a study of hydrodynamics of spiral-wound elements with permeable membranes. The simplifying assumption of an isotropic medium was actually made for the simulations and the flow field in the spacer-filled channel was characterized by computational fluid dynamics (CFD) methods applied for fully developed flow ("unit cell" approach), keeping the flow attack angle fixed. Kodým *et al*. [325] developed a semi-empirical two-dimensional model, based on momentum balance equations for two interacting sub-layers taking into account the anisotropy of spacers (constituted by overlapped filaments) in the anisotropic form of Darcy's law. A subsequent work [319] extended the model by including in the momentum balance equation fluid inertia, which has a significant influence in the inlet and outlet regions where sudden contractions and expansions, respectively, occur. Significant non-uniformities in the flow distribution in the proximity of the manifolds and larger pressure drops were shown. More uniform flow distributions were predicted as the flow rate decreased and the filaments of the spacer were placed more transversally with respect to the main flow direction (by letting the diagonals of the diamond spacer to vary while maintaining the main flow direction bisecting the angle between the two wires). This corresponds to higher pressure drops within the channel, which make also the distribution among channels more uniform [318, 320, 321].

However, in other cases the flow distribution within the channel is improved by less frictional geometries. For example, Güler *et al*. [259] visualized the dispersion of a black ink in a transparent cell equipped with a profiled membrane (Figure 16). A pillar profiled-membrane exhibited an even distribution over the membrane surface and also low pressure drops, while profiled membranes with

continuous structures made by either ridges or waves led to preferential flow paths, and also to higher pressure drops.

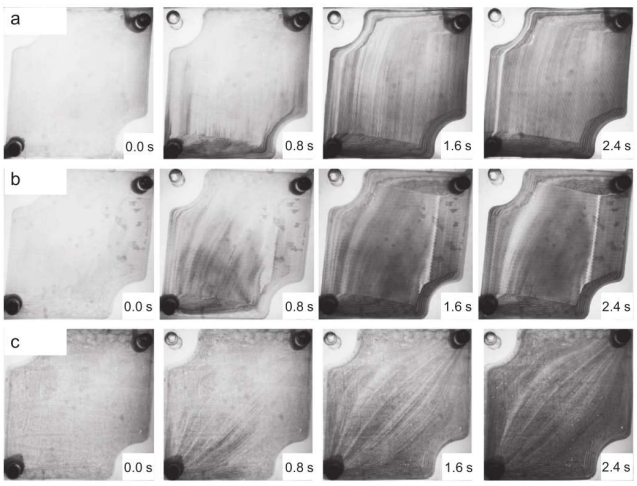

Figure 16. Visualisation of the flow distribution by ink-injection in a flow cell equipped with profiled membrane with (a) ridges, (b) waves, (c) pillars [259].

Turek and Mitko [326] proposed an experimental method for the investigation of residence time distribution in working electrodialyzers, when the applied current causes ion migration and electroosmotic water flux. It was shown that electroosmotic flux, which increases the fluid velocity in the concentrate compartment, changes the hydrodynamic conditions, concluding that (i) the risk of scaling is more pronounced when there are changes in residence time, and (ii) in counter-current mode the flow may be far from the often-assumed plug flow. Enciso *et al*. [327] simulated hydrodynamics and mass transfer in a filter press type electrodialysis reactor (with spacerless channels) by using the finite element method. Simulation results and experiments with a tracer (followed by a digital image analysis) highlighted the presence of stagnant zones, recirculation and preferential flow paths.

In conclusion, both modelling and experimental tools can be effective for the investigation of hydrodynamics in ED units at large scale and reveal interesting perspectives for stack design and optimisation.

5. Process models and simulation tools for electrodialysis and related processes

As already pointed out in the previous sections, in order accurately to describe the ED process and develop effective process simulation tools it is necessary to implement mathematical models able to take into account a number of complex phenomena. These include solution-membrane equilibria, concentration polarisation and fluid flow behaviour along channels, mass transport phenomena and

mass balances in the compartments, electrical phenomena, etc. Several different modelling approaches have been presented so far in the literature, each one addressing in a different way and to a different extent all these aspects. In most cases, the aim was to develop effective design and optimisation tools for ED and RED[1] processes.

In the present section, the different modelling approaches will be critically presented, starting with a classification into simplified and advanced modelling tools.

The first class of process models is characterised by a highly simplified approach based on neglecting most non-ideal phenomena (e.g. DBL, non-Ohmic effects, salt diffusion, water fluxes, etc.) and on the use of lumped parameters equations (i.e. the use of average compartment concentrations to estimate all process variables). Simplified models are commonly adopted for a first rough design of ED equipment, allowing the estimation of figures such as the membrane area required for a given separation problem, and for simplified economic analysis of the process. In this case, empirical coefficients are applied in order to somehow account for all non-idealities, often summarized by a simple *current utilisation factor* (or *current efficiency*).

The second, and wider, class of process models can be divided into 2 sub-categories: 1) rigorous Nernst–Plank (N-P) or Stefan–Maxwell (S-M) based models and 2) semi-empirical models. In both cases, non-ideal phenomena are accounted for and models typically include mass balance differential equations in order to describe the variation or process parameters along the flow direction. The main difference between the two sub-categories is related to the mathematical description of trans-membrane phenomena.

N-P based models (S-M models are even more complex and accurate, with this respect) contain rigorous equations able to almost predictively describe all transport phenomena inside the membrane at the microscopic level (though even in this case some membrane features, such as ions diffusivity, ions mobility, fixed charge density etc. have to be based on empirical information). The simulation is often carried out using Finite Element Methods (or similar approaches) and the process model is practically merged with thermodynamics and mass transfer models, including the description of the fluid dynamics. A limitation of this approach is the very large computational power required to solve the model, which limits the application to very simple channel geometries or to a very small computational domain, thus making the tool unsuitable for whole-stack simulation purposes.

[1] Models developed for RED are based on the same physical principles governing the ED process and are, therefore, useful to complete the scenario of modelling tools for electromembrane processes.

Semi-empirical models, on the contrary, are based on a multi-scale approach, in which lower scale phenomena (such as mass transfer and fluid-flow behaviour, leading also to the characterisation of DBL) are described by means of empirical information or small-scale theoretical analysis, e.g. by means of Computational Fluid Dynamics tools. Thus, also the effect of spacers geometry or membrane profiles can be accounted for. Meso- and higher-scale phenomena are described by means of differential equations for mass balances and algebraic phenomenological equations for fluxes through the membrane, allowing for the achievement of plant-scale description.

Figure 17 gives a graphical representation of the process models classification, while the following sections will illustrate in details the different modelling approaches, reviewing the most important literature contributions to this topic.

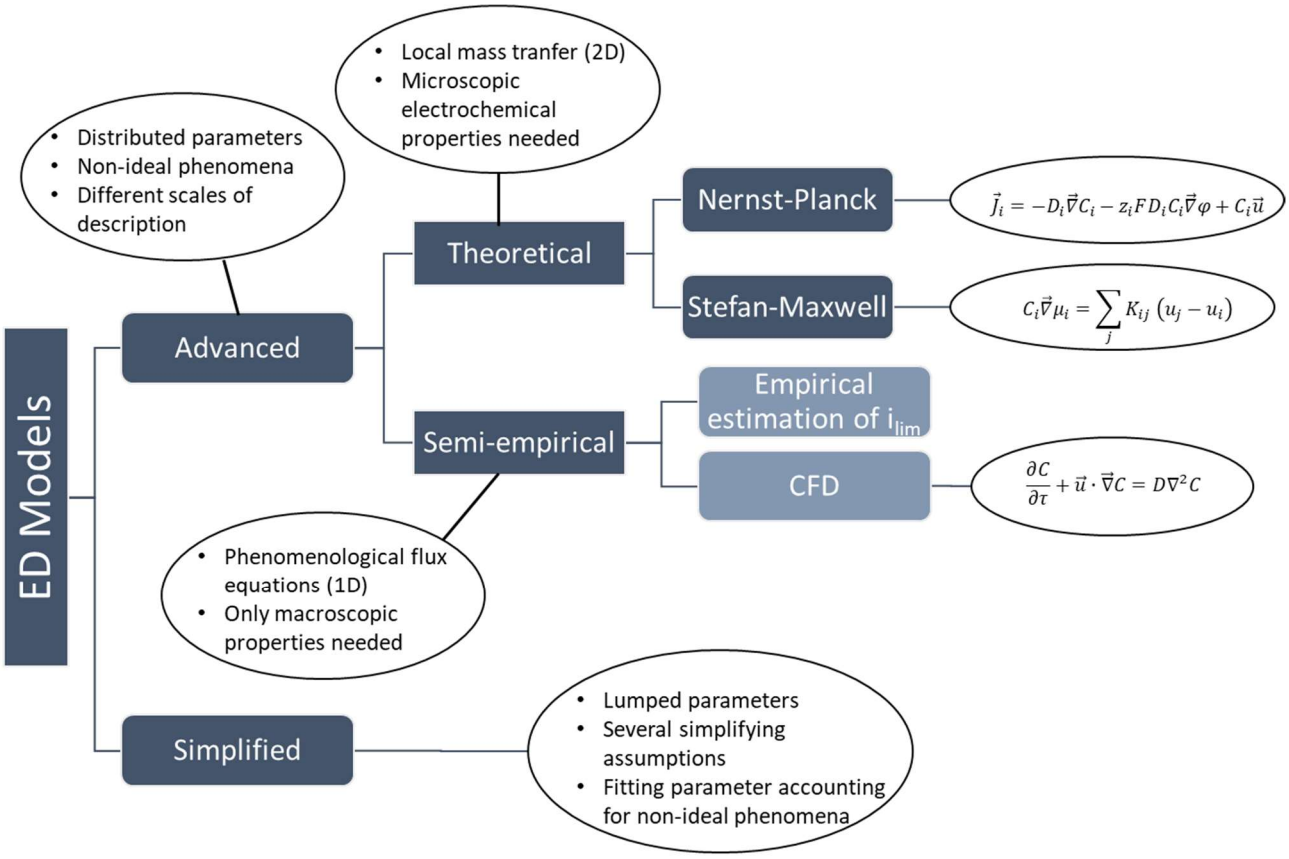

Figure 17. Block diagram showing the classification of modelling tools presented in this work, along with the main features of each class of models.

5.1 Nernst–Planck based models

5.1.1 Mass transfer simulation by the Nernst–Planck equation

Ions in electrolytic solution are charged species that interact with one another as well as with the solvent. These interactions are quite complex and difficult to model, but an effective yet simple approach leads to the Nernst–Planck equation, which is commonly adopted to describe the ionic flux in electromembrane processes. This approach is based on the so-called principle of independence of ionic fluxes: the flux density of a species *i* is determined by its electrochemical potential gradient only, and not by the electrochemical potential gradients of other species [62]. This means that cross-phenomenological coefficients are neglected in the transport equations for ionic species, i.e. short-range interactions among ions are neglected, while only ion-solvent interaction is considered. The Nernst–Planck approach is strictly applicable only to dilute solutions, where the probability that two ions get close is relatively small. The ions flux is expressed as previously reported in eq. (7) (see Section 4.1).

The complete system of equations includes the mass balance of ionic species, the conservation of mass (continuity equation) and momentum (Navier–Stokes equations), a condition for the net charge density (electroneutrality or Poisson's law) and a constitutive equation linking current density and ions flux. Usually, local electroneutrality condition is simply assumed, which states that the local electrical charge density is null everywhere:

$$\sum_i z_i C_i = 0 \tag{26}$$

In this respect, a more rigorous relationship is Poisson's equation, which, for a medium of uniform dielectric constant ε, is:

$$\nabla^2 \varphi = \frac{F}{\varepsilon} \sum_i z_i C_i \tag{27}$$

When Poisson's equation is used (instead of local electroneutrality) to close the system, the so-called Nernst–Planck–Poisson (N-P-P) model is obtained. The proportionality constant F/ε in eq. (27) is quite large (for water $\varepsilon \approx 7.08 \times 10^{-10}$ F/m), so that a negligible deviation from electroneutrality would lead to a considerable deviation from zero of the Laplacian of the electric potential. In other words, an appreciable separation of charge would be associated with very large electric forces [305]. However, deviations from local electroneutrality do occur in the electrical double layer at IEM-solution or electrode-solution interfaces and are confined to a very narrow region (thickness of 1-10 nm [305]). Only at overlimiting currents the *space charge* (or *extended space charge*, *ESC*) region expands beyond the electric double layer. In these conditions, Poisson's equation is needed for the description of transport phenomena.

Due to the small numerical value of the permittivity of water, the N-P-P model is mathematically classified as a singularly perturbed problem [245, 328]. Several techniques have been developed for one-dimensional simulations [203, 245, 263, 328–332] and also for two-dimensional simulations solving the fully coupled N-P-P and Navier-Stokes equations, providing an analysis of the electrokinetic instability that characterizes overlimiting transport phenomena [189, 210, 245, 246, 333–339].

As the energy required to charge a macroscopic system is very high and the double layer is confined in a very narrow region, when transport phenomena are investigated at higher scale and below i_{lim}, electrolytic solutions are assumed to be electrically neutral and Poisson's equation is replaced by the electroneutrality condition. Several works based on the Nernst–Planck approach and local electroneutrality condition have been presented for IEM-based processes (ED/RED) [185, 187, 202, 224, 236, 251, 298, 303, 304, 327, 340–346]. Note that by combining the N-P equations and the mass balances of the two ions of a binary electrolyte with the local electroneutrality condition, the convective-diffusive transport equation is obtained (see Section 5.2.3). Actually, several models based on the N-P approach solve this equation within the fluid domain for calculating the concentration field.

In the N-P based models, some simplifying assumptions are usually done: only 1-D (cross-membrane) or 2-D (axial + cross-membrane) simulations have been carried out, convection has been considered only in some cases [185, 187, 236, 298, 303, 327, 340, 341, 343, 345, 346], while all the components of the cell pair have been simulated only in a few works [187, 298, 327, 341, 343], and the presence of either spacers or membrane profiles has rarely been included [185, 187, 298].

For the sake of completeness, we mention that the applicability of the Nernst–Planck approach has some limitations [347]. In concentrated solutions, each ion is surrounded not only by solvent molecules but also by other ions. In such a situation, short-range interactions become more important, thus additional frictional (interaction) forces are present. In other words, the accurate description of transport processes in concentrated solutions requires more transport coefficients and a more rigorous approach, which can be offered by the Stefan–Maxwell equation. Few examples of application of this approach on ion exchange systems can be found in the literature [301, 348, 349]. However, the N-P model is by far the most adopted due to its simplicity and robustness under a wide range of typical operating conditions of ED and related systems.

5.1.2 Process models based on the Nernst–Planck equation

In order to step from the sole Nernst–Planck mathematical description of transport phenomena to the formulation of a process simulation tool, some of the above mentioned works compute also global

quantities as the voltage-current relationship and the electric power of the stack. The most simplified models are 1-D (cross-membrane) [304, 342, 344], simulate spacerless channels and predict the stack performance by lumped parameters. In other cases, variations along the stack length are taken into account in 2-D (axial + cross-membrane) by simulating the entire channel from inlet to outlet (stack performance predicted by distributed parameters along the axial direction). In some cases fluid dynamics is explicitly simulated by the Navier-Stokes and continuity equations [187, 340, 341], while other models assume either a developed flow field with parabolic velocity profile (Hagen-Poiseuille equation) [303], or even a flat profile [345]. Differently, in Gurreri *et al*. [298] a periodic portion of a single cell pair was simulated, thus allowing a very accurate spatial resolution, suitable for channels with either non-conducting spacers or membrane profiles, while keeping the total number of elements compatible with acceptable RAM requirements and computing time. Tado *et al*. [343] simulated the spacer as a porous domain (Darcy's law) and integrated the governing equations over the channels width, thus obtaining a 1-D axial model. Enciso *et al*. [327] performed 3-D simulations of a stack with spacerless channels by a simplified approach.

Some models have simulated the membranes as a domain with Ohmic behaviour, i.e. by neglecting the effect of concentration variations (secondary current distribution) [187, 327, 341], and in some models membranes were not even included in the computational domain [340, 343], but were modelled by imposing appropriate boundary conditions. Conversely, various simulation tools have explicitly simulated the membranes by the Nernst–Planck equation, taking into account the concentration variation [298, 303, 304, 342, 344, 345]. Water transport has been simulated only in a few cases [343, 345]. Clearly, the complete simulation including the membranes in the computational domain implies that all the coefficients characterizing the transport through the membranes are known. Finally, several models [187, 298, 327, 340, 341] were implemented in multi-physics modelling platforms [350] based on the Finite Element Method (FEM).

As a matter of fact, this general overview shows that, to the best of our knowledge, all models that simulate mass transport by the Nernst–Planck equation have been mostly focused on the membrane modelling, while only little attention has been paid to the modelling of the overall process behaviour for simulation and design purposes. As a consequence, hydrodynamics and associated phenomena of concentration polarization have been taken into account only by a simplified approach. These models have been implemented by either solvers of differential equations or FEM-based software, which are devised for the simulation of simple geometries and would suffer from a prohibitively large memory requirement for the simulation of complex, accurately discretized, 3-D geometries even in the case of a small periodic portion of a cell pair. For example, Gu *et al*. [273] performed FEM simulations of a 3-D periodic domain of a spacer-filled channel discretized with 1.4-2.9 million elements, simulating

only convection-diffusion phenomena inside the channels. In this case, simulations took 3-8 h by using a workstation with 96 GB RAM. Therefore, building up a comprehensive simulation tool for an electromembrane process would be a very hard task and the direct simulation of the complete system by one single tool adopting the N-P approach appears to be almost impossible with currently available computing facilities.

As an alternative to the rigorous N-P-based models, several "semi-empirical" models have been developed, based on a mix of mass and energy balance equations, equations linking electrical and physical variables, and some empirical equations, which are able to predict the voltage drop over the cell pair and, in a more or less rigorous way, a number of physical phenomena characterising the system. This will be discussed in the next section.

5.2 Semi-empirical models

In the present section we have grouped all the models that renounce to resolve the Nernst–Planck equation, but simulate IEMs by using only macroscopic, experimentally accessible, properties (such as transport numbers, Ohmic resistance, salt permeability, osmotic permeability), and allow the channel geometry to be taken into account in a more realistic way. In most cases, semi-empirical models are based on a system of algebraic and differential equations divided into:

1) thermodynamic and electrical equations, leading to the calculation of cell pair potential and resistance, electric current, etc.;
2) mass balance equations accounting for the variation of flow rates and concentrations along the main flow directions and strictly linked with mass transfer equations;
3) transport equations providing mass flux of ions and water through the membrane, on the basis of empirical or separately calculated values for quantities like the Sherwood numbers;
4) other equations allowing the calculation of macroscopic performance parameters such as power requirements, pumping losses, efficiencies, etc., on the basis of empirical or separately calculated values for quantities like the friction factors.

Figure 18 schematically represents a unit cell pair with indication of mass fluxes and of inlet-outlet variables typically adopted in semi-empirical models.

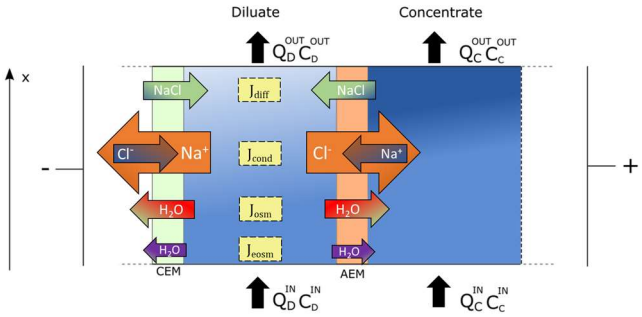

Figure 18. Schematic representation of the transport phenomena involved along the channels and through the membranes of an ED cell pair.

Most semi-empirical models are based on the segmentation modelling approach (see Section 4.3), which, in turn, can be supported either by experiments or by simulations providing Sherwood numbers (Section 5.2.1). Phenomenological expressions of the mass fluxes can thus be written and can be linked to the mass balance equations for the simulation of the whole cell pair length (Section 5.2.2). In particular, when fluid dynamics and mass transfer are simulated at small scale (channel repetitive unit, or unit cell) and the results are transferred to the higher scale at which mass balances and fluxes across the membranes apply (channel-scale, or meso-scale), a multi-scale model is obtained. This represents an integrated simulation tool, built on a hierarchical structure of scales, which can effectively address the full simulation problem [201].

5.2.1 Voltage drop over the cell pair by the segmentation modelling approach

As illustrated in Section 4.3, the total voltage drop over a multi-layer system of solutions and membranes can be assessed as the sum of the various contributions provided by elements in series. For a cell pair, eq. (15) can be rewritten in a more compact form as

$$\Delta V = \eta_{non-Ohm} + r_{Ohm} I \tag{28}$$

where $\eta_{non-Ohm}$ is the overall non-Ohmic voltage drop occurring in DBLs and IEMs (eqs. (19)-(20)), I is the electrical current and R_{Ohm} is the overall Ohmic resistance.

The non-Ohmic term becomes more important when the activity gradient increases, thus generally representing the main contribution on potential drop at the stack outlet when drinking water is obtained. Moreover, the effect of mass transport from bulk to interface, also contributing to the non-Ohmic losses, can be described at different scales of complexity. The simplest approaches adopt the definition of limiting current density, often experimentally determined and empirically correlated to the process conditions. On the other side, several studies have adopted CFD-based or experimental

approaches to determine the values of Sherwood number and link it to the main process variables, thus providing a more complex tool for characterising these phenomena (Section 5.2.3).

In several models, the Ohmic resistance of compartments has been calculated based on the solutions' bulk concentration [6, 141, 174, 254]. Therefore, the Ohmic cell pair resistance can be expressed as

$$r_{Ohm} = r_{CEM} + r_{AEM} + r_C + r_D \tag{29}$$

where r_{CEM} and r_{AEM} are the resistances of the IEMs, while r_C and r_D are the resistances of concentrate and dilute compartments, respectively, which can easily be evaluated as [226]

$$r_C = F_S \frac{h_C}{\lambda_C C_C} \tag{30}$$

$$r_D = F_S \frac{h_D}{\lambda_D C_D} \tag{31}$$

where F_S is a factor accounting for the shadow effect due to spacer filaments or membrane profiles (see below), h is the compartment thickness, λ is the equivalent conductivity, C is the bulk concentration of electrolyte.

Membrane resistance represents the most difficult term to estimate. Fidaleo *et al*. [199] derived the membrane resistance and the effective membrane area from measurements on a stack built with only CEMs or AEMs. Often, a constant value is used for the membrane resistance [174, 254, 297]. However, it has been widely shown that the resistance is strongly affected by the solution concentration, steeply increasing as the solution concentration decreases [75, 142]. Therefore, some models take into account the effect of solutions concentration [6, 141, 247]. Since it is difficult to estimate the actual behaviour of an IEM inside an operating stack, a theoretical approach could represent an effective solution. In this context, Berezina *et al*. [60] proposed a theoretical method for the estimation of conductivity based on the structure of the IEM itself. In particular, membrane conductivity was correlated to the conductivity of individual phases, the volume fraction of each phase and a correction factor accounting for the arrangement of phases inside the material. However, there is still no common approach in experimental methods for membrane resistance measurement and models interpreting the membrane behaviour [76].

The presence of non-conducting net spacers causes an increase of channel Ohmic resistance, referred to as "shadow effect". This aspect has been taken into account in several models by a correction factor defined in different ways, e.g. as the reciprocal of the spacer open area [141], or as the reciprocal of the square of the channel porosity [254]. Pawlowski *et al*. [297] used the reciprocal of the channel porosity but took into account also the increment of the membrane resistance due to the coverage effect of spacers. Clearly, the real effect of spacers depends on their actual geometry. Therefore, more

accurate estimations can be made by experiments [199], or by models, e.g. numerical simulations solving the Laplace equation for the electric potential field [6] decoupled from the concentration field. In addition, also profiled membranes can be simulated, provided the IEM can be treated as a homogeneous resistive material with a uniform electric conductivity. However, in order to reduce the computational effort, such simulations can be restricted to a small number of cases in order to verify/calibrate approximate expressions, more suitable for fast-running models. For example, in the case of a woven spacer with a pitch-to-height ratio of 2 the channel resistance was shown to be inversely proportional to the porosity with a good approximation [6].

5.2.2 Mass balances and transport across membranes

Eq. (28) and all the related equations for the calculation of electric variables can be expressed as functions of the *x* coordinate along the flow direction. Mass balances and transport equations across the membranes allow the variation of concentrations and flow rates along the flow direction to be computed, thus providing all the information needed fully to characterise the system along its entire length [6, 141, 199, 254, 297]. Following an approach similar to the Nernst–Planck one, ions transport within the membrane can be expressed as the sum of an Ohmic conduction flux and a diffusion flux (see Section 4.1). Therefore, the expressions for ions fluxes across the two IEMs of an ED channel can be generalized for monovalent salts as [6, 141, 199, 254]:

$$J_{cond}(x) = \left[t_+^{cem} - (1 - t_-^{aem})\right] \frac{i(x)}{F} \tag{32}$$

$$J_{diff}(x) = \frac{D_{cem}}{h_{cem}}\left[C_C^{cem}(x) - C_D^{cem}(x)\right] + \frac{D_{aem}}{h_{aem}}\left[C_C^{aem}(x) - C_D^{aem}(x)\right] \tag{33}$$

$$J_{tot}(x) = J_{cond}(x) + J_{diff}(x) \tag{34}$$

where t_+^{cem} and t_-^{aem} are the transport numbers of the counter-ions inside the IEMs, D_{aem} and D_{cem} are the salt (diffusion) permeability coefficients through the IEMs, h_{aem} and h_{cem} are the thicknesses of IEMs, C_C^{cem}, C_D^{cem}, C_C^{aem} and C_D^{aem} are the electrolyte concentrations at the various IEM-solution interfaces (solution side) [6, 254] and *i* is the electric current density. Some models simplify eq. (33) by using only one proportionality factor for both IEMs [141, 199, 254] and/or the bulk concentrations instead of those at the interface [141, 199]. The Ohmic conduction is taken as positive, while the diffusion term that contributes to the total flux must be taken with the suitable sign in eq. (34), i.e. in ED channels the diffusion has to be considered negative, since conduction and diffusion are opposite. The Ohmic conduction is the most important as it is directly linked to the ionic current, while the diffusive flux is the result of the non-ideal membrane permselectivity. Therefore, the influence of diffusion through the IEMs on the overall process strongly depends on the specific membrane [315].

Due to the fact that membranes are not perfectly permselective there is also a water flux through them. Two phenomena contribute to this, namely osmosis and electroosmosis, and can be quantified as [6, 141, 199, 254]:

$$J_{osm}(x) = L_{p,cem}[\pi_C^{cem}(x) - \pi_D^{cem}(x)] + L_{p,aem}[\pi_C^{aem}(x) - \pi_D^{aem}(x)] \quad (35)$$

$$J_{eosm}(x) = n_h J_{tot}(x) \quad (36)$$

$$J_w(x) = J_{osm}(x) + J_{eosm}(x) \quad (37)$$

where $L_{p,aem}$ and $L_{p,cem}$ are the water (osmotic) permeability coefficients of IEMs, π_{SOL}^{iem} denotes the osmotic pressure of the solutions at the membrane-solution interface, n_h is the number of water molecules in the solvation shell of salts [6, 141] and J_w is the total water molar flux. Some models totally neglect osmotic phenomena [297], others simplify eq. (35) by using only one proportionality factor (L_p) for both IEMs [141, 199, 254] and/or the bulk osmotic pressures instead of the ones at the membrane-solution interface [141, 199]. In ED units, osmosis and electroosmosis are both from the diluate channel to the concentrate one. Moreover, the flux of water across membranes can be of primary importance for the process performance, especially in stacks with a large membrane area and long residence time.

One-dimensional mass balance equations (global and for the solute) along the flow direction *x* can be expressed by the following differential equations:

$$\frac{d\,Q_D(x)\,C_D(x)}{dx} = -\frac{d\,Q_C(x)\,C_C(x)}{dx} = -b\,J_{tot}(x) \quad (38)$$

$$\frac{d\,Q_D(x)}{dx} = -\frac{d\,Q_C(x)}{dx} = -b\,J'_w(x) \quad (39)$$

where Q represents the volumetric flow rate, b the membrane width and J'_w the volumetric flux of the solvent through IEMs. In order to take the effect of solution density variation into account in eq. (39), more rigorous mass balances should be written [6], though such effect is typically negligible.

Differential mass balance equations are typically solved by numerical methods in several different platforms, thus allowing an easy and reliable characterisation of the unit behaviour along the flow direction in co-current and counter-current stacks.

A particular type of semi-empirical models is represented by the time dependent models. These are used to simulate batch or semi-batch operation [199, 351, 352], usually taking place in laboratory test rigs or in food industry applications. In most cases, batch ED is simulated using a quasi-steady state approach, where a stationary lumped model is coupled with time dependent mass balances applied to recirculation tanks. Although the lumped-parameters approach is less accurate than distributed-

parameters models, this is an acceptable assumption as batch processes are usually characterised by small stacks with time constants much smaller than those of the tanks adopted for recirculation.

5.2.3 Complex approaches for non-Ohmic phenomena and mass transport models

As mentioned in Section 4.3, all the contributions of the DBL to the total voltage drop (Ohmic voltage drop, diffusion potential and concentration overpotential) can be calculated as logarithmic functions of polarization coefficients. In general, in a cell pair there are four different values of polarization coefficient, one for each interface. In turn, polarization coefficients depend on current density, mass transport related to hydrodynamics, which is accounted by the Sherwood number, and transport numbers in membrane and solution (eq. (11)). Often mass transport phenomena within the channel have been characterized by experimental measurements (chronopotentiometry, EIS, limiting current density, see Section 4). Nevertheless, mass transfer characteristics have been computed by numerical simulation of the convective-diffusive transport equation of the electrolyte, predicting the Sherwood number. As mentioned in Section 5.1.1, under the local electroneutrality condition, from the Nernst–Planck equations of the two ions of a binary electrolyte the well-known convective-diffusive transport equation can be obtained [202, 236, 280, 302, 305]:

$$\frac{\partial C}{\partial \tau} + \vec{u} \cdot \vec{\nabla} C = D \nabla^2 C \tag{40}$$

where C denotes the electrolyte concentration. In many works devoted to ED (or RED) systems, ideal mass transport within the channels has been simulated by this equation [6, 185, 193, 281, 288, 291, 296, 297, 303, 304, 342, 353], which, in principle, is valid to the same extent as the Nernst–Planck equation coupled with the electroneutrality condition. However, in the models that limit the domain to one channel, this approach imposes the need to choose the boundary condition at the IEM-solution interface (uniform concentration, uniform flux, or mixed condition). Nevertheless, in typical scenarios the boundary conditions affect mass transfer coefficient only slightly [297], although a larger effect may occur when profiled membranes are adopted.

An important advantage of the convection-diffusion equation is that CFD codes are suitable for the simulation of relatively complex 3-D geometries of spacer-filled and profiled-membrane channels, providing accurate spatial resolution. Under the hypothesis of fully developed conditions, the unit cell (Figure 19) has been simulated in several studies [6, 185, 193, 281, 284, 296, 297] using periodic boundary conditions and solving the convection-diffusion equation along with the Navier-Stokes and continuity equations.

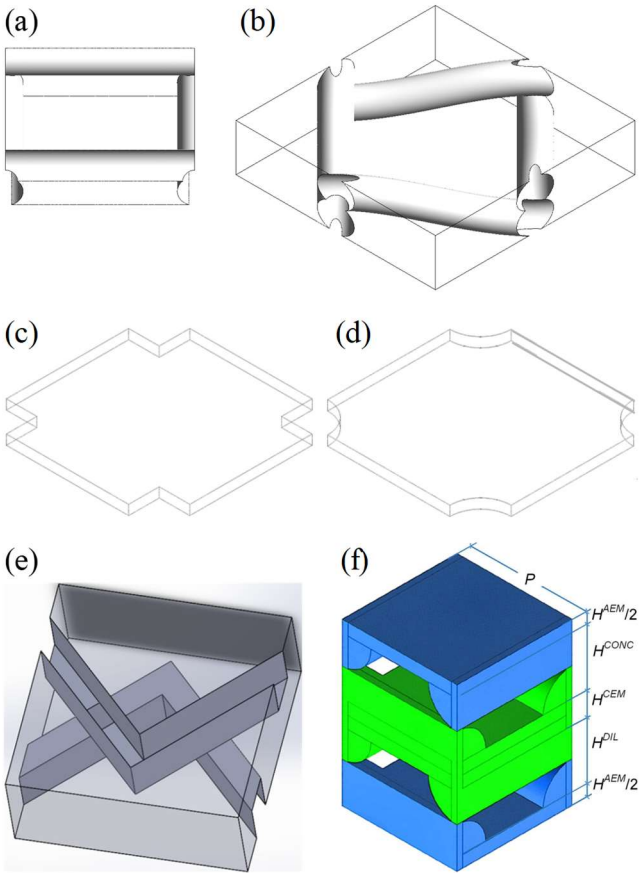

Figure 19. Unit cell for CFD simulations solving the convection-diffusion equation: (a) overlapped and (b) woven spacer [281], (c) square and (d) circular pillar profiled membrane [296], (e) chevron profiled membrane [297], (f) overlapped crossed filaments profiled membrane [6].

Moreover, CFD simulations of narrow channels have general validity for various membrane processes, as reverse osmosis, nanofiltration and others [198, 200, 230, 266, 271–274]; through the heat/mass analogy, the same applies even for simulations of temperature driven processes [269, 275]. Therefore, mass transfer correlations for a large number of channel geometries are available in the literature and are suitable for assessing the effects of concentration polarization in ED modules. For example, CFD results have been used for the calculation of the DBL effects in [6, 141, 297]; in addition, CFD results concerning pressure drops can be used in order to calculate the pumping power consumption, as will be discussed in the next section. Other models have used experimental data on mass transfer [174, 199, 254].

Among the non-Ohmic effects of the DBL, often only the concentration overpotential is taken into account [6, 141, 254, 297], but in other cases also the diffusion potential is considered [174, 199].

In regard to the mathematical expression for ionic fluxes through the IEMs, a more rigorous (but also more complex) description can be provided by the phenomenological approach of Irreversible Thermodynamics (IT) and its derivations such as the Kedem-Katchalsky equations [354–356]. This

class of models is based on the assumption that the flux of an individual component can be described by the sum of each driving force multiplied by its phenomenological coefficient, thus taking the mutual influence of each flux on the other ones into account. Some ED process models used IT [357, 358]. However, the resulting equations are usually complex to solve and require the determination of several coefficients.

5.2.4 Overall process performance parameters

Once the system is characterised in terms of streams properties and electrical variables, the last step for process models is to calculate the macroscopic performance parameters, such as electrical power and specific power consumption, apparent membrane flux, current utilization factor and pumping power requirements.

Electrical power consumption in ED can be easily calculated as the product of the voltage drop over the cell pair (ΔV) and the electric current flowing through the external circuit (I):

$$P_{el} = \Delta V \cdot I \tag{41}$$

P_{el} has to be multiplied by the number of cell pairs in order to obtain the total stack power requirement.

Dividing by the diluate flow rate generated in each cell pair leads to the most commonly used expression of the specific energy consumption:

$$SEC_{el} = \frac{P_{el}}{Q_D^{out}} \tag{42}$$

Less common, yet useful for a comprehensive understanding of the process behaviour, the salt-specific energy consumption ($sSEC_{el}$) indicates the amount of energy required for the passage of one mol (or one kg) of salt from the dilute to the concentrate compartment:

$$sSEC_{el} = \frac{P_{el}}{C_D^{in}Q_D^{in} - C_D^{out}Q_D^{out}} = \frac{P_{el}}{C_C^{out}Q_C^{out} - C_C^{in}Q_C^{in}} \tag{43}$$

Another important parameter for comparison with other membrane separation processes is the apparent diluate flux (J_D^{app}), also named "water productivity" [359], expressing the amount of diluate generated by the ED unit per square meter of cell pair area:

$$J_D^{qpp} = \frac{Q_D^{out}}{A^{cp}} \tag{44}$$

where A^{cp} is the cell pair membrane area.

A simple, yet effective, approach to estimate the effect of parasitic phenomena inside the stack is the definition of the current utilisation factor (or current efficiency) ζ, defined as the ratio between the ideal current calculated from the salt depletion in the diluate channel and the actual current passing though the stack:

$$\zeta = \frac{(C_D^{in} Q_D^{in} - C_D^{out} Q_D^{out}) \cdot F}{I} \tag{45}$$

Typical values of ζ range from 0.5 to 0.95, with the lower end indicating a significant adverse effect of parasitic phenomena such as salt counter-diffusion, low IEMs perm-selectivity, presence of parasitic currents in the manifolds, etc., particularly detrimental when high concentrations are reached. The current utilisation factor is often adopted in simplified models and design tools (see Section 5.3) for a quick calculation of operating current in industrial ED stacks, and ζ values are generally based on empirical equations or practical experience of process designers and operators.

ED models often neglect the pumping power [174, 199], although in some operating conditions this may be significant (see Section 4.4.5). RED models, instead, normally take into account the pumping power [6, 141, 254, 297] because of the relative low gross power densities producible. In both cases, the pumping power per cell pair can be calculated as

$$P_{pump} = \frac{Q_C \Delta p_C + Q_D \Delta p_D}{\chi} \tag{46}$$

where Q is the flow rate, Δp is the total (in-out) pressure drop pressure drop, χ is the pump efficiency, and the subscripts C and D refer to the concentrate and diluate channels, respectively. Δp includes the pressure drop along the channel and the concentrated pressure drop within the manifolds. It can be predicted by in-out pressure drops measurements used as fitting data [254], or by CFD tools providing distributed pressure drops [6, 141, 297], along with experimental data or simulation results on the friction losses through the manifolds [6, 297].

5.3 Simplified models for the simulation and design of ED systems

The last class of models reported in the literature is characterized by a simplified structure [226, 351, 360]. This approach has been mainly followed in order to implement models aiming at the preliminary design of ED units.

In 2002 Lee *et al*. [226] presented a design tool based on a number of simplifying assumptions and simple equations allowing to estimate the main features of an ED stack such as electric current and required membrane area for a fixed applied voltage. In particular, the main assumptions are:

- Both cells have identical geometries and flow condition;
- The stack operates in a co-current flow;
- The unit works below the limiting current density;
- The membranes potential (back electro-motive force) is neglected;
- Concentration polarisation is neglected;
- Diffusion of ions and water transport are neglected;
- The current utilisation factor is fixed.

On this basis, the "degree of desalination" (i.e. the difference between the inlet and the outlet concentration of the diluate stream) can be expressed as:

$$dC^{\Delta} = \frac{i\zeta N}{zFQ} dA \tag{47}$$

where C^{Δ} is the degree of desalination, i is the current density, ζ is the current utilisation factor (already defined in Section 5.2.4), N is the number of cell pairs, z is the valence, Q the volume flow rate and A is the effective membrane area.

The current density is given by:

$$i = \frac{\kappa_{av}\, \Delta V}{2hN} \tag{48}$$

where ΔV is the applied voltage, h is the channel thickness and κ_{av} is the average electrical conductivity, which can be expressed in terms of solution conductivities and membrane resistances:

$$\kappa_{av} = \frac{2h}{\frac{h}{\kappa_C} + \frac{h}{\kappa_D} + r_{AEM} + r_{CEM}} \tag{49}$$

where κ_C is the concentrate conductivity, κ_D is the diluate conductivity, r_{AEM} and r_{CEM} are the membrane's resistances.

By substituting eqs. (48) and (49) in eq. (47), rearranging and integrating this equation (with the boundary conditions $C^{\Delta} = 0$ at $A = 0$ and $C^{\Delta} = C_D^f - C_D$ at the generic A) in order to express the effective area as a function of the other parameters, one has:

$$A = \left[\frac{h}{\lambda} ln \frac{C_C\, C_D^f}{C_D\, C_C^f} + (r_{AEM} + r_{CEM})\left(C_D^f - C_D\right)\right] \frac{zFQ}{\zeta \Delta V} \tag{50}$$

where λ is the equivalent conductivity, C_C and C_D are the outlet concentrations and C_C^f and C_D^f are the feed concentrations.

In the practical design of an ED unit, the process path length can be derived from this equation when working below the limiting current density and including a correction factor to take into account the shadow effects:

$$L_{prac} = \left[\frac{h}{\lambda} ln \frac{C_C\, C_D^f}{C_D\, C_C^f} + (r_{AEM} + r_{CEM})\left(C_D^f - C_D\right)\right] \frac{zFQ_{prac}}{\zeta \Delta V F_S b} \tag{51}$$

where F_S is the shadow factor, b is the cell width and $Q_{prac} = Q\sigma$, with σ being a factor expressing the fluid volume % of a cell (i.e. the porosity of the spacer). In a subsequent work, Brauns [361] modified this equation by replacing the shadow factor with a general experimentally determined model parameter which can account for additional phenomena.

Another example of simplified model was presented in 2007 by Sadrzadeh *et al*. [360]. In this empirical regression-based model, a current efficiency is used to include all phenomena leading to an incomplete current utilisation, without explicitly considering the various contributions different from the migrative flux for the mass transfer through membranes. In this way, the mass balance can be written as

$$u h_D dC = \frac{\zeta}{F} \frac{I}{A} dx \tag{52}$$

where u is the fluid velocity, h_D is the thickness of the diluate compartment, ζ is the current efficiency, F is the Faraday constant, I is the electrical current, while *I/A* represent the current density and A is the effective area of an IEM. *dC* and *dx* represent the differential variation of concentration for a differential increase in the stack length, respectively.

In addition, membrane resistances as well as Nernst potentials are not explicitly calculated but all included in fitting parameters. The result is a lumped model characterised by a single design equation that gives the outlet diluate concentration as a function of the various parameters:

$$\frac{\beta\, Q^{2/3}\, {h_D}^2\, F}{\Delta V\, A^{2/3}} f(C_0, C) = \int_0^l dx \tag{53}$$

$$f(C_0, C) = \int_{C_0}^{C} \frac{1}{C(12.64 - 8.92C^{0.5} + 8.21\, C)} dC \tag{54}$$

where Q is the flow rate and β is a parameter that is fitted by experimental data, resulting in a function of flow rate and applied voltage.

As it was shown, simplified models result in a limited number of equations that can easily be used to estimate the main design parameters. However, a simplified design tool does not provide details on the variables distribution along the channel, such as current profiles, and approximates all non-ideal

phenomena governing the operation of real ED units. This represents a limitation when a model is needed to analyse the behaviour of the ED process in detail, especially for optimisation purposes. Another important limitation is represented by the fact that these basic model formulations strongly rely on experimentally fitted constants, implying that the model has to be finely calibrated according to the specific unit to be simulated.

6. Special applications of electrodialysis

Several ED-related processes, based on the use of IEMs, have been proposed and are still arousing interest among researchers around the world. These special technologies, expanding the application field of ED and promoting the development of system components and the optimization of devices, are discussed in this section.

6.1 Electrodialysis with bipolar membranes

Electrodialysis with BiPolar Membranes (EBPM) is a process based on the use of special IEMs, namely bipolar membranes (BPM, see Section 3.2) constituted by a double layer of adhering anion and cation exchange membranes, mostly used for the production of acids and bases from salt solutions. An EBPM stack is composed by alternating an AEM, a BPM and a CEM. These three membranes together with three channels represent the repeating unit of the EBPM stack (Figure 20). A salt solution flows in between the AEM and the CEM, while an acid and a basic solution flow in the other two channels respectively [10]. When an electrical potential is applied to the electrodes, water trapped inside bipolar membranes is induced to split catalytically into H^+ and OH^- ions, which will pass through the cationic and anionic layer of the BPM, reaching the acidic and alkaline compartment, respectively. At the same time, anions and cations from the salt solution migrate through IEMs, electrically balancing the passage of H^+ and OH^-, thus restoring electroneutrality and generating the acid and base solutions. Although the three cells compartment is the most diffused configuration, sometimes a two compartment scheme is used, in which only one type of product (either acid or base solution) is obtained, while the salt solution absorbs also the excess H^+ or OH^- generated. This can happen especially when it is not possible or convenient to obtain a high purity for both acid and base [362].

EBPM is an industrial competitor of electrolysis for the production of acid and base compounds. Several works in the literature show how EBPM can reach very low energy consumptions, especially assuming ideally conductive and permselective membranes. Nevertheless, in practical applications

energy consumption is considerably increased by the actual stack Ohmic resistance, diffusional losses and non-ideal permselectivity of homopolar and bipolar membranes [362].

A particularly interesting application of EBPM is the treatment and valorisation of waste brines from desalination plants [363–370]. The process is used to convert very concentrated NaCl (plus a number of additional minor elements) solutions into HCl and NaOH products. Through this novel application of EBPM, brine can be diluted to attenuate disposal issues and, at the same time, valuable products are obtained. Despite the clear environmental advantage, this application has to face a number of technical and economic barriers mainly related to membrane cost and performance (i.e. limited permselectivity and electroosmosis) and to the purity of the product streams due to the presence of minor elements in the feed brine. More details on potentials and limitations of this application can be found in [371].

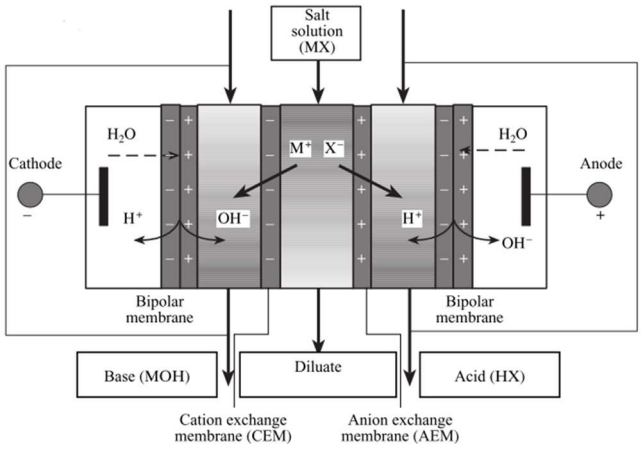

Figure 20. Electrodialysis with bipolar membranes in a conventional three cell compartment configuration [362].

6.2 Continuous electrodeionisation

Continuous ElectroDeIonisation (CEDI) can be considered a hybrid process merging ion exchange deionisation and ED [372]. A typical CEDI unit has a similar configuration to ED, with alternating IEMs, concentrate and diluate compartments where feed solutions flow. Differently from ED, in CEDI at least one channel is filled with ion exchange resins.

CEDI has two possible layouts. In the first the diluate channel is filled with mixed anion and cation exchange resins (Figure 21 (a)), while in the second anionic and cationic resins are placed in two different channels separated by a bipolar membrane (Figure 21 (b)) [10]. The presence of ion exchange resin particles inside the diluate compartment allows for a fast migration of ions through the channel from one membrane to the other, avoiding the limitation of low conductivity of dilute

solutions [373]. This makes CEDI also useful for the production of extremely dilute water solutions in small and medium scale applications. For example, CEDI is often adopted for the production of ultra-pure water in food, pharmaceutical and electronics industry [10, 372, 373]. Another proposed application of CEDI is the removal of heavy metals in wastewater treatment trains [373].

The main advantage of the mixed resins bed is that anions and cations are simultaneously removed, thus avoiding the need for a double passage of the solution (as in case b) and minimising its residence time inside the CEDI unit. However, two separated beds are much more efficient when the solution contains weakly dissociated electrolytes [10]; in this case, the feed solution undergoes the cation exchange step first, where cations are exchanged with the protons generated and released by the bipolar membrane. The resulting acidic solution then flows through the anion exchange channel where anions are exchanged with hydroxide ions from the bipolar membrane, restoring solution neutrality. Nowadays, both layouts (a) and (b) are widely used in the industry.

Interestingly, also novel configurations of CEDI have recently been proposed, based on the use of electrostatic shielding zones instead of membranes [374, 375], though these have not yet reached an industrial applicability scale.

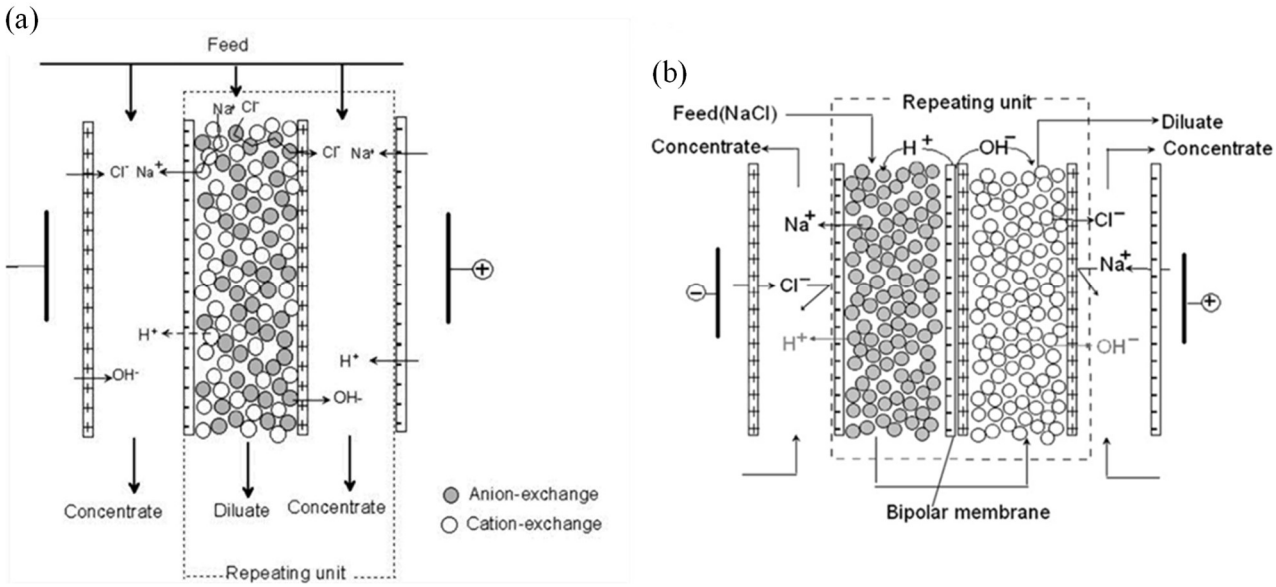

Figure 21. Schematics of the two different layouts of continuous electrodeionisation stacks (from [10]). (a) Conventional stack with diluate channel filled with mixed cation and anion exchange resins, (b) stack with anion and cation exchange resins in two different channels with a bipolar membrane in between.

6.3 Capacitive deionisation

Capacitive DeIonistation (CDI) is a desalination and ion transfer process based on the use of capacitive materials to remove/release ions from/into solutions in a cyclic way [10]. In CDI, a salt solution flows through a channel between the two capacitive electrodes, which are usually covered with an IEM (or, more generally, an ion selective layer) in order to enhance the current efficiency, thus increasing process performance [376]. Applying an electrical potential difference between the electrodes, ions move according to the generated electric field and are eventually absorbed on the capacitive electrodes surface (often consisting in a modified carbon-based matrix), removing salts from the feed water and producing desalinated water. When electrodes reach the saturation condition, polarity is reversed and ions are discharged from the electrodes into a purge stream flowing through the channel, thus regenerating the electrodes and producing a concentrated brine to be disposed. CDI is not yet a fully mature technology, but some commercial manufacturers already exist and some examples of real applications have been reported [377]. Nowadays, CDI suffers from market penetration issues mainly due to upscaling difficulties related to the large quantity and cost of the electrodic material needed for large capacity plants [378].

6.4 Electrodialysis metathesis and selectrodialysis

Since the early '80s the possibility of using an ED stack to carry out a metathesis reaction has been assessed [30–33]. The metathesis reaction allows two salts to be produced by interchanging the anions and cations of two different initial salts:

$$MX + M'X' \rightarrow MX' + M'X \tag{55}$$

Differently from conventional ED, the repetitive unit of electrodialysis metathesis (EDM) is composed by 2 dilute compartments, 2 concentrate compartments, 2 CEMs and 2 AEMs (Figure 22) [33]. Feed channels are alternatively fed with two streams, one containing the first reactant (MX) and the other containing the second ($M'X'$), while a *"sink"* solution flows through the other two channels. The presence of the applied electrical field and of the selective IEMs leads to the passage of ions from feed to compartments containing sink solution and, as a result of this ion shift, product streams are generated in the sink channels. As an example, assuming that the feed solutions contain magnesium chloride and sodium sulphate, the product outlets will contain magnesium sulphate and sodium chloride, which may reach an over-saturation condition and precipitate out of the channel to form solid product salt [33]. In the past years, the possibility of using EDM for the production of different salts such as potassium carbonate, magnesium sulphate and potassium sulphate from more soluble

and less valuable salts has been studied [30, 379]. Recently, EDM was also used for the production of ionic liquids precursors [380]. Another important application of the EDM process is the treatment of RO concentrated brines in zero liquid discharge desalination [31]. In this case, the repeating cell is characterised by a conventional AEM, a conventional CEM, a monovalent selective AEM and a monovalent selective CEM. By feeding the unit with desalination brine and artificial NaCl solution two concentrate product streams are obtained: the first containing sodium with anions and the other containing chloride with cations [31, 33]. In both cases, concentration in the outlet brines can be significantly increased thanks to the high solubility of the salts generated by the metathesis process, thus overtaking the main limitation of RO being the risk of scaling (mainly due to calcium and magnesium carbonates and sulphates) when a recovery ratio of 40-50% is exceeded.

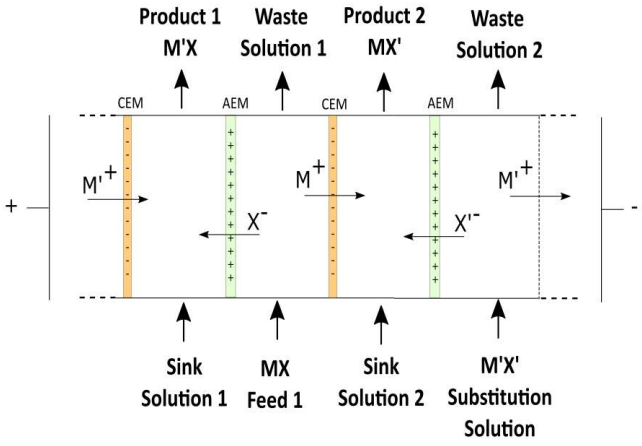

Figure 22. Schematic representation of the electrodialysis metathesis process.

Similarly to EDM in zero liquid discharge applications, selectrodialysis (SED) is a particular technology that makes use of monovalent selective IEMs. A typical SED repeating unit is constituted by 3 compartments with a central monovalent selective IEM (MVA or MVC) between a conventional CEM and an AEM [27]. This configuration allows monovalent and divalent ions to be selectively separated from feed solutions. The scheme reported in Figure 23 refers to the case of separating monovalent and bivalent anions from a feed solution by adopting a monovalent selective anion membrane (MVA) in the centre of the SED repeating unit.

SED is a relatively novel process for which ion fractionation capabilities have generally been claimed [27], but have been practically demonstrated only in a few applications. Examples are the recovery of phosphate from waste streams [28, 381] or the separation of chloride and sulphate compounds from a NaCl and Na_2SO_4 mixture to simulate the application of SED in brine treatment processes [26].

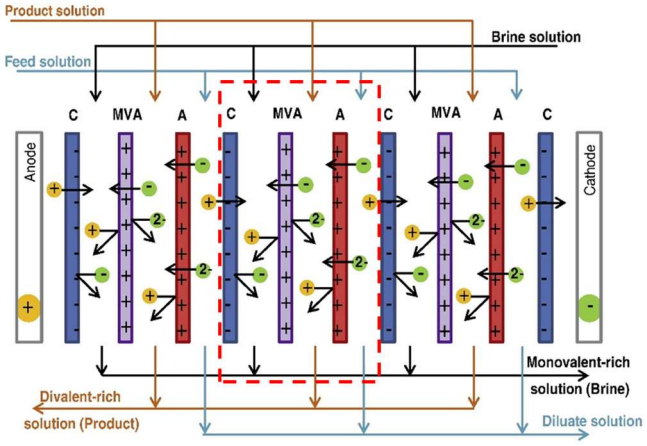

Figure 23. Scheme of a selectrodialysis stack for the separation of salts containing mono- and bi-valent anions (e.g. Cl^- and SO_4^{2-}) showing the functioning principle (adapted from [26]).

6.5 Shock electrodialysis

Limiting and overlimiting currents (see Section 4.3) are possible operating conditions in ED, though they are generally avoided in standard operation [49]. However, the shock electrodialysis concept, recently proposed for water desalination purposes, operates under overlimiting current conditions [382–384]. A shock ED repeating unit is composed by a weakly charged porous medium placed in a channel between two equally-charged ion exchange membranes, such as two CEMs or AEMs (Figure 24). As in conventional ED, electrodes are placed at both ends of a pile comprising a number of repeating units, next to the IEMs. While salted water flows through the channel, a potential is applied at the electrodes. This causes a flux of anions and cations in the two opposite directions. If CEMs are chosen as selective layers (as shown in the example of Figure 24), sodium ions are removed from the channel, creating a depletion zone at one side of the compartment and a salt enriched zone at the opposite side. Conversely, anions move from the depletion to the enriched zone, being blocked in the upper part of the compartment by the CEM. As in ED, when the ion concentration at the membrane interface reaches zero, the limiting current is reached. However, applying an overlimiting current in the presence of the weakly charged porous medium results in a transport of ions much faster than diffusion. The overlimiting current makes the edge of the depletion zone propagate through the pores as a shock wave creating a sharp boundary between the depleted and undepleted zones. Solutions flowing through the two zones are finally separated by a splitter placed in the last part of the channel so that a desalinated water and a brine streams are obtained [384]. Phenomena occurring in shock-ED at overlimiting current condition are still under debate [385–387]. So far, two main phenomena are believed to occur: surface migration and surface convection [385]. The first is typical of sub-micropores; the second is due to electroosmotic flow and is dominant in larger pores.

Shock ED is a very recent technology, still in an early development stage. Although there are no industrial applications, Schlumpberger *et al*. in 2015 showed a small scalable prototype able to remove over 99% of salt from a feed water with a salt concentration up to 100 mM [382]. Also, Deng *et al*. developed a small unit demonstrating the possibility to use shock ED in filtration, separation and disinfection [384].

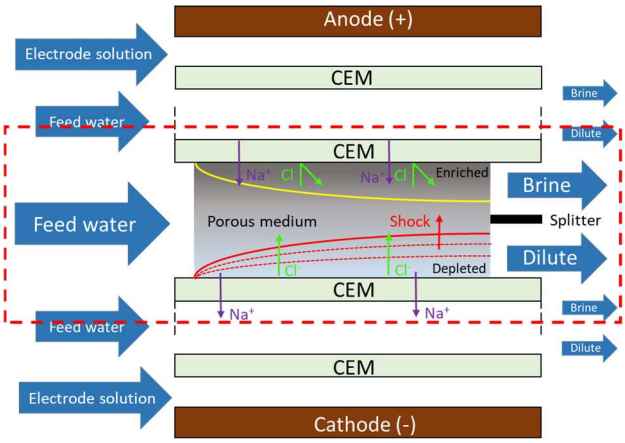

Figure 24. Schematic representation of the shock electrodialysis process with indication of the system repeating unit.

6.6 Reverse electrodialysis for energy generation from salinity gradients

Reverse ElectroDialysis (RED) can be considered as the opposite process of electrodialysis. The latter makes use of electric energy to remove salts from a solution: energy is used to generate a salinity difference between a dilute stream (i.e. the produced fresh water) and a concentrate stream (i.e. the generated brine). Conversely, RED is able to convert the salinity difference, i.e. the chemical potential difference existing between two solutions at different concentrations, into electric energy. RED is one of the most important among the so called Salinity Gradient Power (SGP) technologies, recently arousing the interest of scientists and technologists in the field of water and energy generation from non-conventional sources.

As depicted in Figure 25, the repeating unit of a RED stack (called “cell pair”) consists of a CEM, a dilute compartment, an AEM, and a concentrate compartment. As in ED, anion and cation exchange membranes are also alternatively arranged, and the dilute and concentrate feed solutions flow within channels arranged in an alternate way. Under open circuit conditions (i.e. when the end electrodes are not connected to an external circuit) and assuming ideal membranes, nothing passes through the membranes and the chemical potential difference existing between two adjacent channels is

counterbalanced by the electric potential difference generated in each membrane by the Donnan equilibrium (see Section 3.1). This potential difference is typically addressed as the *open circuit voltage* and represents the electromotive force of the RED generator. When the circuit is closed, ions start to move from the concentrate channels to the dilute ones oriented by the presence of selective IEMs. Thus, positive ions will move towards the cathode passing through CEMs and negative ions will move in the opposite direction, thus generating a net ionic current through the cell pairs. In analogy with ED, the net flux of charges is eventually converted into a flux of electrons in the final compartments of the stack, where electrodes are placed and redox reactions occur. The current of electrons generated at the electrodes can be used to supply an external load [277, 340, 388, 389]. As in standard electric energy generators, also in a RED stack the increase in electric current (related to a reduction in the external load resistance) leads to internal voltage drops, which reduce the available voltage at the stack electrodes, leading to the extreme condition in which a short-cut circuit between electrodes generates the maximum current depleting completely the electromotive force generated in the pile.

It can be demonstrated that the maximum power density can be obtained when the resistance of the external load matches the internal resistance of the stack. Under this condition, only 50% of the available Gibbs free energy of mixing can be theoretically harvested.

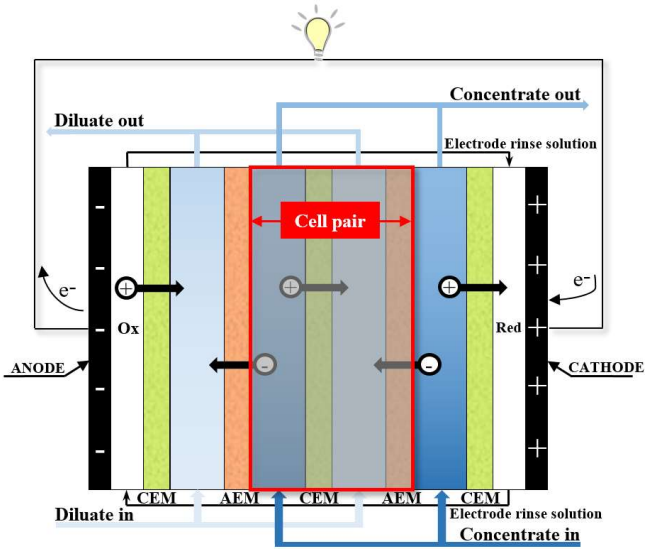

Figure 25. Scheme of Reverse Electrodialysis process.

It is worth mentioning that, under practical conditions, only a portion of this energy can actually be converted into electric energy. Thus, since the amount of electricity producible is not high, all detrimental effects as Ohmic and non-Ohmic resistances and pumping losses due to pressure drops represent matters of crucial importance. In particular, a maximum in the net power density (i.e. gross power density minus pumping power density) is typically found for streams velocity around or below

1 cm/s [284]. At these flow rates, the power output reduction due to pumping power normally amounts to about 10-20% for spacer-filled channels RED units [281] and to about 3-25% in RED systems where profiled membranes are used [4, 259, 260]. The channel thickness is usually in the order of a few hundred microns to keep the channels' electrical resistance low. These aspects mark a difference from ED where thicker channels and larger stream velocities are adopted.

The performance of RED units has rapidly increased during the last years, moving from generated power densities of 0.05 W/m^2 reported in the early '50s by Pattle [390], who first conceptualised the RED process, to values of 1-2 W/m^2 recently obtained by Veerman *et al.* [391] and Veermaas *et al.* [3] mixing solutions simulating river and sea water (see Table 1). The highest values of power density, however, were recently achieved by mixing solutions simulating fresh or brackish water and concentrated brines at temperatures of 40 or 60°C, reaching values up to ~6.70 W/m^2 [5, 392, 393]. A more detailed chronology of the RED technology development is reported in Table 1.

Table 1: Chronological trend of increasing power densities achieved in laboratory scale RED systems. Experimental conditions are also reported (adapted from [393]).

Year	Authors	Power density (W/m^2)	Spacer Thickness (μm)	Solution concentrations (M)	Temperature (°C)
1955	Pattle [390]	0.05	1000	Non specified	39
1976	Weinstein and Leitz [394]	0.17	1000	0.02–0.57	Ambient
1983	Audinos [395]	0.40	1000	4.3	Ambient
1986	Jagur-Grodzinski and Kramer [396]	0.41	250	tap water and seawater	Ambient
2007	Turek and Bandura [397]	0.46	190	0.01–0.5	Ambient
2008	Turek *et al*. [398]	0.87	190	0.01–1.9	Ambient
2008	Veerman *et al*. [391]	0.93	200	0.017–0.5	Ambient
2011	Vermaas *et al*. [3]	2.20	60	0.017–0.5	Ambient
2014	Daniilidis *et al*. [5]	5.30	100	0.01–5	40
2015	Tedesco *et al*. [393]	6.04	270	0.1–5	40
2014	Daniilidis *et al*. [5]	6.70	100	0.01–5	60

During the last years, research achievements have pushed up the RED *Technological Readiness Level* (TRL), allowing the shift from lab-scale units to the first prototypes and pilot plants. Two different pilot plants have been built so far as outcomes of two different projects: Blue Energy and REAPower. Both plants are located in Europe.

The Blue Energy pilot plant is located in Breezanddijk at the Afsluitdijk closure dam (the Netherlands) where seawater and river water are available with an intake capacity of 200 m^3/h. Assuming a technical potential of 1 MJ per m^3 of sea and river water [399], this flow rate has a potential for energy generation of 50 kW [400].

The REAPower pilot plant was installed in Marsala (Sicily, Italy) in 2014 within a saltworks area where solutions at different salinities were available such as: a concentrated brine from evaporating basins, seawater and brackish water from a shoreline well [392, 401]. The concentration of the brine changes during the year ranging between 3 and 5 M (in terms of $NaCl_{equivalent}$ concentration), while the concentration of brackish water is quite constant and equal to 0.03 M (in terms of $NaCl_{equivalent}$ concentration). The pilot plant, consisting of 3 different RED stacks, had a nominal capacity of about 1 kW, reaching under real operation a power output of almost 700 W with artificial solutions and about 330 W with real brackish water and brine [8]. Interestingly, the plant was tested for several months without encountering any performance reduction [401].

Very recently, the RED technology has been also proposed in a closed loop arrangement as a promising way to convert low-temperature waste heat (below 100 °C) into electric energy [402–405]. Two artificial solutions at different salinities are used in a RED unit to produce electricity, exiting as partially mixed streams. These are fed to a regeneration unit powered with low-grade heat where the initial salinity gradient is restored, thereby closing the cycle. Perspective analyses have recently shown that conversion efficiencies up to 10-15% can potentially be achieved in these systems [406]. Closed-loop RED/ED systems have also been proposed for SGP-based energy storage applications, in which energy is stored in the form of salinity gradients. These are converted into electricity in peak demand hours, while, when surplus energy is available, this is used to regenerate the depleted salinity gradient [407, 408].

6.7 RED-ED couplings for low-energy desalination

A very recent development in the field of ED for desalination is represented by the coupling with salinity gradient power or osmotic dilution devices for low-energy desalination [409].

Among the different alternatives that have been theorised, the coupling of RED with ED (or, more in general, with a desalination unit such as RO or even CDI [410]) may result in a technological breakthrough, especially for seawater desalination [9, 411–415]. Figure 26 shows the two main coupling possibilities.

In the first configuration (coupling of unit I and II in the scheme) the RED unit is used as pre-treatment step. When a low-salinity solution, not suitable for drinking water production, is available (e.g. impaired water from a waste water treatment plant) this can be used as the dilute feed of a RED unit, while seawater can be used as the concentrate. In this way, energy is generated from the salinity gradient and seawater exiting the RED device is diluted thanks to the passage of salt into the impaired water, without directly mixing with it. Pre-diluted seawater can thus be fed to a desalination unit in which the energy required to reach the target concentration will be significantly reduced. Additionally, the RED energy generation can be used further to reduce the overall process consumption.

In the second configuration (coupling of unit II and III), the RED unit can be used as a post-treatment in order to mix the brine with impaired water, mitigating disposal issues and recovering energy from the two waste streams. The two configurations can also be used together resulting in the complete scheme of Figure 26.

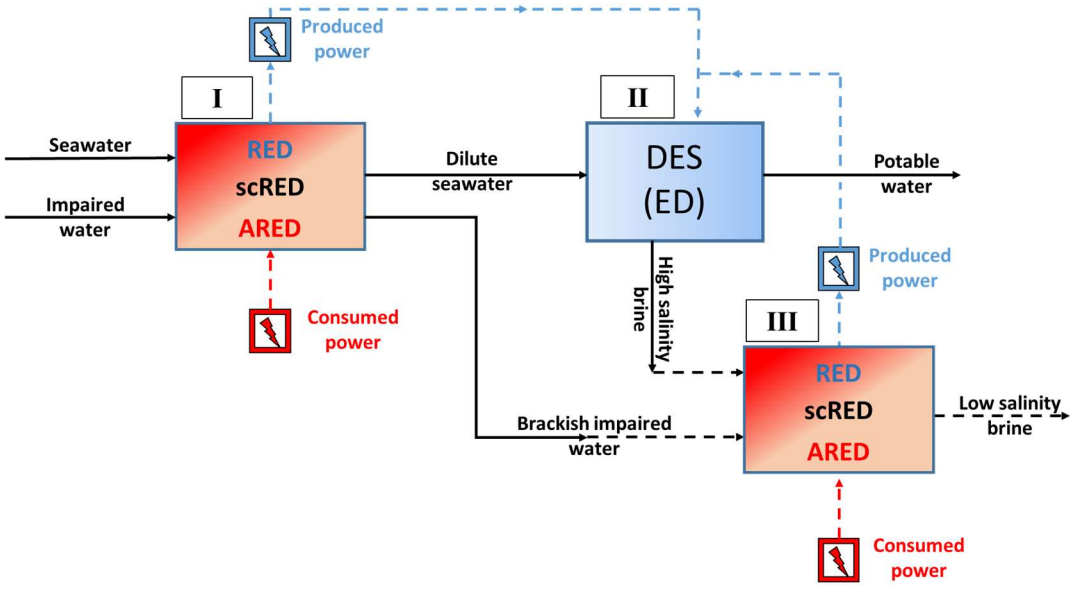

Figure 26. Possibilities of RED/ED integration. Unit I represents RED (or short-circuited RED or assisted RED) used as dilution pre-treatment before feeding the seawater inlet to ED (Unit II). Unit III represents RED used as post-treatment for the recovery of energy from waste brine and relevant dilution with impaired water stream. Coupling Unit I, II and III represents the most complete integration possibility.

Besides the classical SGP operation mode, the RED unit can be operated in two other different modes, thus serving as an enhanced osmotic dilution device [409]:

- Short-circuited Reverse Electrodialysis (scRED)
- Assisted Reverse Electrodialysis (ARED)

In scRED mode the RED unit external load is short-circuited, thus renouncing to energy production in order to maximise the salt transfer rate from the concentrate to the dilute compartment, thus enhancing the dilution effect.

In ARED mode the ionic current inside the scRED unit is further increased by applying an additional external electrical potential to the RED unit, consuming energy in order to "assist" the dilution process, exceeding the maximum achievable current in scRED.

In both cases, the arising benefits are more suitable for the first coupling configuration, where dilution plays a fundamental role in reducing the overall energy consumption, rather than in the second, where dilution is considered beneficial only for environmental reasons.

Due to the complex nature of such processes, it is not possible to determine *a priori* which of the configurations or RED operation mode is the most convenient to achieve the overall minimum energy consumption. In addition to that, pushing the dilution process to high levels will significantly increase the capital costs, mainly depending on the amount of membrane area required. For this reason, optimisation studies are crucial for the development of such hybrid schemes.

In the current literature, the RED-RO coupling has been investigated by several authors, although still at a conceptual level [411–414]. In particular, Li *et al.* [411] explored the RED-RO process through a simple mathematical model, showing that the process can potentially achieve a ~50% lower energy consumption compared to state-of-the-art seawater RO. Vanoppen *et al.* [409] performed a comparative analysis of all RED operational modes coupled to RO, exploring the operational ranges and identifying the benefits in energy consumption reduction. Specific energy consumption below 1 kWh/m^3 were theoretically demonstrated to be feasible, although an important increase of overall membrane area required (including RED membranes) was found in these scenarios.

The RED-ED process has been much less studied, with only one recent publication by Wang *et al.* [415] who focused on the very specific case of desalination of high salinity waste brine containing phenols. They demonstrated an overall reduction of energy consumption of about 30% compared to the stand-alone ED case, though such figures can not be compared with RO, due to the much higher energy consumption of the base case (above 20 kWh/m^3).

It should be noted that, as an alternative to the reverse electrodialysis dilution process, other osmotically-driven processes such as Pressure Retarded Osmosis [414, 416] have been proposed in the literature. Similarly to the RED case, forward osmosis [417–420] and pressure-assisted osmosis [417] have also been proposed for further enhancing the dilution process in order to reduce the overall desalination energy consumption.

7. Conclusions

Electrodialysis represents nowadays an important process option for saline water desalination. The ED history indicates a constant presence in the market, especially in the field of brackish water desalination. A significant interest towards ED and related processes has recently risen due to new IEMs, new industrial actors and several novel proposed applications. In the present review, all these aspects have been addressed aiming at identifying the most important factors influencing the development potentials of this promising class of technologies.

An overview on the state of the art of Ion Exchange Membranes highlighted the key factors currently representing the most important routes for technology developments: 1) the preparation of low resistance and high permselectivity IEMs, when operating with highly saline solutions (which would allow the effective application also to the case of seawater desalination); 2) advances in surface modification techniques, aiming at improving IEMs properties (e.g. permselectivity, but also fouling resistance and overlimiting mass transfer); 3) the development of profiled membranes, allowing the implementation of spacerless ED stacks; 4) the manufacturing cost abatement, which is a key factor for market growth.

Following a comprehensive description of the very complex phenomena governing the process, a detailed review of the most interesting findings on fundamental aspects such as mass transfer, ionic current and fluid flow behaviour in ED and related processes has also been presented. In particular, fluid dynamics and polarisation phenomena have been found to be crucial for process performance. Overlimiting regimes for enhanced mass transfer and reduced membrane area have aroused the interest of researchers and opened room for further investigation and developments. The issues related to stack and channels optimisation (in terms of pressure drop and polarisation phenomena reduction) have led to the new frontier of profiled-IEMs (especially for RED applications), though the study and optimisation of traditional spacers along with the development of alternative geometries (multi-layer, twisted, etc.) is still the objective of several investigations. Another interesting topic concerns the study of oscillating regimes (oscillating current or flow rate), which have been found to improve process performance under certain conditions. Finally, the large-scale study of inlet-outlet distribution manifolds has identified how critical these can be for the optimal flow distribution in feed channels. Misdistribution problems, in fact, can cause significant losses in terms of resistance increase and non-Ohmic voltage drops, in addition to fluid dynamics issues such as solution leakages. Thus, modelling and experimental investigations have pointed out possible solutions for improving manifolds layout, opening the route to novel and optimised stack designs.

The subsequent part of this review has focused on the analysis of process-modelling tools developed so far. These can be divided into a class of simplified models, proposed for preliminary design purposes, and a wider class of advanced modelling tools, more recently proposed for simulation, design and optimisation of ED or other electromembrane processes. These latter are often based on a multi-scale approach, merging the information originated from the CFD or experimental characterisation of mass and momentum transport phenomena with higher-scale mass balances and phenomenological equations. In all cases, the complexity of phenomena governing these processes highlights the need for further development of advanced modelling and optimisation tools for process adaptation to the wide spectrum of novel applications for all ED-related technologies.

Among the main boosters for ED technologies, the development of special applications, based on the use of IEMs, has been critically analysed. This has highlighted how some of these novel applications, such as RED, SED, EDM, shock ED, etc., are still raising the interest of researchers and industrial actors, often leading to the construction of pilot installations and, in some cases, to the first commercialisation examples of such new ideas. Interestingly, this applies not only to the field of saline water desalination, but more in general to water treatment for food, pharmaceutical and electronics industries, industrial brines valorisation, minerals recovery and energy generation from salinity gradients. All this is strongly promoting the overall development of IEMs-based technologies, thus projecting ED and related processes towards a new horizon of applications and new markets.

Acknowledgments

Part of this work has been carried out thanks to the financial support of the European Union's Horizon 2020 research and innovation programme, within the REvivED water project (www.revivedwater.eu), Grant Agreement no. 685579.

Notation

List of abbreviations

AC	Alternate Current
AEM	Anion-Exchange Membrane
BPM	BiPolar Membrane
CDI	Capacitive DeIonisation
CEDI	Continuous ElectroDeIonisation
CEM	Cation-Exchange Membrane
DBL	Diffusion Boundary Layer
DC	Direct Current
DES	DESalination
EBPM	ElectroDialysis with Bipolar Membrane
ED	ElectroDialysis
EDI	Electro DeIonisation
EDL	Electrical Double Layer
EDM	ElectroDialysis Metathesis
EDR	ElectroDialysis Reversal
EDTA	EthyleneDiamineTetraAcetic
EIS	Electrical Impedance Spectroscopy
ER	Electrical Resistance
IEC	Ion-Exchange Capacity
IEM	Ion-Exchange Membrane
IPN	InterPenetrating Network
MV	MonoValent selective membrane
PEF	Pulsed Electrical Field
PV	PhotoVoltaic
RED	Reverse ElectroDialysis
RO	Reverse Osmosis
SED	SelElectroDialyis
SGP	Salinity Gradient Power
sIPN	Semi-InterPenetrating Network
TMS	Teorell-Meyer-Sievers
TRL	Technological Readiness Level
ZLD	Zero Liquid Discharge

List of symbols

A	Membrane area (m^2)
A^{cp}	Cell pair membrane area (m^2)
b	Membrane width (m)
C	Concentration (mol/m^3)
D	Diffusion coefficient (m^2/s)
F	Faraday's constant (C/mol)
F_S	Shadow factor
f	Friction factor
h	Thickness (m)
I	Current (A)
i	Current density (A/m^2)
i_{lim}	Limiting current density (A/m^2)
J	Flux ($mol/m^2/s$)
J'	Volumetric flux ($m^3/m^2/s$)
L	Channel length (m)
n_h	Hydration number
P_{el}	Electrical power consumption (W)
P_{pump}	Pumping power consumption (W)
Δp	Pressure drop (Pa)
Q	Volumetric flow rate (m^3/s)
R	Universal gas constant (J/mol/K)
r	Areal electrical resistance (Ωm^2)
Re	Reynolds number
Sc	Schmidt number
SEC_{el}	Specific energy consumption (J/m^3)
Sh	Sherwood number
$sSEC_{el}$	Salt-specific energy consumption (J/mol)
T^{iem}	Integral transport number within the membrane
T	Temperature (K)
t	Migrational transport number
u	Velocity (m/s)

ΔV	Voltage drop over a cell pair (V)
x	Coordinate in the direction of the main flow
y	Coordinate normal to the membrane surface
z	Valence of ion

Greek letters

α	Permselectivity
γ	Activity coefficient
δ	Diffusion boundary layer thickness (m)
ε	Dielectric constant (F/m)
ζ	Current utilisation factor (or current efficiency)
η	Voltage drop (V)
θ	Polarization coefficient
κ	Conductivity (S/m)
λ	Equivalent conductivity (Sm^2/mol)
σ	Porosity
τ	Time (s)
φ	Electric potential (V)
χ	Pump efficiency

Subscripts and superscripts

AEM	Anion-exchange membrane
$bulk$	Solution bulk
C	Concentrate
CEM	Cation-exchange membrane
COP	Concentration Overpotential
co	Co-ion
$counter$	Counter-ion
D	Dilute
DBL	Diffusion boundary layer
$diff$	Diffusive
Don	Donnan

i	Species *i* (cation or anion)
iem	Ion-exchange membrane
L	Left
Ohm	Ohmic
R	Right
SOL	Solution (dilute or concentrate)

References

[1] IDA, Desalination YearBook 2016-2017, Water Desalination Report, 2017.

[2] J. Veerman, M. Saakes, S. J. Metz, G. J. Harmsen, Reverse electrodialysis: A validated process model for design and optimization, Chem. Eng. J. 166 (2011) 256–268. doi:10.1016/j.cej.2010.10.071.

[3] D. A. Vermaas, M. Saakes, K. Nijmeijer, Doubled power density from salinity gradients at reduced intermembrane distance, Environ. Sci. Technol. 45 (2011) 7089–7095. doi:10.1021/es2012758.

[4] D. A. Vermaas, M. Saakes, K. Nijmeijer, Power generation using profiled membranes in reverse electrodialysis, J. Memb. Sci. 385–386 (2011) 234–242. doi:10.1016/j.memsci.2011.09.043.

[5] A. Daniilidis, D. A. Vermaas, R. Herber, K. Nijmeijer, Experimentally obtainable energy from mixing river water, seawater or brines with reverse electrodialysis, Renew. Energy. 64 (2014) 123–131. doi:10.1016/j.renene.2013.11.001.

[6] M. La Cerva, M. Di Liberto, L. Gurreri, A. Tamburini, A. Cipollina, G. Micale, M. Ciofalo, Coupling CFD with simplified 1-D models to predict the performance of reverse electrodialysis stacks, J. Memb. Sci. 541 (2017) 595–610. doi:10.1016/j.memsci.2017.07.030.

[7] N. Y. Yip, D. A. Vermaas, K. Nijmeijer, M. Elimelech, Thermodynamic, Energy Efficiency, and Power Density Analysis of Reverse Electrodialysis Power Generation with Natural Salinity Gradients, Environ. Sci. Technol. 48 (2014) 4925–4936. doi:10.1021/es5005413.

[8] M. Tedesco, A. Cipollina, A. Tamburini, G. Micale, Towards 1 kW power production in a reverse electrodialysis pilot plant with saline waters and concentrated brines, J. Memb. Sci. 522 (2017) 226–236. doi:10.1016/j.memsci.2016.09.015.

[9] E. U., REvivED water, (2016). https://www.revivedwater.eu/ (accessed November 28, 2017).

[10] H. Strathmann, Electrodialysis, a mature technology with a multitude of new applications, Desalination. 264 (2010) 268–288. doi:10.1016/j.desal.2010.04.069.

[11] T. Yamabe, Present status of electrodialysis in Japan, Desalination. 23 (1977) 195–202. doi:10.1016/S0011-9164(00)82522-9.

[12] E. Vera, J. Ruales, M. Dornier, J. Sandeaux, R. Sandeaux, G. Pourcelly, Deacidification of clarified passion fruit juice using different configurations of electrodialysis, J. Chem. Technol. Biotechnol. 78 (2003) 918–925. doi:10.1002/jctb.827.

[13] M. Fidaleo, M. Moresi, Electrodialysis Applications in The Food Industry, Adv. Food Nutr. Res. 51 (2006) 265–360. doi:10.1016/S1043-4526(06)51005-8.

[14] F. Gonçalves, C. Fernandes, P. Cameira dos Santos, M. N. de Pinho, Wine tartaric stabilization by electrodialysis and its assessment by the saturation temperature, J. Food Eng. 59 (2003) 229–235. doi:10.1016/S0260-8774(02)00462-4.

[15] F. Fu, Q. Wang, Removal of heavy metal ions from wastewaters: A review, J. Environ. Manage. 92 (2011) 407–418. doi:10.1016/j.jenvman.2010.11.011.

[16] L. Marder, A. M. Bernardes, J. Zoppas Ferreira, Cadmium electroplating wastewater treatment using a laboratory-scale electrodialysis system, Sep. Purif. Technol. 37 (2004) 247–255. doi:10.1016/j.seppur.2003.10.011.

[17] M. A. Acheampong, R. J. W. Meulepas, P. N. L. Lens, Removal of heavy metals and cyanide from gold mine wastewater, J. Chem. Technol. Biotechnol. 85 (2010) 590–613. doi:10.1002/jctb.2358.

[18] M. R. Adiga, S. K. Adhikary, P. K. Narayanan, W. P. Harkare, S. D. Gomkale, K. P. Govindan, Performance analysis of photovoltaic electrodialysis desalination plant at Tanote in Thar desert, Desalination. 67 (1987) 59–66. doi:10.1016/0011-9164(87)90232-3.

[19] J. M. Veza, B. Penate, F. Castellano, Electrodialysis desalination designed for off-grid wind energy, Desalination. 160 (2004) 211–221. doi:10.1016/S0011-9164(04)90024-0.

[20] K. Nagasubramanian, F. P. Chlanda, K. J. Liu, Use of bipolar membranes for generation of acid and base - an engineering and economic analysis, J. Memb. Sci. 2 (1977) 109–124. doi:10.1016/S0376-7388(00)83237-8.

[21] L. Bazinet, D. Ippersiel, C. Gendron, J. René-Paradis, C. Tétrault, J. Beaudry, M. Britten, B. Mahdavi, J. Amiot, F. Lamarche, Bipolar Membrane Electroacidification of Demineralized Skim Milk, J. Agric. Food Chem. 49 (2001) 2812–2818. doi:10.1021/jf000982r.

[22] X. Tongwen, Electrodialysis processes with bipolar membranes (EDBM) in environmental protection—a review, Resour. Conserv. Recycl. 37 (2002) 1–22. doi:10.1016/S0921-3449(02)00032-0.

[23] V. J. Frilette, Preparation and Characterization of Bipolar Ion Exchange Membranes, J. Phys. Chem. 60 (1956) 435–439. doi:10.1021/j150538a013.

[24] Y. C. Chiao, F. P. Chlanda, K. N. Mani, Bipolar membranes for purification of acids and bases, J. Memb. Sci. 61 (1991) 239–252. doi:10.1016/0376-7388(91)80018-2.

[25] L. Bazinet, F. Lamarche, D. Ippersiel, Bipolar-membrane electrodialysis: Applications of electrodialysis in the food industry, Trends Food Sci. Technol. 9 (1998) 107–113. doi:10.1016/S0924-2244(98)00026-0.

[26] M. Reig, C. Valderrama, O. Gibert, J. L. Cortina, Selectrodialysis and bipolar membrane electrodialysis combination for industrial process brines treatment: Monovalent-divalent ions

separation and acid and base production, Desalination. 399 (2016) 88–95. doi:10.1016/j.desal.2016.08.010.

[27] Y. Zhang, S. Paepen, L. Pinoy, B. Meesschaert, B. Van der Bruggen, Selectrodialysis: Fractionation of divalent ions from monovalent ions in a novel electrodialysis stack, Sep. Purif. Technol. 88 (2012) 191–201. doi:10.1016/j.seppur.2011.12.017.

[28] A. T. K. Tran, Phosphate Pre-Concentrate from Wastewater for Phosphate Recovery by Selectrodialysis, in: Institute of Electrical and Electronics Engineers Inc., 2016: pp. 55–58. doi:10.1109/GTSD.2016.23.

[29] Y. Zhang, E. Desmidt, A. Van Looveren, L. Pinoy, B. Meesschaert, B. Van Der Bruggen, Phosphate separation and recovery from wastewater by novel electrodialysis, Environ. Sci. Technol. 47 (2013) 5888–5895. doi:10.1021/es4004476.

[30] C. Alhéritière, W. R. Ernst, T. A. Davis, Metathesis of magnesium and solium salt systems by electrodialysis, Desalination. 115 (1998) 189–198. doi:10.1016/S0011-9164(98)00037-X.

[31] R. Bond, B. Batchelor, T. A. Davis, B. Klayman, Zero liquid discharge desalination of brackish water with an innovative form of electrodialysis: Electrodialysis metathesis, in: Florida Water Resour. J., 2011: pp. 36–44.

[32] S. K. Thampy, B. S. Joshi, K. P. Govindan, Preparation of potassium bicarbonate by electrodialysis technique, Indian J. Technol. 12 (1985) 454–457.

[33] L. M. Camacho, J. A. Fox, J. O. Ajedegba, Optimization of electrodialysis metathesis (EDM) desalination using factorial design methodology, Desalination. 403 (2017) 136–143. doi:10.1016/j.desal.2016.07.028.

[34] V. A. Shaposhnik, K. Kesore, An early history of electrodialysis with permselective membranes, J. Memb. Sci. 136 (1997) 35–39. doi:10.1016/S0376-7388(97)00149-X.

[35] V. D. Grebenyuk, O. V. Grebenyuk, Electrodialysis: From an idea to realization, Russ. J. Electrochem. 38 (2002) 806–809. doi:10.1023/A:1016897224948.

[36] F. G. Donnan, The Theory of Membrane Equilibria., Chem. Rev. 1 (1924) 73–90. doi:10.1021/cr60001a003.

[37] T. Teorell, An Attempt to Formulate a Quantitative Theory of Membrane Permeability, Exp. Biol. Med. 33 (1935) 282–285. doi:10.3181/00379727-33-8339C.

[38] E. R. Reahl, Half A Century of Desalination With Electrodialysis, GE Water Process Technol. (2004) 1–617.

[39] G. Belfort, G. A. Guter, An experimental study of electrodialysis hydrodynamics, Desalination. 10 (1972) 221–262. doi:10.1016/S0011-9164(00)82001-9.

[40] G. Grossman, A. A. Sonin, Experimental study of the effects of hydrodynamics and membrane fouling in electrodialysis, Desalination. 10 (1972) 157–180. doi:10.1016/S0011-9164(00)80084-3.

[41] J.-M. Chiapello, M. Bernard, Improved spacer design and cost reduction in an electrodialysis system, J. Memb. Sci. 80 (1993) 251–256. doi:10.1016/0376-7388(93)85149-Q.

[42] A. H. Galama, M. Saakes, H. Bruning, H. H. M. Rijnaarts, J. W. Post, Seawater predesalination with electrodialysis, Desalination. 342 (2014) 61–69. doi:10.1016/j.desal.2013.07.012.

[43] M. Demircioglu, N. Kabay, I. Kurucaovali, E. Ersoz, Demineralization by electrodialysis (ED) - Separation performance and cost comparison for monovalent salts, Desalination. 153 (2003) 329–333. doi:10.1016/S0011-9164(02)01119-0.

[44] E. J. Parsi, Large Electrodialysis Stack Development, Desalination. 19 (1976) 139–151. doi:10.1016/S0011-9164(00)88024-8.

[45] A. von Gottberg, New High-Performance Spacers in Electro- Dialysis Reversal (EDR) Systems, in: Proc. 1998 AWWA Anu. Conf., Dallas, Texas, 1998.

[46] O. Kedem, Reduction of polarization in electrodialysis by ion-conducting spacers, Desalination. 16 (1975) 105–118. doi:10.1016/S0011-9164(00)84095-3.

[47] O. Kedem, Y. Maoz, Ion conducting spacer for improved ed, Desalination. 19 (1976) 465–470. doi:10.1016/S0011-9164(00)88055-8.

[48] Y. Winograd, A. Solan, M. Toren, Mass transfer in narrow channels in the presence of turbulence promoters, Desalination. 13 (1973) 171–186. doi:10.1016/S0011-9164(00)82043-3.

[49] H. Strathmann, Ion-exchange membrane separation processes, First ed., Elsevier, Amsterdam, 2004.

[50] C. Larchet, V. I. Zabolotsky, N. Pismenskaya, V. V. Nikonenko, A. Tskhay, K. Tastanov, G. Pourcelly, Comparison of different ED stack conceptions when applied for drinking water

production from brackish waters, Desalination. 222 (2008) 489–496. doi:10.1016/j.desal.2007.02.067.

[51] B. Van der Bruggen, Advances in electrodialysis for water treatment, in: A. Basile, A. Cassano, N.K. Rastogi (Eds.), Adv. Membr. Technol. Water Treat. Mater. Process. Appl., Woodhead Publishing, 2015: pp. 185–203. doi:10.1016/B978-1-78242-121-4.00006-X.

[52] D. A. Vermaas, S. Bajracharya, B. B. Sales, M. Saakes, B. Hamelers, K. Nijmeijer, Clean energy generation using capacitive electrodes in reverse electrodialysis, Energy Environ. Sci. 6 (2013) 643–651. doi:10.1039/C2EE23562E.

[53] O. N. Demirer, R. L. Clifton, C. A. R. Perez, R. Naylor, C. Hidrovo, Characterization of Ion Transport and -Sorption in a Carbon Based Porous Electrode for Desalination Purposes, J. Fluids Eng. 135 (2013) 41201–41208.

[54] D. A. Vermaas, M. Saakes, K. Nijmeijer, Capacitive Electrodes for Energy Generation by Reverse Electrodialysis, Procedia Eng. 44 (2012) 496–497. doi:10.1016/j.proeng.2012.08.463.

[55] Y. Tanaka, Regularity in ion-exchange membrane characteristics and concentration of sea water, J. Memb. Sci. 163 (1999) 277–287. doi:10.1016/S0376-7388(99)00169-6.

[56] A. V. Demin, V. I. Zabolotskii, Model verification of limiting concentration by electrodialysis of an electrolyte solution, Russ. J. Electrochem. 44 (2008) 1058–1064. doi:10.1134/S1023193508090115.

[57] H. Strathmann, A. Grabowski, G. Eigenberger, Ion-Exchange Membranes in the Chemical Process Industry, Ind. Eng. Chem. Res. 52 (2013) 10364–10379. doi:10.1021/ie4002102.

[58] A. H. Galama, J. W. Post, M. A. Cohen Stuart, P. M. Biesheuvel, Validity of the Boltzmann equation to describe Donnan equilibrium at the membrane–solution interface, J. Memb. Sci. 442 (2013) 131–139. doi:10.1016/j.memsci.2013.04.022.

[59] J. Ran, L. Wu, Y. He, Z. Yang, Y. Wang, C. Jiang, L. Ge, E. Bakangura, T. Xu, Ion exchange membranes: New developments and applications, J. Memb. Sci. 522 (2017) 267–291. doi:10.1016/j.memsci.2016.09.033.

[60] N. P. Berezina, N. A. Kononenko, O. A. Dyomina, N. P. Gnusin, Characterization of ion-exchange membrane materials: Properties vs structure, Adv. Colloid Interface Sci. 139 (2008) 3–28. doi:10.1016/j.cis.2008.01.002.

[61] C. Larchet, L. Dammak, B. Auclair, S. Parchikov, V. V. Nikonenko, A simplified procedure for ion-exchange membrane characterisation, New J. Chem. 28 (2004) 1260. doi:10.1039/b316725a.

[62] K. Kontturi, M. Lasse, J. A. Manzanares, Ionic Transport Processes in Electrochemistry and Membrane Science, Oxford University Press Inc., New York, 2008. doi:10.1093/acprof:oso/9780199533817.001.0001.

[63] N. Lakshminarayanaiah, Transport phenomena in artificial membranes, Chem. Rev. 65 (1965) 492–565.

[64] A. H. Galama, J. W. Post, H. V. M. Hamelers, V. V. Nikonenko, P. M. Biesheuvel, On the Origin of the Membrane Potential Arising Across Densely Charged Ion Exchange Membranes:

How Well Does the Teorell-Meyer-Sievers Theory Work?, J. Membr. Sci. Res. 2 (2016) 128–140.

[65] M. B. Kristensen, A. Bentien, M. Tedesco, J. Catalano, Counter-ion transport number and membrane potential in working membrane systems, J. Colloid Interface Sci. 504 (2017) 800–813. doi:10.1016/j.jcis.2017.06.010.

[66] R. K. Nagarale, G. S. Gohil, V. K. Shahi, Recent developments on ion-exchange membranes and electro-membrane processes, Adv. Colloid Interface Sci. 119 (2006) 97–130. doi:10.1016/j.cis.2005.09.005.

[67] G. E. Molau, Heterogeneous ion-exchange membranes, J. Memb. Sci. 8 (1981) 309–330. doi:10.1016/S0376-7388(00)82318-2.

[68] W. Garcia-Vasquez, L. Dammak, C. Larchet, V. V. Nikonenko, N. Pismenskaya, D. Grande, Evolution of anion-exchange membrane properties in a full scale electrodialysis stack, J. Memb. Sci. 446 (2013) 255–265. doi:10.1016/j.memsci.2013.06.042.

[69] C. Genies, R. Mercier, B. Sillion, N. Cornet, G. Gebel, M. Pineri, Soluble sulfonated naphthalenic polyimides as materials for proton exchange membranes, Polymer (Guildf). 42 (2001) 359–373. doi:10.1016/S0032-3861(00)00384-0.

[70] T. Sata, Studies on anion exchange membranes having permselectivity for specific anions in electrodialysis - Effect of hydrophilicity of anion exchange membranes on permselectivity of anions, J. Memb. Sci. 167 (2000) 1–31. doi:10.1016/S0376-7388(99)00277-X.

[71] V. K. Shahi, S. K. Thampy, R. Rangarajan, Preparation and electrochemical characterization of sulfonated interpolymer of polyethylene and styrene–divinylbenzene copolymer membranes, React. Funct. Polym. 46 (2000) 39–47. doi:10.1016/S1381-5148(00)00031-6.

[72] Y. Woo, S. Y. Oh, Y. S. Kang, B. Jung, Synthesis and characterization of sulfonated polyimide membranes for direct methanol fuel cell, J. Memb. Sci. 220 (2003) 31–45. doi:10.1016/S0376-7388(03)00185-6.

[73] V. I. Zabolotsky, V. V. Nikonenko, Effect of structural membrane inhomogeneity on transport properties, J. Memb. Sci. 79 (1993) 181–198. doi:10.1016/0376-7388(93)85115-D.

[74] C. Larchet, S. Nouri, B. Auclair, L. Dammak, V. V. Nikonenko, Application of chronopotentiometry to determine the thickness of diffusion layer adjacent to an ion-exchange

membrane under natural convection, Adv. Colloid Interface Sci. 139 (2008) 45–61. doi:10.1016/j.cis.2008.01.007.

[75] A. H. Galama, D. A. Vermaas, J. Veerman, M. Saakes, H. H. M. Rijnaarts, J. W. Post, K. Nijmeijer, Membrane resistance: The effect of salinity gradients over a cation exchange membrane, J. Memb. Sci. 467 (2014) 279–291. doi:10.1016/j.memsci.2014.05.046.

[76] J. Kamcev, R. Sujanani, E.-S. Jang, N. Yan, N. Moe, D. R. Paul, B. D. Freeman, Salt concentration dependence of ionic conductivity in ion exchange membranes, J. Memb. Sci. 547 (2018) 123–133. doi:10.1016/J.MEMSCI.2017.10.024.

[77] T. Xu, Ion exchange membranes: State of their development and perspective, J. Memb. Sci. 263 (2005) 1–29. doi:10.1016/j.memsci.2005.05.002.

[78] B. D. Gupta, A. Chapiró, Preparation of ion-exchange membranes by grafting acrylic acid into pre-irradiated polymer films-1. grafting into polyethylene, Eur. Polym. J. 25 (1989) 1137–1143. doi:10.1016/0014-3057(89)90170-5.

[79] J.-L. Gineste, J.-L. Garaud, G. Pourcelly, Grafting of acrylic acid with diethyleneglycol–dimethacrylate onto radioperoxided polyethylene, J. Appl. Polym. Sci. 48 (1993) 2113–2122. doi:10.1002/app.1993.070481206.

[80] E.-S. A. Hegazy, N. H. Taher, A. R. Ebaid, Preparation and some properties of hydrophilic membranes obtained by radiation grafting of methacrylic acid onto fluorinated polymers, J. Appl. Polym. Sci. 41 (1990) 2637–2647. doi:10.1002/app.1990.070411111.

[81] S.-H. Choi, Y. C. Nho, Radiation-induced graft copolymerization of binary monomer mixture containing acrylonitrile onto polyethylene films, Radiat. Phys. Chem. 58 (2000) 157–168. doi:10.1016/S0969-806X(99)00367-9.

[82] J. A. Horsfall, K. V. Lovell, Synthesis and characterization of acrylic acid-grafted hydrocarbon and fluorocarbon polymers with the simultaneous or mutual grafting technique, J. Appl. Polym. Sci. 87 (2003) 230–243. doi:10.1002/app.11358.

[83] B. Gupta, F. N. Büchi, G. G. Scherer, A. Chapiró, Crosslinked ion exchange membranes by radiation grafting of styrene/divinylbenzene into FEP films, J. Memb. Sci. 118 (1996) 231–238. doi:10.1016/0376-7388(96)00093-2.

[84] M. V. Rouilly, E. R. Kötz, O. Haas, G. G. Scherer, A. Chapiró, Proton exchange membranes prepared by simultaneous radiation grafting of styrene onto Teflon-FEP films. Synthesis and characterization, J. Memb. Sci. 81 (1993) 89–95. doi:10.1016/0376-7388(93)85033-S.

[85] M. M. Nasef, H. Saidi, A. M. Dessouki, E. M. EI-Nesr, Radiation-induced grafting of styrene onto poly(tetrafluoroethylene) (PTFE) films. I. Effect of grafting conditions and properties of the grafted films, Polym. Int. 49 (2000) 399–406. doi:10.1002/(SICI)1097-0126(200004)49:4<399::AID-PI393>3.0.CO;2-W.

[86] T. Yamaki, M. Asano, Y. Maekawa, Y. Morita, T. Suwa, J. Chen, N. Tsubokawa, K. Kobayashi, H. Kubota, M. Yoshida, Radiation grafting of styrene into crosslinked PTEE films and subsequent sulfonation for fuel cell applications, Radiat. Phys. Chem. 67 (2003) 403–407. doi:10.1016/S0969-806X(03)00075-6.

[87] H. Herman, R. C. Slade, J. R. Varcoe, The radiation-grafting of vinylbenzyl chloride onto poly(hexafluoropropylene-co-tetrafluoroethylene) films with subsequent conversion to alkaline anion-exchange membranes: optimisation of the experimental conditions and characterisation, J. Memb. Sci. 218 (2003) 147–163. doi:10.1016/S0376-7388(03)00167-4.

[88] W. Lee, K. Saito, S. Furusaki, T. Sugo, K. Makuuchi, Design of urea-permeable anion-exchange membrane by radiation-induced graft polymerization, J. Memb. Sci. 81 (1993) 295–305. doi:10.1016/0376-7388(93)85181-U.

[89] R. K. Nagarale, G. S. Gohil, V. K. Shahi, R. Rangarajan, Preparation and electrochemical characterization of sulfonated polysulfone cation-exchange membranes: Effects of the solvents on the degree of sulfonation, J. Appl. Polym. Sci. 96 (2005) 2344–2351. doi:10.1002/app.21630.

[90] F. Wang, M. A. Hickner, Y. S. Kim, T. A. Zawodzinski, J. E. McGrath, Direct polymerization of sulfonated poly(arylene ether sulfone) random (statistical) copolymers: candidates for new proton exchange membranes, J. Memb. Sci. 197 (2002) 231–242. doi:10.1016/S0376-7388(01)00620-2.

[91] M.-S. Kang, Electrochemical characterization of sulfonated poly(arylene ether sulfone) (S-PES) cation-exchange membranes, J. Memb. Sci. 216 (2003) 39–53. doi:10.1016/S0376-7388(03)00045-0.

[92] J. Kerres, W. Cui, S. Reichle, New Sulfonated Eengineering Polymers via the Metalation Route. II. Sulfinated/Sulfonated Poly(ether sulfone) PSU Udel via metalation-sulfination-

oxidation, J. Polym. Sci. Part A Polym. Chem. 34 (1996) 2421–2438. doi:10.1002/(SICI)1099-0518(19980715)36:9<1441::AID-POLA12>3.0.CO;2-4.

[93] G.-J. Hwang, H. Ohya, Preparation of anion exchange membrane based on block copolymers. Part II: the effect of the formation of macroreticular structure on the membrane properties, J. Memb. Sci. 149 (1998) 163–169. doi:10.1016/S0376-7388(98)00194-X.

[94] G.-J. Hwang, H. Ohya, T. Nagai, Ion exchange membrane based on block copolymers. Part III: preparation of cation exchange membrane, J. Memb. Sci. 156 (1999) 61–65. doi:10.1016/S0376-7388(98)00331-7.

[95] P. Zschocke, D. Quellmalz, Novel ion exchange membranes based on an aromatic polyethersulfone, J. Memb. Sci. 22 (1985) 325–332. doi:10.1016/S0376-7388(00)81290-9.

[96] R. K. Nagarale, V. K. Shahi, R. Rangarajan, Preparation of polyvinyl alcohol–silica hybrid heterogeneous anion-exchange membranes by sol–gel method and their characterization, J. Memb. Sci. 248 (2005) 37–44. doi:10.1016/j.memsci.2004.09.025.

[97] P. V Vyas, B. Shah, G. Trivedi, P. Ray, S. K. Adhikary, R. Rangarajan, Characterization of heterogeneous anion-exchange membrane, J. Memb. Sci. 187 (2001) 39–46. doi:10.1016/S0376-7388(00)00613-X.

[98] X. Wu, G. He, S. Gu, Z. Hu, P. Yao, Novel interpenetrating polymer network sulfonated poly (phthalazinone ether sulfone ketone)/polyacrylic acid proton exchange membranes for fuel cell, J. Memb. Sci. 295 (2007) 80–87. doi:10.1016/j.memsci.2007.02.039.

[99] C. W. Lin, Y. F. Huang, A. M. Kannan, Semi-interpenetrating network based on cross-linked poly(vinyl alcohol) and poly(styrene sulfonic acid-co-maleic anhydride) as proton exchange

fuel cell membranes, J. Power Sources. 164 (2007) 449–456. doi:10.1016/j.jpowsour.2006.10.081.

[100] J. Wang, R. He, Q. Che, Anion exchange membranes based on semi-interpenetrating polymer network of quaternized chitosan and polystyrene, J. Colloid Interface Sci. 361 (2011) 219–225. doi:10.1016/j.jcis.2011.05.039.

[101] Y.-J. Choi, M.-S. Kang, S.-H. Moon, Characterization of semi-interpenetrating polymer network polystyrene cation-exchange membranes, J. Appl. Polym. Sci. 88 (2003) 1488–1496. doi:10.1002/app.11860.

[102] L. Lebrun, E. Da Silva, M. Metayer, Elaboration of ion-exchange membranes with semi-interpenetrating polymer networks containing poly(vinyl alcohol) as polymer matrix, J. Appl. Polym. Sci. 84 (2002) 1572–1580. doi:10.1002/app.10420.

[103] L. Lebrun, N. Follain, M. Metayer, Elaboration of a new anion-exchange membrane with semi-interpenetrating polymer networks and characterisation, Electrochim. Acta. 50 (2004) 985–993. doi:10.1016/j.electacta.2004.07.040.

[104] H.-P. Brack, H. G. Bührer, L. Bonorand, G. G. Scherer, Grafting of pre-irradiated poly(ethylene-alt-tetrafluoroethylene) films with styrene: influence of base polymer film properties and processing parameters, J. Mater. Chem. 10 (2000) 1795–1803. doi:10.1039/b0018511.

[105] G. K. Kostov, O. Matsuda, S. Machi, Y. Tabata, Radiation synthesis of ion-exchange carboxylic fluorine containing membranes, J. Memb. Sci. 68 (1992) 133–140. doi:10.1016/0376-7388(92)80156-E.

[106] G. K. Kostov, A. N. Atanassov, Properties of cation-exchange membranes prepared by radiation grafting of acrylic acid onto tetrafluoroethylene–ethylene copolymers, J. Appl. Polym. Sci. 47 (1993) 1269–1276. doi:10.1002/app.1993.070470715.

[107] G. K. Kostov, S. C. Turmanova, Radiation-initiated graft copolymerization of 4-vinylpyridine onto polyethylene and polytetrafluoroethylene films and anion-exchange membranes therefrom, J. Appl. Polym. Sci. 64 (1997) 1469–1475. doi:10.1002/(SICI)1097-4628(19970523)64:8<1469::AID-APP3>3.0.CO;2-F.

[108] M. M. Nasef, H. Saidi, H. M. Nor, Proton exchange membranes prepared by simultaneous radiation grafting of styrene onto poly(tetrafluoroethylene-co-hexafluoropropylene) films. I.

Effect of grafting conditions, J. Appl. Polym. Sci. 76 (2000) 220–227. doi:10.1002/(SICI)1097-4628(20000411)76:2<220::AID-APP11>3.0.CO;2-M.

[109] K. A. Mauritz, D. A. Mountz, D. A. Reuschle, R. I. Blackwell, Self-assembled organic/inorganic hybrids as membrane materials, Electrochim. Acta. 50 (2004) 565–569. doi:10.1016/j.electacta.2003.09.051.

[110] J. Zou, Y. Zhao, W. Shi, Preparation and properties of proton conducting organic–inorganic hybrid membranes based on hyperbranched aliphatic polyester and phosphoric acid, J. Memb. Sci. 245 (2004) 35–40. doi:10.1016/j.memsci.2004.07.015.

[111] I. Gautier-Luneau, A. Denoyelle, J. Y. Sanchez, C. Poinsignon, Organic—inorganic protonic polymer electrolytes as membrane for low-temperature fuel cell, Electrochim. Acta. 37 (1992) 1615–1618. doi:10.1016/0013-4686(92)80122-3.

[112] L. Depre, J. Kappel, M. Popall, Inorganic–organic proton conductors based on alkylsulfone functionalities and their patterning by photoinduced methods, Electrochim. Acta. 43 (1998) 1301–1306. doi:10.1016/S0013-4686(97)10034-2.

[113] L. Depre, M. Ingram, C. Poinsignon, M. Popall, Proton conducting sulfon/sulfonamide functionalized materials based on inorganic–organic matrices, Electrochim. Acta. 45 (2000) 1377–1383. doi:10.1016/S0013-4686(99)00346-1.

[114] R. K. Nagarale, G. S. Gohil, V. K. Shahi, R. Rangarajan, Organic−Inorganic Hybrid Membrane: Thermally Stable Cation-Exchange Membrane Prepared by the Sol−Gel Method, Macromolecules. 37 (2004) 10023–10030. doi:10.1021/ma048404p.

[115] A. Walcarius, Electrochemical Applications of Silica-Based Organic−Inorganic Hybrid Materials, Chem. Mater. 13 (2001) 3351–3372. doi:10.1021/cm0110167.

[116] D. S. Kim, H. B. Park, J. W. Rhim, Y. M. Lee, Proton conductivity and methanol transport behavior of cross-linked PVA/PAA/silica hybrid membranes, Solid State Ionics. 176 (2005) 117–126. doi:10.1016/j.ssi.2004.07.011.

[117] D. S. Kim, H. B. Park, J. W. Rhim, Y. M. Lee, Preparation and characterization of crosslinked PVA/SiO2 hybrid membranes containing sulfonic acid groups for direct methanol fuel cell applications, J. Memb. Sci. 240 (2004) 37–48. doi:10.1016/j.memsci.2004.04.010.

[118] H. Ohya, R. Paterson, T. Nomura, S. McFadzean, T. Suzuki, M. Kogure, Properties of new inorganic membranes prepared by metal alkoxide methods Part I: A new permselective cation

exchange membrane based on Si/Ta oxides, J. Memb. Sci. 105 (1995) 103–112. doi:10.1016/0376-7388(95)00054-G.

[119] M. Kogure, H. Ohya, R. Paterson, M. Hosaka, J.-J. Kim, S. McFadzean, Properties of new inorganic membranes prepared by metal alkoxide methods Part II: New inorganic-organic anion-exchange membranes prepared by the modified metal alkoxide methods with silane coupling agents, J. Memb. Sci. 126 (1997) 161–169. doi:10.1016/S0376-7388(96)00289-X.

[120] J. H. Hao, C. Chen, L. Li, L. Yu, W. Jiang, Preparation of Bipolar Membranes (I), J. Appl. Polym. Sci. 80 (2001) 1658–1663. doi:10.1002/app.1260.

[121] R. Q. Fu, T. W. Xu, W. H. Yang, Z. X. Pan, Preparation of a mono-sheet bipolar membrane by simultaneous irradiation grafting polymerization of acrylic acid and chloromethylstyrene, J. Appl. Polym. Sci. 90 (2003) 572–576. doi:10.1002/app.12776.

[122] A. Jendrychowska-Bonamour, Semipermeable membranes synthesized by grafting poly (tetrafluoroethylene) films. Synthesis and study of properties. II. Anionic and cationic mixed, J. Chim. Phys. Phys. Chim. Biol. (1973).

[123] X. Zhili, G. Haifeng, Q. Mengping, Y. Ye, W. Guoxiong, C. Baokang, Preparation of bipolar membranes via radiation peroxidation grafting, Radiat. Phys. Chem. 42 (1993) 963–966. doi:10.1016/0969-806X(93)90413-O.

[124] H. H. Rachid El Moussaoui, Single-film membrane, process for obtaining it and use thereof, US Patent 5840192 A, 1994.

[125] M. Higa, D. Masuda, E. Kobayashi, M. Nishimura, Y. Sugio, T. Kusudou, N. Fujiwara, Charge mosaic membranes prepared from laminated structures of PVA-based charged layers. 1.

Preparation and transport properties of charged mosaic membranes, J. Memb. Sci. 310 (2008) 466–473. doi:10.1016/j.memsci.2007.11.024.

[126] K. Wang, A. A. Abdalla, M. A. Khaleel, N. Hilal, M. K. Khraisheh, Mechanical properties of water desalination and wastewater treatment membranes, Desalination. 401 (2017) 190–205. doi:10.1016/j.desal.2016.06.032.

[127] P. W. Majsztrik, A. B. Bocarsly, J. B. Benziger, Viscoelastic Response of Nafion. Effects of Temperature and Hydration on Tensile Creep, Macromolecules. 41 (2008) 9849–9862. doi:10.1021/ma801811m.

[128] Y. Kawano, Y. Wang, R. A. Palmer, S. R. Aubuchon, Stress-Strain Curves of Nafion Membranes in Acid and Salt Forms, Polímeros. 12 (2002) 96–101. doi:10.1590/S0104-14282002000200008.

[129] E. Y. Safronova, D. V. Golubenko, N. V. Shevlyakova, M. G. D'yakova, V. A. Tverskoi, L. Dammak, D. Grande, A. B. Yaroslavtsev, New cation-exchange membranes based on cross-linked sulfonated polystyrene and polyethylene for power generation systems, J. Memb. Sci. 515 (2016) 196–203. doi:10.1016/j.memsci.2016.05.006.

[130] N. Liang, Y. Liu, X. Liao, Z. Luo, D. Chen, X. Liu, H. Zhang, Preparation and characterization of anion-exchange membranes derived from poly(vinylbenzyl chloride-co-styrene) and intercalated montmorillonite, Polym. Adv. Technol. 28 (2017) 728–735. doi:10.1002/pat.3959.

[131] N. Ataollahi, K. Vezzù, G. Nawn, G. Pace, G. Cavinato, F. Girardi, P. Scardi, V. Di Noto, R. Di Maggio, A Polyketone-based Anion Exchange Membrane for Electrochemical

Applications: Synthesis and Characterization, Electrochim. Acta. 226 (2017) 148–157. doi:10.1016/j.electacta.2016.12.150.

[132] M. Nemati, S. M. Hosseini, M. Shabanian, Novel electrodialysis cation exchange membrane prepared by 2-acrylamido-2-methylpropane sulfonic acid; heavy metal ions removal, J. Hazard. Mater. 337 (2017) 90–104. doi:10.1016/j.jhazmat.2017.04.074.

[133] M. Tedesco, A. Cipollina, A. Tamburini, W. van Baak, G. Micale, Modelling the Reverse ElectroDialysis process with seawater and concentrated brines, Desalin. Water Treat. 49 (2012) 1–21. doi:10.1080/19443994.2012.699355.

[134] R. Lteif, L. Dammak, C. Larchet, B. Auclair, Determination du nombre de transport d'un contre-ion dans une membrane echangeuse d'ions en utilisant la methode de la pile de concentration, Eur. Polym. J. 37 (2001) 627–639. doi:10.1016/S0014-3057(00)00163-4.

[135] Y. Zhang, R. Liu, Q. Lang, M. Tan, Y. Zhang, Composite anion exchange membrane made by layer-by-layer method for selective ion separation and water migration control, Sep. Purif. Technol. 192 (2018) 278–286. doi:10.1016/j.seppur.2017.10.022.

[136] G. Ramachandraiah, P. Ray, Electroassisted Transport Phenomenon of Strong and Weak Electrolytes across Ion-Exchange Membranes: Chronopotentiometric Study on Deactivation

of Anion Exchange Membranes by Higher Homologous Monocarboxylates, J. Phys. Chem. B. 101 (1997) 7892–7900. doi:10.1021/jp9701698.

[137] R. Audinos, G. Pichelin, Characterization of electrodialysis membranes by chronopotentiometry, Desalination. 68 (1988) 251–263. doi:10.1016/0011-9164(88)80059-6.

[138] J. Balster, M. H. Yildirim, D. F. Stamatialis, R. Ibañez, R. G. H. Lammertink, V. Jordan, M. Wessling, Morphology and Microtopology of Cation-Exchange Polymers and the Origin of the Overlimiting Current, J. Phys. Chem. B. (2006). doi:10.1021/jp068474t.

[139] S. Pawlowski, P. Sistat, J. G. Crespo, S. Velizarov, Mass transfer in reverse electrodialysis: Flow entrance effects and diffusion boundary layer thickness, J. Memb. Sci. 471 (2014) 72–83. doi:10.1016/j.memsci.2014.07.075.

[140] P. Długołecki, B. Anet, S. J. Metz, K. Nijmeijer, M. Wessling, Transport limitations in ion exchange membranes at low salt concentrations, J. Memb. Sci. 346 (2010) 163–171. doi:10.1016/j.memsci.2009.09.033.

[141] M. Tedesco, A. Cipollina, A. Tamburini, I. D. L. Bogle, G. Micale, A simulation tool for analysis and design of reverse electrodialysis using concentrated brines, Chem. Eng. Res. Des. 93 (2015) 441–456. doi:10.1016/j.cherd.2014.05.009.

[142] A. H. Galama, N. A. Hoog, D. R. Yntema, Method for determining ion exchange membrane resistance for electrodialysis systems, Desalination. 380 (2016) 1–11. doi:10.1016/j.desal.2015.11.018.

[143] A. Elattar, A. Elmidaoui, N. Pismenskaia, C. Gavach, G. Pourcelly, Comparison of transport properties of monovalent anions through anion-exchange membranes, J. Memb. Sci. 143 (1998) 249–261. doi:10.1016/S0376-7388(98)00013-1.

[144] V. K. Shahi, S. K. Thampy, R. Rangarajan, The effect of conducting spacers on transport properties of ion-exchange membranes in electrodriven separation, Desalination. 133 (2001) 245–258. doi:10.1016/S0011-9164(01)00105-9.

[145] G. S. Gohil, V. K. Shahi, R. Rangarajan, Comparative studies on electrochemical characterization of homogeneous and heterogeneous type of ion-exchange membranes, J. Memb. Sci. 240 (2004) 211–219. doi:10.1016/j.memsci.2004.04.022.

[146] V. K. Shahi, A. P. Murugesh, B. S. Makwana, S. K. Thampy, R. Rangarajan, Comparative investigations on electrical conductance of ion-exchange membranes, Indian Joumal Chem. 39 (2000) 1264–1269.

[147] B. Auclair, V. V. Nikonenko, C. Larchet, M. Métayer, L. Dammak, Correlation between transport parameters of ion-exchange membranes, J. Memb. Sci. 195 (2002) 89–102. doi:10.1016/S0376-7388(01)00556-7.

[148] R. F. Silva, M. De Francesco, A. Pozio, Tangential and normal conductivities of Nafion® membranes used in polymer electrolyte fuel cells, J. Power Sources. 134 (2004) 18–26. doi:10.1016/j.jpowsour.2004.03.028.

[149] A. Alcaraz, H. Holdik, T. Ruffing, P. Ramírez, S. Mafé, AC impedance spectra of bipolar membranes: an experimental study, J. Memb. Sci. 150 (1998) 43–56. doi:10.1016/S0376-7388(98)00201-4.

[150] F. Valero, R. Arbós, Desalination of brackish river water using Electrodialysis Reversal (EDR): Control of the THMs formation in the Barcelona (NE Spain) area, Desalination. 253 (2010) 170–174. doi:10.1016/j.desal.2009.11.011.

[151] V. Lindstrand, G. Sundström, A. S. Jönsson, Fouling of electrodialysis membranes by organic substances, Desalination. 128 (2000) 91–102. doi:10.1016/S0011-9164(00)00026-6.

[152] J. S. Park, J.-H. Choi, K. H. Yeon, S. H. Moon, An approach to fouling characterization of an ion-exchange membrane using current-voltage relation and electrical impedance spectroscopy, J. Colloid Interface Sci. 294 (2006) 129–138. doi:10.1016/j.jcis.2005.07.016.

[153] H.-J. Lee, S.-H. Moon, S.-P. Tsai, Effects of pulsed electric fields on membrane fouling in electrodialysis of NaCl solution containing humate, Sep. Purif. Technol. 27 (2002) 89–95. doi:10.1016/S1383-5866(01)00167-8.

[154] I. Ben Salah Sayadi, P. Sistat, M. M. Tlili, Assess of physical antiscale-treatments on conventional electrodialysis pilot unit during brackish water desalination, Chem. Eng. Process. Process Intensif. 88 (2015) 47–57. doi:10.1016/j.cep.2014.11.013.

[155] W. Garcia-Vasquez, L. Dammak, C. Larchet, V. V. Nikonenko, D. Grande, Effects of acid–base cleaning procedure on structure and properties of anion-exchange membranes used in electrodialysis, J. Memb. Sci. 507 (2016) 12–23. doi:10.1016/j.memsci.2016.02.006.

[156] R. Audinos, Fouling of ion-selective membranes during electrodialysis of grape must, J. Memb. Sci. 41 (1989) 115–126. doi:10.1016/S0376-7388(00)82395-9.

[157] R. P. Allison, Electrodialysis reversal in water reuse applications, Desalination. 103 (1995) 11–18. doi:10.1016/0011-9164(95)00082-8.

[158] N. Tanaka, M. Nagase, M. Higa, Organic fouling behavior of commercially available hydrocarbon-based anion-exchange membranes by various organic-fouling substances, Desalination. 296 (2012) 81–86. doi:10.1016/j.desal.2012.04.010.

[159] E. Korngold, F. de Körösy, R. Rahav, M. F. Taboch, Fouling of anionselective membranes in electrodialysis, Desalination. 8 (1970) 195–220. doi:10.1016/S0011-9164(00)80230-1.

[160] V. D. Grebenyuk, R. D. Chebotareva, S. Peters, V. Linkov, Surface modification of anion-exchange electrodialysis membranes to enhance anti-fouling characteristics, Desalination. 115 (1998) 313–329. doi:10.1016/S0011-9164(98)00051-4.

[161] S. Mulyati, R. Takagi, A. Fujii, Y. Ohmukai, T. Maruyama, H. Matsuyama, Improvement of the antifouling potential of an anion exchange membrane by surface modification with a polyelectrolyte for an electrodialysis process, J. Memb. Sci. 417–418 (2012) 137–143. doi:10.1016/j.memsci.2012.06.024.

[162] M. Vaselbehagh, H. Karkhanechi, S. Mulyati, R. Takagi, H. Matsuyama, Improved antifouling of anion-exchange membrane by polydopamine coating in electrodialysis process, Desalination. 332 (2014) 126–133. doi:10.1016/j.desal.2013.10.031.

[163] W. E. Katz, The electrodialysis reversal (EDR) process, Desalination. 28 (1979) 31–40. doi:10.1016/S0011-9164(00)88124-2.

[164] M. Turek, P. Dydo, J. Waś, Electrodialysis reversal in high CaSO4 supersaturation mode, Desalination. 198 (2006) 288–294. doi:10.1016/j.desal.2006.01.029.

[165] N. Cifuentes-Araya, G. Pourcelly, L. Bazinet, Impact of pulsed electric field on electrodialysis process performance and membrane fouling during consecutive demineralization of a model

salt solution containing a high magnesium/calcium ratio, J. Colloid Interface Sci. 361 (2011) 79–89. doi:10.1016/j.jcis.2011.05.044.

[166] C. Casademont, P. Sistat, B. Ruiz, G. Pourcelly, L. Bazinet, Electrodialysis of model salt solution containing whey proteins: Enhancement by pulsed electric field and modified cell configuration, J. Memb. Sci. 328 (2009) 238–345. doi:10.1016/j.memsci.2008.12.013.

[167] S. Suwal, J. Amiot, L. Beaulieu, L. Bazinet, Effect of pulsed electric field and polarity reversal on peptide/amino acid migration, selectivity and fouling mitigation, J. Memb. Sci. 510 (2016) 405–416. doi:10.1016/j.memsci.2016.03.010.

[168] B. A. Cooke, Concentration polarization in electrodialysis—I. The electrometric measurement of interfacial concentration, Electrochim. Acta. 3 (1961) 307–317. doi:10.1016/0013-4686(61)85007-X.

[169] K. S. Spiegler, Polarization at ion exchange membrane-solution interfaces, Desalination. 9 (1971) 367–385. doi:10.1016/0011-9164(71)80005-X.

[170] C. Forgacs, N. Ishibashi, J. Leibovitz, J. Sinkovic, K. S. Spiegler, Polarization at ion-exchange membranes in electrodialysis, Desalination. 10 (1972) 181–214. doi:10.1016/S0011-9164(00)80085-5.

[171] F. Helfferich, Ion exchange, McGraw-Hill, New York, 1962.

[172] V. G. Levich, Physicochemical Hydrodynamics, Prentice-Hall, Englewood Cliffs, N.J., 1962.

[173] V. V. Nikonenko, N. D. Pismenskaya, E. I. Belova, P. Sistat, P. Huguet, G. Pourcelly, C. Larchet, Intensive current transfer in membrane systems: Modelling, mechanisms and

application in electrodialysis, Adv. Colloid Interface Sci. 160 (2010) 101–123. doi:10.1016/j.cis.2010.08.001.

[174] R. K. McGovern, S. M. Zubair, J. H. Lienhard V, The cost effectiveness of electrodialysis for diverse salinity applications, Desalination. 348 (2014) 57–65. doi:10.1016/j.desal.2014.06.010.

[175] J. J. Krol, M. Wessling, H. Strathmann, Concentration polarization with monopolar ion exchange membranes : current - voltage curves and water dissociation, J. Memb. Sci. 162 (1999) 145–154. doi:10.1016/S0376-7388(99)00133-7.

[176] J. Krol, Chronopotentiometry and overlimiting ion transport through monopolar ion exchange membranes, J. Memb. Sci. 162 (1999) 155–164. doi:10.1016/S0376-7388(99)00134-9.

[177] R. Valerdi-Pérez, J. Ibáñez-Mengual, Current—voltage curves for an electrodialysis reversal pilot plant: determination of limiting currents, Desalination. 141 (2001) 23–37. doi:10.1016/S0011-9164(01)00386-1.

[178] J. G. D. Tadimeti, S. Chattopadhyay, Uninterrupted swirling motion facilitating ion transport in electrodialysis, Desalination. 392 (2016) 54–62. doi:10.1016/j.desal.2016.04.007.

[179] J.-H. Choi, J.-S. Park, S.-H. Moon, Direct Measurement of Concentration Distribution within the Boundary Layer of an Ion-Exchange Membrane, J. Colloid Interface Sci. 251 (2002) 311–317. doi:10.1006/jcis.2002.8407.

[180] Y. Tanaka, Concentration polarization in ion exchange membrane electrodialysis, J. Memb. Sci. 57 (1991) 217–235. doi:10.1016/S0376-7388(00)80680-8.

[181] Y. Tanaka, Concentration polarization in ion-exchange membrane electrodialysis The events arising in an unforced flowing solution in a desalting cell, J. Memb. Sci. 244 (2004) 1–16. doi:10.1016/j.memsci.2004.02.041.

[182] C. Forgacs, J. Leibovitz, R. N. O'Brien, K. S. Spiegler, Interferometric study of concentration profiles in solutions near membrane surfaces, Electrochim. Acta. 20 (1975) 555–563. doi:10.1016/0013-4686(75)80006-5.

[183] V. A. Shaposhnik, V. I. Vasil'eva, D. B. Praslov, Concentration fields of solutions under electrodialysis with ion-exchange membranes, J. Memb. Sci. 101 (1995) 23–30. doi:10.1016/0376-7388(94)00270-9.

[184] V. A. Shaposhnik, V. A. Kuzminykh, O. V. Grigorchuk, V. I. Vasil'eva, Analytical model of laminar flow electrodialysis with ion-exchange membranes, J. Memb. Sci. 133 (1997) 27–37. doi:10.1016/S0376-7388(97)00063-X.

[185] V. A. Shaposhnik, O. V. Grigorchuk, E. N. Korzhov, V. I. Vasil'eva, V. Y. Klimov, The effect of ion-conducting spacers on mass transfer - Numerical analysis and concentration field visualization by means of laser interferometry, J. Memb. Sci. 139 (1998) 85–96. doi:10.1016/S0376-7388(97)00247-0.

[186] V. I. Vasil'eva, V. A. Shaposhnik, O. V. Grigorchuk, I. P. Petrunya, The membrane–solution interface under high-performance current regimes of electrodialysis by means of laser interferometry, Desalination. 192 (2006) 408–414. doi:10.1016/j.desal.2005.06.055.

[187] J. G. D. Tadimeti, V. Kurian, A. Chandra, S. Chattopadhyay, Corrugated membrane surfaces for effective ion transport in electrodialysis, J. Memb. Sci. 499 (2016) 418–428. doi:10.1016/j.memsci.2015.11.001.

[188] R. Kwak, G. Guan, W. K. Peng, J. Han, Microscale electrodialysis: Concentration profiling and vortex visualization, Desalination. 308 (2013) 138–146. doi:10.1016/j.desal.2012.07.017.

[189] B. Kim, S. Choi, V. S. Pham, R. Kwak, J. Han, Energy efficiency enhancement of electromembrane desalination systems by local flow redistribution optimized for the asymmetry of cation/anion diffusivity, J. Memb. Sci. 524 (2017) 280–287. doi:10.1016/j.memsci.2016.11.046.

[190] V. M. Barragán, C. Ruíz-Bauzá, Current–Voltage Curves for Ion-Exchange Membranes: A Method for Determining the Limiting Current Density, J. Colloid Interface Sci. 205 (1998) 365–373. doi:10.1006/jcis.1998.5649.

[191] P. Malek, J. M. Ortiz, B. S. Richards, A. I. Schäfer, Electrodialytic removal of NaCl from water: Impacts of using pulsed electric potential on ion transport and water dissociation phenomena, J. Memb. Sci. 435 (2013) 99–109. doi:10.1016/j.memsci.2013.01.060.

[192] V. V. Nikonenko, N. D. Pismenskaya, A. G. Istoshin, V. I. Zabolotsky, A. A. Shudrenko, Description of mass transfer characteristics of ED and EDI apparatuses by using the similarity

theory and compartmentation method, Chem. Eng. Process. Process Intensif. 47 (2008) 1118–1127. doi:10.1016/j.cep.2007.12.005.

[193] L. Gurreri, A. Tamburini, A. Cipollina, G. Micale, M. Ciofalo, CFD prediction of concentration polarization phenomena in spacer-filled channels for reverse electrodialysis, J. Memb. Sci. 468 (2014) 133–148. doi:10.1016/j.memsci.2014.05.058.

[194] R. F. Probstein, A. A. Sonin, E. Gur-Arie, A turbulent flow theory of electrodialysis, Desalination. 11 (1972) 165–187. doi:10.1016/S0011-9164(00)80066-1.

[195] M. S. Isaacson, A. A. Sonin, Sherwood Number and Friction Factor Correlations for Electrodialysis Systems, with Application to Process Optimization, Ind. Eng. Chem. Process Des. Dev. 15 (1976) 313–321. doi:10.1021/i260058a017.

[196] G. Schock, A. Miquel, Mass transfer and pressure loss in spiral wound modules, Desalination. 64 (1987) 339–352. doi:10.1016/0011-9164(87)90107-X.

[197] A. R. Da Costa, A. G. Fane, C. J. D. Fell, A. C. M. Franken, Optimal channel spacer design for ultrafiltration, J. Memb. Sci. 62 (1991) 275–291. doi:10.1016/0376-7388(91)80043-6.

[198] F. Li, W. Meindersma, A. B. de Haan, T. Reith, Optimization of commercial net spacers in spiral wound membrane modules, J. Memb. Sci. 208 (2002) 289–302. doi:10.1016/S0376-7388(02)00307-1.

[199] M. Fidaleo, M. Moresi, Optimal strategy to model the electrodialytic recovery of a strong electrolyte, J. Memb. Sci. 260 (2005) 90–111. doi:10.1016/j.memsci.2005.01.048.

[200] C. P. Koutsou, S. G. Yiantsios, A. J. Karabelas, A numerical and experimental study of mass transfer in spacer-filled channels: Effects of spacer geometrical characteristics and Schmidt number, J. Memb. Sci. 326 (2009) 234–251. doi:10.1016/j.memsci.2008.10.007.

[201] A. J. Karabelas, M. Kostoglou, C. P. Koutsou, Modeling of spiral wound membrane desalination modules and plants – review and research priorities, Desalination. 356 (2015) 165–186. doi:10.1016/j.desal.2014.10.002.

[202] P. Sistat, G. Pourcelly, Chronopotentiometric response of an ion-exchange membrane in the underlimiting current-range. Transport phenomena within the diffusion layers, J. Memb. Sci. 123 (1997) 121–131. doi:10.1016/S0376-7388(96)00210-4.

[203] S. Mareev, D. Yu Butylskii, N. Pismenskaya, V. V. Nikonenko, Chronopotentiometry of ion-exchange membranes in the overlimiting current range. Transition time for a finite-length

diffusion layer: modeling and experiment, J. Memb. Sci. 500 (2016) 171–179. doi:10.1016/j.memsci.2015.11.026.

[204] W. Zhang, J. Ma, P. Wang, Z. Wang, F. Shi, H. Liu, Investigations on the interfacial capacitance and the diffusion boundary layer thickness of ion exchange membrane using electrochemical impedance spectroscopy, J. Memb. Sci. 502 (2016). doi:10.1016/j.memsci.2015.12.007.

[205] B. Zhang, J. G. Hong, S. Xie, S. Xia, Y. Chen, An integrative modeling and experimental study on the ionic resistance of ion-exchange membranes, J. Memb. Sci. 524 (2017). doi:10.1016/j.memsci.2016.11.050.

[206] I. Rubinstein, L. Shtilman, Voltage against current curves of cation exchange membranes, J. Chem. Soc. Faraday Trans. 2 Mol. Chem. Phys. 75 (1979) 231. doi:10.1039/f29797500231.

[207] I. Rubinstein, F. Maletzki, Electroconvection at an electrically inhomogeneous permselective membrane surface, J. Chem. Soc. Faraday Trans. 87 (1991) 2079. doi:10.1039/ft9918702079.

[208] J.-H. Choi, H. J. Lee, S.-H. Moon, Effects of Electrolytes on the Transport Phenomena in a Cation-Exchange Membrane, J. Colloid Interface Sci. 238 (2001) 188–195. doi:10.1006/jcis.2001.7510.

[209] H. J. Lee, H. Strathmann, S. H. Moon, Determination of the limiting current density in electrodialysis desalination as an empirical function of linear velocity, Desalination. 190 (2006) 43–50. doi:10.1016/j.desal.2005.08.004.

[210] M. K. Urtenov, A. M. Uzdenova, A. V. Kovalenko, V. V. Nikonenko, N. D. Pismenskaya, V. I. Vasil'eva, P. Sistat, G. Pourcelly, Basic mathematical model of overlimiting transfer enhanced by electroconvection in flow-through electrodialysis membrane cells, J. Memb. Sci. 447 (2013) 190–202. doi:10.1016/j.memsci.2013.07.033.

[211] I. Rubinstein, E. Staude, O. Kedem, Role of the membrane surface in concentration polarization at ion-exchange membrane, Desalination. 69 (1988) 101–114. doi:10.1016/0011-9164(88)80013-4.

[212] F. Maletzki, H.-W. Rösler, E. Staude, Ion transfer across electrodialysis membranes in the overlimiting current range: stationary voltage current characteristics and current noise power

spectra under different conditions of free convection, J. Memb. Sci. 71 (1992) 105–116. doi:10.1016/0376-7388(92)85010-G.

[213] H.-W. Rösler, F. Maletzki, E. Staude, Ion transfer across electrodialysis membranes in the overlimiting current range: chronopotentiometric studies, J. Memb. Sci. 72 (1992) 171–179. doi:10.1016/0376-7388(92)80197-R.

[214] R. Ibañez, D. F. Stamatialis, M. Wessling, Role of membrane surface in concentration polarization at cation exchange membranes, J. Memb. Sci. 239 (2004) 119–128. doi:10.1016/j.memsci.2003.12.032.

[215] N. Pismenskaia, P. Sistat, P. Huguet, V. V. Nikonenko, G. Pourcelly, Chronopotentiometry applied to the study of ion transfer through anion exchange membranes, J. Memb. Sci. 228 (2004) 65–76. doi:10.1016/j.memsci.2003.09.012.

[216] E. Volodina, N. Pismenskaya, V. V. Nikonenko, C. Larchet, G. Pourcelly, Ion transfer across ion-exchange membranes with homogeneous and heterogeneous surfaces, J. Colloid Interface Sci. 285 (2005) 247–258. doi:10.1016/j.jcis.2004.11.017.

[217] V. V. Nikonenko, A. V. Kovalenko, M. K. Urtenov, N. D. Pismenskaya, J. Han, P. Sistat, G. Pourcelly, Desalination at overlimiting currents: State-of-the-art and perspectives, Desalination. 342 (2014) 85–106. doi:10.1016/j.desal.2014.01.008.

[218] K. A. Nebavskaya, V. V. Sarapulova, K. G. Sabbatovskiy, V. D. Sobolev, N. D. Pismenskaya, P. Sistat, M. Cretin, V. V. Nikonenko, Impact of ion exchange membrane surface charge and hydrophobicity on electroconvection at underlimiting and overlimiting currents, J. Memb. Sci. 523 (2017) 36–44. doi:10.1016/j.memsci.2016.09.038.

[219] V. V. Nikonenko, S. A. Mareev, N. D. Pis'menskaya, A. M. Uzdenova, A. V. Kovalenko, M. K. Urtenov, G. Pourcelly, Effect of electroconvection and its use in intensifying the mass

transfer in electrodialysis (Review), Russ. J. Electrochem. 53 (2017) 1122–1144. doi:10.1134/S1023193517090099.

[220] D. A. Cowan, J. H. Brown, Effect of Turbulence on Limiting Current in Electrodialysis Cells, Ind. Eng. Chem. 51 (1959) 1445–1448. doi:10.1021/ie50600a026.

[221] W. G. B. Mandersloot, R. E. Hicks, Concertration Polarization on Ion Exchange Resin Membranes in Electrodialytic Demineralization, Ind. Eng. Chem. Process Des. Dev. 4 (1965) 304–308. doi:10.1021/i260015a014.

[222] J. Balster, I. Pünt, D. F. Stamatialis, M. Wessling, Multi-layer spacer geometries with improved mass transport, J. Memb. Sci. 282 (2006) 351–361. doi:10.1016/j.memsci.2006.05.039.

[223] J. Balster, D. F. Stamatialis, M. Wessling, Towards spacer free electrodialysis, J. Memb. Sci. 341 (2009) 131–138. doi:10.1016/j.memsci.2009.05.048.

[224] V. Geraldes, M. D. Afonso, Limiting current density in the electrodialysis of multi-ionic solutions, J. Memb. Sci. 360 (2010) 499–508. doi:10.1016/j.memsci.2010.05.054.

[225] P. Saremirad, H. G. Gomaa, J. Zhu, Effect of flow oscillations on mass transfer in electrodialysis with bipolar membrane, J. Memb. Sci. 405–406 (2012) 158–166. doi:10.1016/j.memsci.2012.03.006.

[226] H. Lee, F. Sarfert, H. Strathmann, S. H. Moon, Designing of an electrodialysis desalination plant, Desalination. 142 (2002) 267–286. doi:10.1016/S0011-9164(02)00208-4.

[227] Y. Tanaka, Limiting current density of an ion-exchange membrane and of an electrodialyzer, J. Memb. Sci. 266 (2005) 6–17. doi:10.1016/j.memsci.2005.05.005.

[228] X. W. Zhong, W. R. Zhang, Z. Y. Hu, H. C. Li, Effect of characterizations of spacer in electrodialysis cells on mass transfer, Desalination. 46 (1983) 243–252. doi:10.1016/0011-9164(83)87161-6.

[229] F. Li, W. Meindersma, A. B. de Haan, T. Reith, Experimental validation of CFD mass transfer simulations in flat channels with non-woven net spacers, J. Memb. Sci. 232 (2004) 19–30. doi:10.1016/j.memsci.2003.11.015.

[230] F. Li, W. Meindersma, A. B. de Haan, T. Reith, Novel spacers for mass transfer enhancement in membrane separations, J. Memb. Sci. 253 (2005) 1–12. doi:10.1016/j.memsci.2004.12.019.

[231] C. Rodrigues, V. Geraldes, M. N. de Pinho, V. Semião, Mass-transfer entrance effects in narrow rectangular channels with ribbed walls or mesh-type spacers, Chem. Eng. Sci. 78 (2012) 38–45. doi:10.1016/j.ces.2012.04.023.

[232] C. Rodrigues, M. Rodrigues, V. Semiao, V. Geraldes, Enhancement of mass transfer in spacer-filled channels under laminar regime by pulsatile flow, Chem. Eng. Sci. 123 (2015) 536–541. doi:10.1016/j.ces.2014.11.047.

[233] E. V. Laktionov, N. D. Pismenskaya, V. V. Nikonenko, V. I. Zabolotsky, Method of electrodialysis stack testing with the feed solution concentration regulation, Desalination. 151 (2003) 101–116. doi:10.1016/S0011-9164(02)00988-8.

[234] A. A. Sonin, M. S. Isaacson, Optimization of Flow Design in Forced Flow Electrochemical Systems, with Special Application to Electrodialysis, Ind. Eng. Chem. Process Des. Dev. 13 (1974) 241–248. doi:10.1021/i260051a009.

[235] L. Karimi, A. Ghassemi, An empirical/theoretical model with dimensionless numbers to predict the performance of electrodialysis systems on the basis of operating conditions, Water Res. 98 (2016) 270–279. doi:10.1016/j.watres.2016.04.014.

[236] A. A. Sonin, R. F. Probstein, A hydrodynamic theory of desalination by electrodialysis, Desalination. 5 (1968) 293–329. doi:10.1016/S0011-9164(00)80105-8.

[237] Y. I. Kharkats, The mechanism of supralimiting currents at ion-exchange membrane/electrolyte interfaces, Sov. Electrochem. 21 (1985) 917.

[238] R. Simons, The origin and elimination of water splitting in ion exchange membranes during water demineralisation by electrodialysis, Desalination. 28 (1979) 41–42. doi:10.1016/S0011-9164(00)88125-4.

[239] R. Simons, Water splitting in ion exchange membranes, Electrochim. Acta. 30 (1985) 275–282. doi:10.1016/0013-4686(85)80184-5.

[240] I. Rubinstein, A. Warshawsky, L. Schechtman, O. Kedem, Elimination of acid-base generation ("water-splitting") in electrodialysis, Desalination. 51 (1984) 55–60. doi:10.1016/0011-9164(84)85052-3.

[241] V. I. Zabolotsky, V. V. Nikonenko, N. D. Pismenskaya, On the role of gravitational convection in the transfer enhancement of salt ions in the course of dilute solution electrodialysis, J. Memb. Sci. 119 (1996) 171–181. doi:10.1016/0376-7388(96)00121-4.

[242] V. I. Zabolotsky, V. V. Nikonenko, N. D. Pismenskaya, E. V. Laktionov, M. K. Urtenov, H. Strathmann, M. Wessling, G. H. Koops, Coupled transport phenomena in overlimiting current electrodialysis, Sep. Purif. Technol. 14 (1998) 255–267. doi:10.1016/S1383-5866(98)00080-X.

[243] S. S. Dukhin, Electrokinetic phenomena of the second kind and their applications, Adv. Colloid Interface Sci. 35 (1991) 173–196. doi:10.1016/0001-8686(91)80022-C.

[244] I. Rubinstein, B. Zaltzman, O. Kedem, Electric fields in and around ion-exchange membranes1, J. Memb. Sci. 125 (1997) 17–21. doi:10.1016/S0376-7388(96)00194-9.

[245] B. Zaltzman, I. Rubinstein, Electro-osmotic slip and electroconvective instability, J. Fluid Mech. 579 (2007) 173–226.

[246] R. Kwak, V. S. Pham, K. M. Lim, J. Han, Shear Flow of an Electrically Charged Fluid by Ion Concentration Polarization: Scaling Laws for Electroconvective Vortices, Phys. Rev. Lett. 110 (2013). doi:10.1103/PhysRevLett.110.114501.

[247] P. Sistat, G. Pourcelly, Steady-state ion transport through homopolar ion-exchange membranes: an analytical solution of the Nernst–Planck equations for a 1:1 electrolyte under the electroneutrality assumption, J. Electroanal. Chem. 460 (1999) 53–62. doi:10.1016/S0022-0728(98)00339-8.

[248] V.M. Aguilella, S. Mafe, J.A. Manzanares, J. Pellicer, Current-voltage curves for ion-exchange membranes. Contributions to the total potential drop, J. Memb. Sci. 61 (1991) 177–190. doi:10.1016/0376-7388(91)80014-W.

[249] M. Taky, G. Pourcelly, F. Lebon, C. Gavach, Polarization phenomena at the interfaces between an electrolyte solution and an ion exchange membrane: Part I. Ion transfer with a cation

exchange membrane, J. Electroanal. Chem. 336 (1992) 171–194. doi:10.1016/0022-0728(92)80270-E.

[250] R. Q. Fu, T. W. Xu, W. H. Yang, Z. X. Pan, A new derivation and numerical analysis of current-voltage characteristics for an ion-exchange membrane under limiting current density, Desalination. 173 (2005) 143–155. doi:10.1016/j.desal.2004.07.047.

[251] P. Sistat, A. Kozmai, N. Pismenskaya, C. Larchet, G. Pourcelly, V. V. Nikonenko, Low-frequency impedance of an ion-exchange membrane system, Electrochim. Acta. 53 (2008) 6380–6390. doi:10.1016/j.electacta.2008.04.041.

[252] Y. Kim, W. S. Walker, D. F. Lawler, Electrodialysis with spacers: Effects of variation and correlation of boundary layer thickness, Desalination. 274 (2011) 54–63. doi:10.1016/j.desal.2011.01.076.

[253] Y. Kim, W. S. Walker, D. F. Lawler, Competitive separation of di- vs. mono-valent cations in electrodialysis: Effects of the boundary layer properties, Water Res. 46 (2012) 2042–2056. doi:10.1016/j.watres.2012.01.004.

[254] A. M. Weiner, R. K. McGovern, J. H. Lienhard V, Increasing the power density and reducing the levelized cost of electricity of a reverse electrodialysis stack through blending, Desalination. 369 (2015) 140–148. doi:10.1016/j.desal.2015.04.031.

[255] M. Block, J. A. Kitchener, Polarization Phenomena in Commercial Ion-Exchange Membranes, J. Electrochem. Soc. 113 (1966) 947. doi:10.1149/1.2424162.

[256] S. J. Judd, G. S. Solt, T. Wen, Polarization and back em.f. in electrodialysis, J. Appl. Electrochem. 23 (1993) 1117–1124. doi:10.1007/BF00625584.

[257] T. Wen, G. S. Solt, D. W. Gao, Electrical resistance and coulomb efficiency of electrodialysis (ED) apparatus in polarization, J. Memb. Sci. 114 (1996) 255–262. doi:10.1016/0376-7388(96)00005-1.

[258] M. Law, T. Wen, G. S. Solt, Thickness and concentration profile of the boundary layer in electrodialysis, Desalination. 109 (1997) 95–103. doi:10.1016/S0011-9164(97)00055-6.

[259] E. Güler, R. Elizen, M. Saakes, K. Nijmeijer, Micro-structured membranes for electricity generation by reverse electrodialysis, J. Memb. Sci. 458 (2014) 136–148. doi:10.1016/j.memsci.2014.01.060.

[260] D. A. Vermaas, M. Saakes, K. Nijmeijer, Enhanced mixing in the diffusive boundary layer for energy generation in reverse electrodialysis, J. Memb. Sci. 453 (2014) 312–319. doi:10.1016/j.memsci.2013.11.005.

[261] J. Liu, G. M. Geise, X. Luo, H. Hou, F. Zhang, Y. Feng, M. A. Hickner, B. E. Logan, Patterned ion exchange membranes for improved power production in microbial reverse-electrodialysis cells, J. Power Sources. 271 (2014) 437–443. doi:10.1016/j.jpowsour.2014.08.026.

[262] J. Moreno, E. Slouwerhof, D. A. Vermaas, M. Saakes, K. Nijmeijer, The Breathing Cell: Cyclic Intermembrane Distance Variation in Reverse Electrodialysis, Environ. Sci. Technol. 50 (2016) 11386–11393. doi:10.1021/acs.est.6b02668.

[263] A. A. Moya, Electrochemical Impedance of Ion-Exchange Membranes with Interfacial Charge Transfer Resistances, J. Phys. Chem. C. 120 (2016) 6543–6552. doi:10.1021/acs.jpcc.5b12087.

[264] R. Abu-Rjal, V. Chinaryan, M. Z. Bazant, I. Rubinstein, B. Zaltzman, Effect of concentration polarization on permselectivity, Phys. Rev. E. 89 (2014) 12302. doi:10.1103/PhysRevE.89.012302.

[265] A. R. Da Costa, A. G. Fane, D. E. Wiley, Spacer characterization and pressure drop modelling in spacer-filled channels for ultrafiltration, J. Memb. Sci. 87 (1994) 79–98. doi:10.1016/0376-7388(93)E0076-P.

[266] C. P. Koutsou, S. G. Yiantsios, A. J. Karabelas, Direct numerical simulation of flow in spacer-filled channels: Effect of spacer geometrical characteristics, J. Memb. Sci. 291 (2007) 53–69. doi:10.1016/j.memsci.2006.12.032.

[267] G. A. Fimbres-Weihs, D. E. Wiley, Review of 3D CFD modeling of flow and mass transfer in narrow spacer-filled channels in membrane modules, Chem. Eng. Process. 49 (2010) 759–781. doi:10.1016/j.cep.2010.01.007.

[268] P. A. Araújo, D. J. Miller, P. B. Correia, M. C. M. van Loosdrecht, J. C. Kruithof, B. D. Freeman, D. R. Paul, J. S. Vrouwenvelder, Impact of feed spacer and membrane modification

by hydrophilic, bactericidal and biocidal coating on biofouling control, Desalination. 295 (2012) 1–10. doi:10.1016/j.desal.2012.02.026.

[269] S. Al-Sharif, M. Albeirutty, A. Cipollina, G. Micale, Modelling flow and heat transfer in spacer-filled membrane distillation channels using open source CFD code, Desalination. 311 (2013) 103–112. doi:10.1016/j.desal.2012.11.005.

[270] S. S. Bucs, A. I. Radu, V. Lavric, J. S. Vrouwenvelder, C. Picioreanu, Effect of different commercial feed spacers on biofouling of reverse osmosis membrane systems: A numerical study, Desalination. 343 (2014) 26–37. doi:10.1016/j.desal.2013.11.007.

[271] C. P. Koutsou, A. J. Karabelas, A novel retentate spacer geometry for improved spiral wound membrane (SWM) module performance, J. Memb. Sci. 488 (2015) 129–142. doi:10.1016/j.memsci.2015.03.064.

[272] A. Siddiqui, N. Farhat, S. S. Bucs, R. V. Linares, C. Picioreanu, J. C. Kruithof, M. C. M. van Loosdrecht, J. Kidwell, J. S. Vrouwenvelder, Development and characterization of 3D-printed feed spacers for spiral wound membrane systems, Water Res. 91 (2016) 55–67. doi:10.1016/j.watres.2015.12.052.

[273] B. Gu, C. S. Adjiman, X. Y. Xu, The effect of feed spacer geometry on membrane performance and concentration polarisation based on 3D CFD simulations, J. Memb. Sci. 527 (2017) 78–91. doi:10.1016/j.memsci.2016.12.058.

[274] V. A. Haaksman, A. Siddiqui, C. Schellenberg, J. Kidwell, J. S. Vrouwenvelder, C. Picioreanu, Characterization of feed channel spacer performance using geometries obtained by X-ray

computed tomography, J. Memb. Sci. 522 (2017) 124–139. doi:10.1016/j.memsci.2016.09.005.

[275] M. La Cerva, M. Ciofalo, L. Gurreri, A. Tamburini, A. Cipollina, G. Micale, On some issues in the computational modelling of spacer-filled channels for membrane distillation, Desalination. 411 (2017) 101–111. doi:10.1016/j.desal.2017.02.016.

[276] Y. Taamneh, K. Bataineh, Improving the performance of direct contact membrane distillation utilizing spacer-filled channel, Desalination. 408 (2017) 25–35. doi:10.1016/j.desal.2017.01.004.

[277] D. A. Vermaas, J. Veerman, N. Y. Yip, M. Elimelech, M. Saakes, K. Nijmeijer, High Efficiency in Energy Generation from Salinity Gradients with Reverse Electrodialysis, ACS Sustain. Chem. Eng. 1 (2013) 1295–1302. doi:10.1021/sc400150w.

[278] F. B. Leitz, L. Marinčić, Enhanced mass transfer in electrochemical cells using turbulence promoters, J. Appl. Electrochem. 7 (1977) 473–484. doi:10.1007/BF00616758.

[279] O. Kuroda, S. Takahashi, M. Nomura, Characteristics of flow and mass transfer rate in an electrodialyzer compartment including spacer, Desalination. 46 (1983) 225–232. doi:10.1016/0011-9164(83)87159-8.

[280] A. Kitamoto, Y. Takashima, Transfer rates in electrodialysis with ion exchange membranes, Desalination. 9 (1971) 51–87. doi:10.1016/S0011-9164(00)80129-0.

[281] L. Gurreri, A. Tamburini, A. Cipollina, G. Micale, M. Ciofalo, Flow and mass transfer in spacer-filled channels for reverse electrodialysis: a CFD parametrical study, J. Memb. Sci. 497 (2016) 300–317. doi:10.1016/j.memsci.2015.09.006.

[282] J. Schwinge, D. E. Wiley, A. G. Fane, Novel spacer design improves observed flux, J. Memb. Sci. 229 (2004) 53–61. doi:10.1016/j.memsci.2003.09.015.

[283] D. Dendukuri, S. K. Karode, A. Kumar, Flow visualization through spacer filled channels by computational fluid dynamics-II: Improved feed spacer designs, J. Memb. Sci. 249 (2005) 41–49. doi:10.1016/j.memsci.2004.06.062.

[284] L. Gurreri, A. Tamburini, A. Cipollina, G. Micale, M. Ciofalo, Pressure drop at low reynolds numbers in woven-spacer-filled channels for membrane processes: CFD prediction and

experimental validation, Desalin. Water Treat. 61 (2017) 170–182. doi:10.5004/dwt.2016.11279.

[285] E. Korngold, L. Aronov, O. Kedem, Novel ion-exchange spacer for improving electrodialysis I. Reacted spacer, J. Memb. Sci. 138 (1998) 165–170. doi:10.1016/S0376-7388(97)00216-0.

[286] R. Messalem, Y. Mirsky, N. Daltrophe, G. Saveliev, O. Kedem, Novel ion-exchange spacer for improving electrodialysis II. Coated spacer, J. Memb. Sci. 138 (1998) 171–180. doi:10.1016/S0376-7388(97)00217-2.

[287] K. Kesore, F. Janowski, V. A. Shaposhnik, Highly effective electrodialysis for selective elimination of nitrates from drinking water, J. Memb. Sci. 127 (1997) 17–24. doi:10.1016/S0376-7388(96)00282-7.

[288] V. V. Nikonenko, A. G. Istoshin, M. K. Urtenov, V. I. Zabolotsky, C. Larchet, J. Benzaria, Analysis of electrodialysis water desalination costs by convective-diffusion model, Desalination. 126 (1999) 207–211. doi:10.1016/S0011-9164(99)00176-9.

[289] D. A. Vermaas, D. Kunteng, M. Saakes, K. Nijmeijer, Fouling in reverse electrodialysis under natural conditions, Water Res. 47 (2013) 1289–1298. doi:10.1016/j.watres.2012.11.053.

[290] J. Balster, D. F. F. Stamatialis, M. Wessling, Membrane with integrated spacer, J. Memb. Sci. 360 (2010) 185–189. doi:10.1016/j.memsci.2010.05.011.

[291] Y. Zhao, H. Wang, C. Jiang, L. Wu, T. Xu, Electrodialysis with notched ion exchange membranes: Experimental investigations and computational fluid dynamics simulations, Sep. Purif. Technol. 130 (2014) 102–111. doi:10.1016/j.seppur.2014.04.010.

[292] S. Pawlowski, T. Rijnaarts, M. Saakes, K. Nijmeijer, J. G. Crespo, S. Velizarov, Improved fluid mixing and power density in reverse electrodialysis stacks with chevron-profiled membranes, J. Memb. Sci. 531 (2017) 111–121. doi:10.1016/j.memsci.2017.03.003.

[293] D. W. Hall, K. Scott, R. J. J. Jachuck, Determination of mass transfer coefficient of a cross-corrugated membrane reactor by the limiting-current technique, Int. J. Heat Mass Transf. 44 (2001) 2201–2207. doi:10.1016/S0017-9310(00)00274-X.

[294] K. Scott, J. Lobato, Mass transfer characteristics of cross-corrugated membranes, Desalination. 146 (2002) 255–258. doi:10.1016/S0011-9164(02)00483-6.

[295] N. Tzanetakis, W. M. Taama, K. Scott, R. J. J. Jachuck, R. S. Slade, J. Varcoe, Comparative performance of ion exchange membranes for electrodialysis of nickel and cobalt, Sep. Purif. Technol. 30 (2003) 113–127. doi:10.1016/S1383-5866(02)00139-9.

[296] L. Gurreri, M. Ciofalo, A. Cipollina, A. Tamburini, W. Van Baak, G. Micale, CFD modelling of profiled-membrane channels for reverse electrodialysis, Desalin. Water Treat. 55 (2015) 1–20. doi:10.1080/19443994.2014.940651.

[297] S. Pawlowski, V. Geraldes, J. G. Crespo, S. Velizarov, Computational fluid dynamics (CFD) assisted analysis of profiled membranes performance in reverse electrodialysis, J. Memb. Sci. 502 (2016) 179–190. doi:10.1016/j.memsci.2015.11.031.

[298] L. Gurreri, G. Battaglia, A. Tamburini, A. Cipollina, G. Micale, M. Ciofalo, Multi-physical modelling of reverse electrodialysis, Desalination. 423 (2017) 52–64. doi:10.1016/j.desal.2017.09.006.

[299] S. M. Mojab, A. Pollard, J. G. Pharoah, S. B. Beale, E. S. Hanff, Unsteady laminar to turbulent flow in a spacer-filled channel, Flow, Turbul. Combust. 92 (2014) 563–577. doi:10.1007/s10494-013-9514-4.

[300] F. N. Ponzio, A. Tamburini, A. Cipollina, G. Micale, M. Ciofalo, Experimental and computational investigation of heat transfer in channels filled by woven spacers, Int. J. Heat Mass Transf. 104 (2017) 163–177. doi:10.1016/j.ijheatmasstransfer.2016.08.023.

[301] G. Kraaijeveld, V. Sumberova, S. Kuindersma, H. Wesselingh, Modelling electrodialysis using the Maxwell-Stefan description, Chem. Eng. J. Biochem. Eng. J. 57 (1995) 163–176. doi:10.1016/0923-0467(94)02940-7.

[302] A. Nakayama, Y. Sano, X. Bai, K. Tado, A boundary layer analysis for determination of the limiting current density in an electrodialysis desalination, Desalination. 404 (2017) 41–49. doi:10.1016/j.desal.2016.10.013.

[303] M. Tedesco, H. V. M. Hamelers, P. M. Biesheuvel, Nernst-Planck transport theory for (reverse) electrodialysis: I. Effect of co-ion transport through the membranes, J. Memb. Sci. 510 (2016) 370–381. doi:10.1016/j.memsci.2016.03.012.

[304] A. A. Moya, Numerical simulation of ionic transport processes through bilayer ion- exchange membranes in reverse electrodialysis stacks, J. Memb. Sci. 524 (2016) 400–408. doi:10.1016/j.memsci.2016.11.051.

[305] J. S. Newman, Electrochemical Systems, second, Prentice Hall, Englewood Cliffs, 1991.

[306] R. B. Bird, W. E. Stewart, E. N. Lightfoot, Transport Phenomena, second, John Wiley & Sons, Inc., New York, 2002.

[307] T.-C. Huang, Correlations of ionic mass transfer rate in ion exchange membrane electrodialysis, J. Chem. Eng. Data. 22 (1977) 422–426. doi:10.1021/je60075a006.

[308] T.-C. Huang, I.-Y. Yu, Correlation of ionic transfer rate in electrodialysis under limiting current density conditions, J. Memb. Sci. 35 (1988) 193–206. doi:10.1016/S0376-7388(00)82443-6.

[309] M. Shakaib, S. M. F. Hasani, M. Mahmood, CFD modeling for flow and mass transfer in spacer-obstructed membrane feed channels, J. Memb. Sci. 326 (2009) 270–284. doi:10.1016/j.memsci.2008.09.052.

[310] M. Turek, Optimization of electrodialytic desalination in diluted solutions, Desalination. 153 (2003) 383–387. doi:10.1016/S0011-9164(02)01132-3.

[311] V. Pérez-Herranz, J. L. Guiñón, J. García-Antón, Analysis of mass and momentum transfer in an annular electrodialysis cell in pulsed flow, Chem. Eng. Sci. 54 (1999) 1667–1675. doi:10.1016/S0009-2509(98)00537-5.

[312] N. A. Mishchuk, L. K. Koopal, F. Gonzalez-Caballero, Intensification of electrodialysis by applying a non-stationary electric field, Colloids Surfaces A Physicochem. Eng. Asp. 176 (2001) 195–212.

[313] P. Sistat, P. Huguet, B. Ruiz, G. Pourcelly, S. A. Mareev, V. V. Nikonenko, Effect of pulsed electric field on electrodialysis of a NaCl solution in sub-limiting current regime, Electrochim. Acta. 164 (2015) 267–280. doi:10.1016/j.electacta.2015.02.197.

[314] M. H. Dirkse, W. K. P. van Loon, J. D. Stigter, J. W. Post, J. Veerman, G. P. a Bot, Extending potential flow modelling of flat-sheet geometries as applied in membrane-based systems, J. Memb. Sci. 325 (2008) 537–545. doi:10.1016/j.memsci.2008.08.022.

[315] J. Veerman, R. M. de Jong, M. Saakes, S. J. Metz, G. J. Harmsen, Reverse electrodialysis: Comparison of six commercial membrane pairs on the thermodynamic efficiency and power density, J. Memb. Sci. 343 (2009) 7–15. doi:10.1016/j.memsci.2009.05.047.

[316] J. Veerman, M. Saakes, S. J. Metz, G. J. Harmsen, Electrical power from sea and river water by reverse electrodialysis: A first step from the laboratory to a real power plant, Environ. Sci. Technol. 44 (2010) 9207–9212. doi:10.1021/es1009345.

[317] D. A. Vermaas, E. Guler, M. Saakes, K. Nijmeijer, Theoretical power density from salinity gradients using reverse electrodialysis, Energy Procedia. 20 (2012) 170–184. doi:10.1016/j.egypro.2012.03.018.

[318] S. Pawlowski, J. G. Crespo, S. Velizarov, Pressure drop in reverse electrodialysis: Experimental and modeling studies for stacks with variable number of cell pairs, J. Memb. Sci. 462 (2014) 96–111. doi:10.1016/j.memsci.2014.03.020.

[319] P. Pánek, R. Kodým, D. Šnita, K. Bouzek, Spatially two-dimensional mathematical model of the flow hydrodynamics in a spacer-filled channel – The effect of inertial forces, J. Memb. Sci. 492 (2015) 588–599. doi:10.1016/j.memsci.2015.03.099.

[320] L. Gurreri, A. Tamburini, A. Cipollina, G. Micale, CFD analysis of the fluid flow behavior in a reverse electrodialysis stack, Desalin. Water Treat. (2012) 1–14. doi:10.1080/19443994.2012.705966.

[321] S.-K. Hong, C.-S. Kim, K.-S. Hwang, J.-H. Han, H.-K. Kim, N.-J. Jeong, K.-S. Choi, Experimental and numerical studies on pressure drop in reverse electrodialysis: Effect of unit

cell configuration, J. Mech. Sci. Technol. 30 (2016) 5287–5292. doi:10.1007/s12206-016-1047-z.

[322] Y. Tanaka, Pressure distribution, hydrodynamics, mass transport and solution leakage in an ion-exchange membrane electrodialyzer, J. Memb. Sci. 234 (2004) 23–39. doi:10.1016/j.memsci.2004.01.008.

[323] Z. He, X. Gao, Y. Zhang, Y. Wang, J. Wang, Revised spacer design to improve hydrodynamics and anti-fouling behavior in reverse electrodialysis processes, Desalin. Water Treat. 57 (2016) 28176–28186. doi:10.1080/19443994.2016.1186569.

[324] M. Kostoglou, A. J. Karabelas, On the Fluid Mechanics of Spiral-Wound Membrane Modules, Ind. Eng. Chem. Res. 48 (2009) 10025–10036. doi:10.1021/ie901129j.

[325] R. Kodým, F. Vlasák, D. Snita, A. Cernín, K. Bouzek, Spatially two-dimensional mathematical model of the flow hydrodynamics in a channel filled with a net-like spacer, J. Memb. Sci. 368 (2010) 171–183. doi:10.1016/j.memsci.2010.11.042.

[326] M. Turek, K. Mitko, Residence time distribution of the electrodialyzer under electric field conditions, Desalination. 342 (2014) 139–147. doi:10.1016/j.desal.2013.11.042.

[327] R. Enciso, J. A. Delgadillo, O. Domínguez, I. Rodríguez-Torres, Analysis and validation of the hydrodynamics of an electrodialysis cell using computational fluid dynamics, Desalination. 408 (2017) 127–132. doi:10.1016/j.desal.2017.01.015.

[328] M. A.-K. Urtenov, E. V. Kirillova, N. M. Seidova, V. V. Nikonenko, Decoupling of the Nernst−Planck and Poisson Equations. Application to a Membrane System at Overlimiting Currents, J. Phys. Chem. B. 111 (2007) 14208–14222. doi:10.1021/jp073103d.

[329] T. R. Brumleve, R. P. Buck, Numerical solution of the Nernst-Planck and poisson equation system with applications to membrane electrochemistry and solid state physics, J. Electroanal. Chem. Interfacial Electrochem. 90 (1978) 1–31. doi:10.1016/S0022-0728(78)80137-5.

[330] J. Manzanares, W. Murphy, Numerical simulation of the nonequilibrium diffuse double layer in ion-exchange membranes, J. Phys. Chem. 97 (1993) 8524–8530. doi:10.1021/j100134a023.

[331] V. M. Volgin, A. D. Davydov, Ionic transport through ion-exchange and bipolar membranes, J. Memb. Sci. 259 (2005) 110–121. doi:v.

[332] J. Lim, J. Whitcomb, J. Boyd, J. Varghese, Transient finite element analysis of electric double layer using Nernst–Planck–Poisson equations with a modified Stern layer, J. Colloid Interface Sci. 305 (2007) 159–174. doi:10.1016/j.jcis.2006.08.049.

[333] V. S. Pham, Z. Li, K. M. Lim, J. K. White, J. Han, Direct numerical simulation of electroconvective instability and hysteretic current-voltage response of a permselective

membrane, Phys. Rev. E - Stat. Nonlinear, Soft Matter Phys. 86 (2012) 46310. doi:10.1103/PhysRevE.86.046310.

[334] E. A. Demekhin, N. V. Nikitin, V. S. Shelistov, Direct numerical simulation of electrokinetic instability and transition to chaotic motion, Phys. Fluids. 25 (2013) 122001. doi:10.1063/1.4843095.

[335] C. L. Druzgalski, M. B. Andersen, A. Mani, Direct numerical simulation of electroconvective instability and hydrodynamic chaos near an ion-selective surface, Phys. Fluids. 25 (2013) 110804. doi:10.1063/1.4818995.

[336] I. Rubinstein, B. Zaltzman, Equilibrium electroconvective instability, Phys. Rev. Lett. 114 (2015) 114502. doi:10.1103/PhysRevLett.114.114502.

[337] A. M. Uzdenova, A. V. Kovalenko, M. K. Urtenov, V. V. Nikonenko, Effect of electroconvection during pulsed electric field electrodialysis. Numerical experiments, Electrochem. Commun. 51 (2015) 1–5. doi:10.1016/j.elecom.2014.11.021.

[338] E. Karatay, C. L. Druzgalski, A. Mani, Simulation of chaotic electrokinetic transport: Performance of commercial software versus custom-built direct numerical simulation codes, J. Colloid Interface Sci. 446 (2015) 67–76. doi:10.1016/j.jcis.2014.12.081.

[339] E. Karatay, M. B. Andersen, M. Wessling, A. Mani, Coupling between Buoyancy Forces and Electroconvective Instability near Ion-Selective Surfaces, Phys. Rev. Lett. 116 (2016) 194501. doi:10.1103/PhysRevLett.116.194501.

[340] H.-I. Jeong, H. J. Kim, D.-K. Kim, Numerical analysis of transport phenomena in reverse electrodialysis for system design and optimization, Energy. 68 (2014) 229–237. doi:10.1016/j.energy.2014.03.013.

[341] Z. Zourmand, F. Faridirad, N. Kasiri, T. Mohammadi, Mass transfer modeling of desalination through an electrodialysis cell, Desalination. 359 (2015) 41–51. doi:10.1016/j.desal.2014.12.008.

[342] A. A. Moya, A numerical comparison of optimal load and internal resistances in ion-exchange membrane systems under reverse electrodialysis conditions, Desalination. 392 (2016) 25–33. doi:10.1016/j.desal.2016.04.016.

[343] K. Tado, F. Sakai, Y. Sano, A. Nakayama, An analysis on ion transport process in electrodialysis desalination, Desalination. 378 (2016) 60–66. doi:10.1016/j.desal.2015.10.001.

[344] A. A. Moya, A Nernst-Planck analysis on the contributions of the ionic transport in permeable ion-exchange membranes to the open circuit voltage and the membrane resistance in reverse electrodialysis stacks, Electrochim. Acta. 238 (2017) 134–141. doi:10.1016/j.electacta.2017.04.022.

[345] M. Tedesco, H. V. M. Hamelers, P. M. Biesheuvel, Nernst-Planck transport theory for (reverse) electrodialysis: II. Effect of water transport through ion-exchange membranes, J. Memb. Sci. 531 (2017) 172–182. doi:10.1016/j.memsci.2017.02.031.

[346] Y. Tanaka, Concentration polarization in ion-exchange membrane electrodialysis: The events arising in an unforced flowing solution in a desalting cell, J. Memb. Sci. 244 (2004) 1–16. doi:10.1016/j.memsci.2004.02.041.

[347] R. P. Buck, Kinetics of bulk and interfacial ionic motion: microscopic bases and limits for the nernst—planck equation applied to membrane systems, J. Memb. Sci. 17 (1984) 1–62. doi:10.1016/S0376-7388(00)81386-1.

[348] P. N. Pintauro, D. N. Bennion, Mass transport of electrolytes in membranes. 1. Development of mathematical transport model, Ind. Eng. Chem. 23 (1984) 230–234. doi:10.1021/i100014a016.

[349] J. A. Wesselingh, P. Vonk, G. Kraaijeveld, Exploring the Maxwell-Stefan description of ion exchange, Chem. Eng. J. Biochem. Eng. J. 57 (1995) 75–89. doi:10.1016/0923-0467(94)02932-6.

[350] COMSOL, (2015). http://www.comsol.com (accessed September 29, 2017).

[351] S. Casas, N. Bonet, C. Aladjem, J. L. Cortina, E. Larrotcha, L. V. Cremades, Modelling Sodium Chloride Concentration from Seawater Reverse Osmosis Brine by Electrodialysis:

Preliminary Results, Solvent Extr. Ion Exch. 29 (2011) 488–508. doi:10.1080/07366299.2011.573451.

[352] J. M. Ortiz, J. A. Sotoca, E. Expósito, F. Gallud, V. García-García, V. Montiel, A. Aldaz, Brackish water desalination by electrodialysis: Batch recirculation operation modeling, J. Memb. Sci. 252 (2005) 65–75. doi:10.1016/j.memsci.2004.11.021.

[353] K. S. Kim, W. Ryoo, M. S. Chun, G. Y. Chung, Simulation of enhanced power generation by reverse electrodialysis stack module in serial configuration, Desalination. 318 (2013) 79–87. doi:doi.org/10.1016/j.desal.2013.03.023.

[354] O. Kedem, A. Katchalsky, Permeability of composite membranes. Part 1.—Electric current, volume flow and flow of solute through membranes, Trans. Faraday Soc. 59 (1963) 1918–1930. doi:10.1039/TF9635901918.

[355] O. Kedem, A. Katchalsky, Permeability of composite membranes. Part 2.—Parallel elements, Trans. Faraday Soc. 59 (1963) 1931–1940. doi:10.1039/TF9635901931.

[356] O. Kedem, A. Katchalsky, Permeability of composite membranes. Part 3.—Series array of elements, Trans. Faraday Soc. 59 (1963) 1941–1953. doi:10.1039/TF9635901941.

[357] Y. Tanaka, Irreversible thermodynamics and overall mass transport in ion-exchange membrane electrodialysis, J. Memb. Sci. 281 (2006) 517–531. doi:10.1016/j.memsci.2006.04.022.

[358] Y. Gong, X. L. Wang, L. X. Yu, Process simulation of desalination by electrodialysis of an aqueous solution containing a neutral solute, Desalination. 172 (2005) 157–172. doi:10.1016/j.desal.2004.06.200.

[359] A. M. Lopez, M. Williams, M. Paiva, D. Demydov, T. D. Do, J. L. Fairey, Y. J. Lin, J. A. Hestekin, Potential of electrodialytic techniques in brackish desalination and recovery of industrial process water for reuse, Desalination. 409 (2017) 108–114. doi:10.1016/j.desal.2017.01.010.

[360] M. Sadrzadeh, A. Kaviani, T. Mohammadi, Mathematical modeling of desalination by electrodialysis, Desalination. 206 (2007) 538–546. doi:10.1016/j.desal.2006.04.062.

[361] E. Brauns, W. De Wilde, B. Van den Bosch, P. Lens, L. Pinoy, M. Empsten, On the experimental verification of an electrodialysis simulation model for optimal stack

configuration design through solver software, Desalination. 249 (2009) 1030–1038. doi:10.1016/j.desal.2009.04.015.

[362] G. Pourcelly, Electrodialysis with Bipolar Membranes: Principles, Optimization, and Applications, Russ. J. Electrochem. 38 (2002) 919–926. doi:10.1023/A:1016882216287.

[363] C. Fernandez-Gonzalez, A. Dominguez-Ramos, R. Ibañez, Y. Chen, A. Irabien, Valorization of desalination brines by electrodialysis with bipolar membranes using nanocomposite anion exchange membranes, Desalination. 406 (2017) 16–24. doi:10.1016/j.desal.2016.07.033.

[364] M. Reig, S. Casas, O. Gibert, C. Valderrama, J. L. Cortina, Integration of nanofiltration and bipolar electrodialysis for valorization of seawater desalination brines: Production of drinking and waste water treatment chemicals, Desalination. 382 (2016) 13–20. doi:10.1016/j.desal.2015.12.013.

[365] S. Koter, A. Warszawski, A new model for characterization of bipolar membrane electrodialysis of brine, Desalination. 198 (2006) 111–123. doi:10.1016/j.desal.2006.09.016.

[366] V. Mavrov, H. Chmiel, B. Heitele, F. Rögener, Desalination of surface water to industrial water with lower impact on the environment Part 4: Treatment of effluents from water desalination

stages for reuse and balance of the new technological concept for water desalination, Desalination. 124 (1999) 205–216. doi:10.1016/S0011-9164(99)00105-8.

[367] M. Wang, K. Kai Wang, Y.-X. Jia, Q. Chun Ren, The reclamation of brine generated from desalination process by bipolar membrane electrodialysis, J. Memb. Sci. 452 (2014) 54–61. doi:10.1016/j.memsci.2013.10.029.

[368] M. Badruzzaman, J. Oppenheimer, S. Adham, M. Kumar, Innovative beneficial reuse of reverse osmosis concentrate using bipolar membrane electrodialysis and electrochlorination processes, J. Memb. Sci. 326 (2009) 392–399. doi:10.1016/j.memsci.2008.10.018.

[369] R. Ibañez, A. Pérez-González, P. Gómez, A. M. Urtiaga, I. Ortiz, Acid and base recovery from softened reverse osmosis (RO) brines. Experimental assessment using model concentrates, Desalination. 309 (2013) 165–170. doi:10.1016/j.desal.2012.10.006.

[370] Y. Yang, X. Gao, A. Fan, L. Fu, C. Gao, An innovative beneficial reuse of seawater concentrate using bipolar membrane electrodialysis, J. Memb. Sci. 449 (2014) 119–126. doi:10.1016/j.memsci.2013.07.066.

[371] C. Fernandez-Gonzalez, A. Dominguez-Ramos, R. Ibañez, A. Irabien, Electrodialysis with Bipolar Membranes for Valorization of Brines, Sep. Purif. Rev. 45 (2016) 275–287. doi:10.1080/15422119.2015.1128951.

[372] J. Wood, J. Gifford, J. Arba, M. Shaw, Production of ultrapure water by continuous electrodeionization, Desalination. 250 (2010) 973–976. doi:10.1016/j.desal.2009.09.084.

[373] L. Alvarado, A. Chen, Electrodeionization: Principles, Strategies and Applications, Electrochim. Acta. 132 (2014) 583–597. doi:10.1016/j.electacta.2014.03.165.

[374] K. Dermentzis, Continuous electrodeionization through electrostatic shielding, Electrochim. Acta. 53 (2008) 2953–2962. doi:10.1016/j.electacta.2007.11.006.

[375] K. Dermentzis, Removal of nickel from electroplating rinse waters using electrostatic shielding electrodialysis/electrodeionization, J. Hazard. Mater. 173 (2010) 647–652. doi:10.1016/j.jhazmat.2009.08.133.

[376] M. Andelman, Flow through capacitor basics, Sep. Purif. Technol. 80 (2011) 262–269. doi:10.1016/j.seppur.2011.05.004.

[377] Y. Oren, Capacitive deionization (CDI) for desalination and water treatment - past, present and future (a review), Desalination. 228 (2008) 10–29. doi:10.1016/j.desal.2007.08.005.

[378] M. A. Anderson, A. L. Cudero, J. Palma, Capacitive deionization as an electrochemical means of saving energy and delivering clean water. Comparison to present desalination practices: Will it compete?, Electrochim. Acta. 55 (2010) 3845–3856. doi:10.1016/j.electacta.2010.02.012.

[379] B. Pisarska, Transport of co-ions across ion exchange membranes in electrodialytic metathesis MgSO4 + 2KCl → K2SO4 + MgCl2, Desalination. 230 (2008) 298–304. doi:10.1016/j.desal.2007.10.021.

[380] K. Haerens, P. De Vreese, E. Matthijs, L. Pinoy, K. Binnemans, B. Van Der Bruggen, Production of ionic liquids by electrodialysis, Sep. Purif. Technol. 97 (2012) 90–95. doi:10.1016/j.seppur.2012.02.017.

[381] A. T. K. Tran, Y. Zhang, D. De Corte, J.-B. Hannes, W. Ye, P. Mondal, N. Jullok, B. Meesschaert, L. Pinoy, B. Van Der Bruggen, P-recovery as calcium phosphate from

wastewater using an integrated selectrodialysis/crystallization process, J. Clean. Prod. 77 (2014). doi:10.1016/j.jclepro.2014.01.069.

[382] S. Schlumpberger, N. B. Lu, M. E. Suss, M. Z. Bazant, Scalable and Continuous Water Deionization by Shock Electrodialysis, Environ. Sci. Technol. Lett. 2 (2015) 367–372. doi:10.1021/acs.estlett.5b00303.

[383] D. Deng, E. V. Dydek, J.-H. Han, S. Schlumpberger, A. Mani, B. Zaltzman, M. Z. Bazant, Overlimiting Current and Shock Electrodialysis in Porous Media, Langmuir. 29 (2013) 16167–16177. doi:10.1021/la4040547.

[384] D. Deng, W. Aouad, W. A. Braff, S. Schlumpberger, M. E. Suss, M. Z. Bazant, Water purification by shock electrodialysis: Deionization, filtration, separation, and disinfection, Desalination. 357 (2015) 77–83. doi:10.1016/j.desal.2014.11.011.

[385] E. V. Dydek, B. Zaltzman, I. Rubinstein, D. S. Deng, A. Mani, M. Z. Bazant, Overlimiting Current in a Microchannel, Phys. Rev. Lett. 107 (2011) 118301. doi:10.1103/PhysRevLett.107.118301.

[386] A. Yaroshchuk, Over-limiting currents and deionization “shocks” in current-induced polarization: Local-equilibrium analysis, Adv. Colloid Interface Sci. 183 (2012) 68–81. doi:10.1016/j.cis.2012.08.004.

[387] A. Mani, T. A. Zangle, J. G. Santiago, On the Propagation of Concentration Polarization from Microchannel−Nanochannel Interfaces Part I: Analytical Model and Characteristic Analysis, Langmuir. 25 (2009) 3898–3908. doi:10.1021/la803317p.

[388] A. Tamburini, G. La Barbera, A. Cipollina, G. Micale, M. Ciofalo, CFD prediction of scalar transport in thin channels for reverse electrodialysis, Desalin. Water Treat. 55 (2015) 3424–3445. doi:10.1080/19443994.2014.959735.

[389] A. H. Avci, P. Sarkar, R. A. Tufa, D. Messana, P. Argurio, E. Fontananova, G. Di Profio, E. Curcio, Effect of Mg 2+ ions on energy generation by Reverse Electrodialysis, J. Memb. Sci. 520 (2016) 499–506. doi:10.1016/j.memsci.2016.08.007.

[390] R.E. Pattle, Production of electric power by mixing fresh and salt water in the hydroelectric pile, Nature. 174 (1954) 660.

[391] J. Veerman, M. Saakes, S. J. Metz, G. J. Harmsen, Reverse electrodialysis: Performance of a stack with 50 cells on the mixing of sea and river water, J. Memb. Sci. 327 (2009) 136–144. doi:10.1016/j.memsci.2008.11.015.

[392] REAPower, (2014). http://www.reapower.eu/ (accessed September 10, 2017).

[393] M. Tedesco, E. Brauns, A. Cipollina, G. Micale, P. Modica, G. Russo, J. Helsen, Reverse electrodialysis with saline waters and concentrated brines: A laboratory investigation towards technology scale-up, J. Memb. Sci. 492 (2015) 9–20. doi:10.1016/j.memsci.2015.05.020.

[394] J. N. Weinstein, F. B. Leitz, Electric Power from Differences in Salinity: The Dialytic Battery, Science (80-.). 191 (1976) 557–559. doi:10.1126/science.191.4227.557.

[395] R. Audinos, Reverse electrodialysis. Study of the electric energy obtained by mixing two solutions of different salinity., J. Power Sources. 10 (1983) 203–217.

[396] J. Jagur-Grodzinski, R. Kramer, Novel process for direct conversion of free energy of mixing into electric power, Ind. Eng. Chem. Process Des. Dev. 25 (1986) 443–449. doi:10.1021/i200033a016.

[397] M. Turek, B. Bandura, Renewable energy by reverse electrodialysis, Desalination. 205 (2007) 67–74. doi:10.1016/J.DESAL.2006.04.041.

[398] M. Turek, B. Bandura, P. Dydo, Power production from coal-mine brine utilizing reversed electrodialysis, Desalination. 221 (2008) 462–466. doi:10.1016/J.DESAL.2007.01.106.

[399] J. W. Post, C. H. Goeting, J. Valk, S. Goinga, J. Veerman, H.V.M. Hamelers, P.J.F.M. Hack, Towards implementation of reverse electrodialysis for power generation from salinity gradients, Desalin. Water Treat. 16 (2010) 182–193. doi:10.5004/dwt.2010.1093.

[400] A. Cipollina, G. Micale, A. Tamburini, M. Tedesco, L. Gurreri, J. Veerman, S. Grasman, Reverse electrodialysis, in: Sustain. Energy from Salin. Gradients, Elsevier, 2016: pp. 135–180. doi:10.1016/B978-0-08-100312-1.00005-5.

[401] M. Tedesco, C. Scalici, D. Vaccari, A. Cipollina, A. Tamburini, G. Micale, Performance of the first reverse electrodialysis pilot plant for power production from saline waters and concentrated brines, J. Memb. Sci. 500 (2016) 33–45. doi:10.1016/j.memsci.2015.10.057.

[402] B. E. Logan, M. Elimelech, Membrane-based processes for sustainable power generation using water, Nature. 488 (2012) 313–319.

[403] A. Tamburini, A. Cipollina, M. Papapetrou, A. Piacentino, G. Micale, Salinity gradient engines, in: Sustain. Energy from Salin. Gradients, 2016: pp. 219–256. doi:10.1016/B978-0-08-100312-1.00007-9.

[404] M. Bevacqua, A. Tamburini, M. Papapetrou, A. Cipollina, G. Micale, A. Piacentino, Reverse electrodialysis with NH4HCO3 -water systems for heat-to-power conversion, Energy. 137 (2017) 1293–1307. doi:10.1016/j.energy.2017.07.012.

[405] K. Kwon, B. H. Park, D. H. Kim, D. Kim, Parametric study of reverse electrodialysis using ammonium bicarbonate solution for low-grade waste heat recovery, Energy Convers. Manag. 103 (2015) 104–110. doi:10.1016/j.enconman.2015.06.051.

[406] A. Tamburini, M. Tedesco, A. Cipollina, G. Micale, M. Ciofalo, M. Papapetrou, W. Van Baak, A. Piacentino, Reverse electrodialysis heat engine for sustainable power production, Appl. Energy. 206 (2017) 1334–1353. doi:10.1016/j.apenergy.2017.10.008.

[407] W. J. van Egmond, M. Saakes, S. Porada, T. Meuwissen, C. J. N. Buisman, H. V. M. Hamelers, The concentration gradient flow battery as electricity storage system: Technology potential and energy dissipation, J. Power Sources. 325 (2016) 129–139. doi:10.1016/J.JPOWSOUR.2016.05.130.

[408] W. J. van Egmond, M. Saakes, I. Noor, S. Porada, C. J. N. Buisman, H. V. M. Hamelers, Performance of an environmentally benign acid base flow battery at high energy density, Int. J. Energy Res. (2017). doi:10.1002/er.3941.

[409] M. Vanoppen, G. Blandin, S. Derese, P. Le Clech, J. Post, A. R. D. Verliefde, Salinity gradient power and desalination, in: Sustain. Energy from Salin. Gradients, Elsevier, 2016: pp. 281–313. doi:10.1016/B978-0-08-100312-1.00009-2.

[410] Y. A. C. Jande, W. S. Kim, Integrating reverse electrodialysis with constant current operating capacitive deionization, J. Environ. Manage. 146 (2014) 463–469. doi:10.1016/j.jenvman.2014.07.039.

[411] W. Li, W. B. Krantz, E. R. Cornelissen, J. W. Post, A. R. D. Verliefde, C. Y. Tang, A novel hybrid process of reverse electrodialysis and reverse osmosis for low energy seawater

desalination and brine management, Appl. Energy. 104 (2013) 592–602. doi:10.1016/j.apenergy.2012.11.064.

[412] Y. Mei, C. Y. Tang, Co-locating reverse electrodialysis with reverse osmosis desalination: Synergies and implications, J. Memb. Sci. 539 (2017) 305–312. doi:10.1016/J.MEMSCI.2017.06.014.

[413] K. Kwon, J. Han, B. H. Park, Y. Shin, D. Kim, Brine recovery using reverse electrodialysis in membrane-based desalination processes, Desalination. 362 (2015) 1–10. doi:10.1016/j.desal.2015.01.047.

[414] B. J. Feinberg, G. Z. Ramon, E. M. V. Hoek, Thermodynamic Analysis of Osmotic Energy Recovery at a Reverse Osmosis Desalination Plant, Environ. Sci. Technol. 47 (2013) 2982–2989. doi:10.1021/es304224b.

[415] Q. Wang, X. Gao, Y. Zhang, Z. He, Z. Ji, X. Wang, C. Gao, Hybrid RED/ED system: Simultaneous osmotic energy recovery and desalination of high-salinity wastewater, Desalination. 405 (2017) 59–67. doi:10.1016/j.desal.2016.12.005.

[416] J. Kim, M. Park, S. A. Snyder, J. H. Kim, Reverse osmosis (RO) and pressure retarded osmosis (PRO) hybrid processes: Model-based scenario study, Desalination. 322 (2013) 121–130. doi:10.1016/j.desal.2013.05.010.

[417] G. Blandin, A. R. D. Verliefde, C. Y. Tang, P. Le-Clech, Opportunities to reach economic sustainability in forward osmosis-reverse osmosis hybrids for seawater desalination, Desalination. 363 (2015) 26–36. doi:10.1016/j.desal.2014.12.011.

[418] T. Y. Cath, N. T. Hancock, C. D. Lundin, C. Hoppe-Jones, J. E. Drewes, A multi-barrier osmotic dilution process for simultaneous desalination and purification of impaired water, J. Memb. Sci. 362 (2010) 417–426. doi:10.1016/j.memsci.2010.06.056.

[419] V. Yangali-Quintanilla, Z. Li, R. Valladares, Q. Li, G. L. Amy, Indirect desalination of Red Sea water with forward osmosis and low pressure reverse osmosis for water reuse, Desalination. 280 (2011) 160–166. doi:10.1016/j.desal.2011.06.066.

[420] V. Yangali-Quintanilla, L. Olesen, J. Lorenzen, C. Rasmussen, H. Laursen, E. Vestergaard, K. Keiding, Lowering desalination costs by alternative desalination and water reuse scenarios, Desalin. Water Treat. 55 (2015) 2437–2445. doi:10.1080/19443994.2014.940660.